AN ABSTRACT OF THE THESIS OF

Cynthia M. Bowline for the degree of Doctor of Philosophy in Civil Engineering presented on November 24, 1993.

Title: Chaos in a Long Rectangular Wave Channel

Redacted for Privacy

Abstract approved: _____

Robert T. Hudspeth

The Melnikov method is applied to a model of parametrically generated cross-waves in a long rectangular channel in order to determine if these cross-waves are chaotic. A great deal of preparation is involved in order to obtain a suitable form for the application of the Melnikov method. The Lagrangian for water waves, which consists of the volume integrals of the kinetic energy density, potential energy density, and a dynamic pressure component, is transformed to surface integrals in order to avoid constant conjugate momenta. The Lagrangian is simplified by subtracting the zero variation integrals and written in terms of generalized coordinates, the time dependent components of the cross-wave and progressive wave velocity potentials. The conjugate momenta are calculated after expanding the Lagrangian in a Taylor series. The Hamiltonian is then determined by a Legendre transformation of the Lagrangian.

Ordinarily, the first order evolution equations obtained from derivatives of the Hamiltonian are suitable for applications of the Melnikov method. However, the cross-wave model results in extremely complicated evolution equations which must be simplified

before a Melnikov analysis is possible. A sequence of seven canonical transformations are applied and yield a final set of evolution equations in fairly simple form. The unperturbed system is analyzed to determine hyperbolic fixed points and the equations describing the heteroclinic orbits for near resonance cases. The Melnikov function is calculated for the perturbed system which must also satisfy KAM conditions.

The Melnikov results indicate the system is chaotic near resonance. Furthermore, the heteroclinic orbits, about which chaotic motions occur, are transformed back to the original set of variables and found to be extremely complicated; this orbit would be impossible to determine analytically without the canonical transformations.

The theoretical results were verified by experiments. Poincaré maps obtained from measurements of the free surface displacement indicate both quasi-periodic and chaotic motions of the water surface. Power spectra and time series of the water surface displacement are also analyzed for chaotic behavior, with less conclusive results. Stability diagrams of cross-wave generation confirm behavior consistent with parametric excitation.

© Copyright by Cynthia M. Bowline
November 24, 1993

All Rights Reserved

CHAOS IN A LONG RECTANGULAR WAVE CHANNEL

by

Cynthia M. Bowline

A THESIS

submitted to

Oregon State University

in partial fulfillment of
the requirements for the
degree of

Doctor of Philosophy

Completed November 24, 1993

Commencement June 1994

APPROVED:

Redacted for Privacy

Professor of Civil Engineering in charge of major

Redacted for Privacy

Head of Department of Civil Engineering

Redacted for Privacy

Dean of Graduate School

Date thesis is presented: November 24, 1993

Typed by: Cynthia M. Bowline

ACKNOWLEDGEMENT

There are a number of people that I would like to thank for their help along the way as I pursued my Ph.D. research. The help provided has been professional, financial, and personal, and all of it has been very welcome.

First and foremost I would like to thank my major professor and thesis advisor, Dr. Robert Hudspeth. It is directly due to Dr. Hudspeth that I ever entered the Ocean Engineering program. As I was nearing completion of my studies in the oceanography program, I decided that I wanted to take a class called Forces on Marine Structures, for which I did not have the prerequisites, so I went to ask the instructor if I could take the class anyway. The instructor was Dr. Hudspeth, who not only said that I could take the class, but also suggested that I apply to the Ph.D. program in ocean engineering. I did apply, and Dr. Hudspeth became my major professor.

Dr. Hudspeth has played a very prominent role in the research involved in this dissertation. It was his idea that cross-waves might be chaotic, and his idea on how to approach the basic problem. At every twist and turn of my research, he was there to discuss all of the possibilities and problems, and to provide insight and intuition into solving them.

Dr. Ronald Guenther has also been very involved in the chaotic cross-wave search, and he was also responsible for the ideas included in this research. As my unofficial "major advisor" when Dr. Hudspeth was on sabbatical, we spent many hours working together on Lagrangians and Hamiltonians. I would also like to say that I have never yet found an integral that Dr. Guenther did not know how to evaluate.

I would also like to thank those involved in additional professional help. Terry Dibble was lots of fun to work with while we generated all sorts of cross-waves in the lab. Dave Standley was always willing to send me new data files from the lab work, especially when

I discovered months after the fact that I had stored some of my data on improperly formatted discs: Mac 1, PC 0. Speaking of PCs, I would like to thank my brother Steve Bowline for letting me use his to analyze all of my experimental data, and for discovering exactly why it was that 1/4 of my data was missing, prompting my emergency phone call to Dave.

My degree would have been very hard to achieve without financial assistance. The Office of Naval Research funded my graduate research assistantship, and wsa also the funding source for the National Defense Science and Engineering Graduate Fellowship that I was awarded for three years. I am very thankful for all of this monetary support. I would also like to thank my parents, Rose and Jerry Bowline, for loaning me the money some years back to buy a computer that has lasted for two theses. They waited patiently for six years for me to pay them back, and never charged any interest.

On a more personal note, I would like to thank my former Corvallis roommates, Dan Kvitka and Jennefer Wood. They teased me endlessly about my hour-long phone calls every evening to my newlywed husband who was stuck in Bakersfield.

Which brings me to my final expression of appreciation, to my husband Mike Parker. Mike has provided love and affection, companionship, comic relief, entertainment, and a wonderful and happy life ever since we met at the beginning of our grad school days. It's not an easy thing to marry a graduate student, and then to have your spouse sometimes with you and sometimes in another state working on their degree, but Mike handled it all with maturity, emotional support, and humor.

TABLE OF CONTENTS

LIST OF FIGURES

Figure

LIST OF TABLES

Tables

CHAOS IN A LONG RECTANGULAR WAVE CHANNEL

Chapter I. Introduction

A long rectangular wave basin has a horizontal flat bottom, two rigid vertical side walls, a wavemaker at one end, and a sloping beach at the far end. Waves of a variety of frequencies and heights can be generated by the wavemaker which propagate down the channel and dissipate on the beach. The wavemaker may be a piston, a flap on a hinge, or a combination of the two. The wave generated by the forcing is called a progressive wave since it travels from the wavemaker and dissipates on the beach.

Sometimes a standing wave develops between the side walls of the channel. This standing wave can be forced if the wavemaker is configured to have an amplitude variation across the tank. An example of this type of wavemaker motion is a series of narrow flaps, all hinged at the bottom, but moving independently of one another. The standing wave that develops from this type of wavemaker forcing will be called a *sloshing* wave.

The particular wave of interest here is also a standing wave between the side walls, but one that forms without any wavemaker variation across the channel, and forms in addition to the progressive wave. This type of standing wave will be called a *cross-wave* and is a result of parametric forcing.

The terms sloshing wave and cross-wave are used here to distinguish between standing waves generated by different forcing mechanisms, but the distinction in name is not consistent throughout the literature. The terminology used here is the same as that used by Kit, Shemer, and Miloh [1987]. Sloshing waves are not studied here, but the following references are provided: Barnard, Mahony, and Pritchard [1977], Shemer, Kit, and Miloh [1987], Kit, Shemer, and Miloh [1987], and Miles [1988].

The parametrically generated cross-waves are of particular interest. Again it is emphasized that they form in addition to a progressive wave that travels from the wavemaker to the end of the channel and dissipates on the beach. Cross-waves generally

oscillate with a frequency half that of the forcing, but as will be shown, this is not always the case. The channel width determines the wavelengths λ_{cn} of possible cross-wave modes, $\lambda_{cn} = 2(\text{basin width})/n$, where n is the mode number, which is equal to the number of half-wavelengths across the channel. The amplitude of the cross-wave can be much larger than both the wavemaker forcing amplitude and the progressive wave amplitude.

The cross-waves studied here form in a long channel, although they may be generated in much shorter channels as well. A short channel generally has a vertical wall opposite the wavemaker, instead of a sloping beach, and the longitudinal wave generated by the wavemaker will also be a standing wave. Some references on cross-waves in short channels include the important theoretical work by Garrett [1970], which will be discussed in some detail, and the theoretical papers by Miles [1988], Shemer [1990], and Tsai, Yue, and Yip [1990]. Lin and Howard [1960] provide experimental work on cross-waves in short channels.

Garrett [1970] seems to have compiled one of the earliest theoretical works on cross-waves and identified them as an example of parametric resonance. Garrett proposed a channel that had two wavemakers opposite each other, rigid vertical side walls, and a flat bottom. The wavemaker motions were assumed to be of small amplitude, so the wavemaker boundary conditions were linearized. The free surface boundary conditions included second order terms and the free surface position and the velocity potential were assumed to be the sums of the primary motion (longitudinal wave) plus all the free modes of the channel. Garrett's analysis showed that the amplitude of the cross-waves was governed by a form of Mathieu's equation, an example of parametric forcing, and thus accounted for the cross-wave frequency being half that of the forcing.

Garrett takes some pains to point out that the general theory of parametric forcing [see Bogoliubov and Mitropolsky, 1961] allows for the phenomenon of resonance to occur whenever the forcing frequency is close to $2\omega/M$, where M is an integer and ω is the

free oscillation frequency, in this case the cross-wave frequency. The strongest resonance is for the case $M = 1$, which is called the primary resonance. Garrett provided the analysis for the primary resonance only, as other cases would have required higher order terms in the free boundary conditions. This discussion is significant because later papers often fail to mention the possibility that cross-wave frequencies can be other than half that of the forcing. A further significance is that cross-waves for $M = 2$ (or the cross-wave frequency equals the forcing frequency) have been observed in experiments at the O. H. Hinsdale Wave Research Laboratory at Oregon State University. The analysis carried out in this research initially assumes many resonance cases are possible, although at some point $M = 1$ must be specified since higher order terms would also be needed to carry out analyses of $M > 1$ resonances.

Finally, Garrett determined that the cross-wave growth is due to the rate of working of the wavemaker against the transverse stresses associated with the cross-waves, one at the surface and one equal to the depth-independent second order pressure. The energy of the cross-waves comes from the wavemaker, not the primary wave field.

An early theoretical work on cross-waves in long channels is that of Mahony [1972]. Mahony assumed a slight transverse disturbance of order ε in the free surface position and the velocity potential, and ignored order ε^2 and higher terms in the free surface boundary conditions. Mahony found a smaller order of magnitude of resonance bandwidth and growth of cross-waves than Garrett did. Mahony also found that the long channel results in some small amount of damping, requiring some minimum amplitude of excitation in order for a cross-wave to occur. Mahony suggested, as did Garrett, that the wavemaker motion and not the primary progressive wave field is responsible for the instability leading to the cross-waves.

Jones [1984] also studied cross-waves in a long wave channel. He used an approach that initially retained all the nonlinear terms and developed a uniformly asymptotic solution based on the small amplitude of the wavemaker. An important result of Jones' work is that

only the order ε interactions of the cross-waves with cross-waves and the cross-waves with progressive waves contributed to resonance effects. The order ε interaction of progressive waves with progressive waves did not contribute to resonance.

Lichter and Chen [1987] used the perturbation method of multiple scales to study cross-waves in long channels. Kit and Shemer [1989] sought to include the effects of dissipation on cross-waves in long channels. Miles and Becker [1988] have formulated the cross-waves in a long channel in terms of a Lagrangian formulation.

This research seeks to expand the understanding of cross-waves in a long tank by formulating the problem in terms of Hamiltonian mechanics. This method builds on the Lagrangian formulation of Miles and Becker [1988].

Experimental studies of cross-waves in long channels begin with Barnard and Pritchard [1972]. Stability diagrams were determined for various cross-wave modes; these diagrams indicate the regions in which cross-waves occur, each mode requiring some minimum amplitude of wavemaker forcing, and the cross-waves occur in a narrow band about a forcing frequency twice that of the cross-wave. (This corresponds to the primary resonance described by Garrett.) Barnard and Pritchard also showed that the amplitude of the cross-wave varied with time, indicating a continual growth and decay of the waves. Cross-wave amplitudes decreased with distance from the wavemaker. The channel used was 30.6 cm wide, the water depth was 16 cm, and the length was 270 cm; although the channel was long compared to its width and depth, it was also small enough that surface effects were profoundly important. In particular, an absorbent cotton bandage was placed on the wavemaker, the channel sides at the waterline, and on the beach to reduce the effects of uneven wetting. Water surface contamination was a crucial factor, necessitating skimming the water surface before each experimental run.

Lichter and Shemer [1986], Shemer and Lichter [1987], and Shemer and Kit [1989] all used a channel 1.2 m wide, 0.9 m deep, and 18 m long, where surface effects were negligible. All experiments used the primary parametric resonance case. Lichter and

Shemer studied the evolution of the wave energy spectrum with distance from the wavemaker. Shemer and Lichter classified different regions in the stability diagrams based on the presence or absence of an amplitude modulation. Shemer and Kit studied the long-time modulation patterns of the cross-waves.

Underhill, Lichter, and Bernoff [1991] studied parametrically forced cross-waves and found three prominent frequencies present: the primary subharmonic and two slow temporal modulations. The stability diagrams were very precisely divided into regions where the cross-wave motion was periodic, quasi-periodic, or chaotic. As this channel was also fairly small (30.9 cm wide, 30 cm deep, and 121 cm long), surface tension effects were notable and a surfactant was added to the water. Shemer and Lichter [1987] also defined the neutral stability curve for a cross-wave and the boundaries between steady, quasi-periodic, and chaotic behavior.

Quasi-periodic behavior is motion that consists of two or more incommensurate frequencies. Chaotic behavior describes a motion that is sensitive to different initial conditions. Motion from one set of initial conditions cannot be used to predict the motion when the conditions are slightly varied. It is the chaotic behavior of cross-waves that is studied here.

There are various theoretical tools for studying chaotic behavior. One common strategy is to obtain the homoclinic orbit in the mathematical model of a dynamical system and then to apply a mathematical technique called the Melnikov method to determine if the system has chaotic motions. The strategy requires that the system be described in terms of a set of first order ordinary differential equations of the phase space variables. In a classical mechanics problem, these are the evolution equations which are the derivatives of the Hamiltonian. The unperturbed (or free oscillation) system is then studied in the phase space to find the location of any saddle points and the time-dependent equations describing the motion along the homoclinic orbit, which is the orbit that results when the stable and

unstable manifolds of the saddle point intersect. The Melnikov method is then applied to the Poincaré map of the perturbed system.

The Melnikov method, which has been described by Moon [1987] as a Reynolds-numberlike criteria for chaos, is a method used to measure the distance between the stable and unstable manifolds of Poincaré maps of continuous phase space flows. When the manifolds intersect, the Melnikov function has a simple zero, which indicates the presence of Smale horseshoes and therefore indicates chaotic motion. For more background on this method and homoclinic orbits, see the original work by Melnikov [1963], Guckenheimer and Holmes [1983], and Wiggins [1988 &1990]. A more general review may be found in Moon [1987 & 1992] or Abraham and Shaw [1992].

The original method [Melnikov, 1963] was applied only to two phase space variables (a one-degree of freedom problem), but has been expanded to include higher dimensional problems [Wiggins and Holmes, 1987; Wiggins, 1988; and Wiggins, 1990]. This technique has also been applied to other water wave problems, including Holmes [1986] and Allen, Samelson, and Newberger [1992].

There are also various experimental tools available for studying chaotic motions. Moon [1987] provides a good summary of these methods. The two simplest tools are the Fourier spectrum and the Poincaré map. The Fourier spectrum of a chaotic signal has a broad band of frequencies present, even if the input is of a single frequency. The Poincaré map is a periodic sampling of the phase space variables. A single point in a Poincaré map indicates periodic motion; additional finite points show subharmonic oscillation; a closed curve indicates quasi-periodic motion; a fractal collection of points, or points filling a strange attractor, indicates chaotic motions. As mentioned earlier, Underhill, Lichter, and Bernoff [1991] applied these two techniques to their experimental cross-wave data. They also calculate the Lyapunov exponent, a positive exponent indicating chaotic motion.

The purpose of this research is to apply the global perturbation technique of the Melnikov function to determine if cross-waves parametrically excited in a long wave

channel are chaotic. Experiments were performed in the O. H. Hinsdale Wave Research Laboratory to support the theoretical analysis. The channel is quite large, 12 ft. wide, 12 ft. deep, and over 300 ft. long, making surface tension effects entirely irrelevant. The most striking observation of the cross-waves was the simultaneous generation of cross-waves of the primary resonance (2:1) and secondary resonance (1:1). This effect has not been reported before.

This chapter serves as an introduction to Chapters II and III, each of which are complete on their own, and it contains some material redundant to each. Chapter II describes the theoretical analysis, which is the set-up involved to apply the Melnikov method and the calculation of the Melnikov function indicating chaos. Chapter III provides all the experimental results and discussions. Chapters II and III each have their own conclusion and reference sections. Chapter IV is a brief discussion of recommended future research.

Chapter II. Theoretical Results

1. Cross-waves in a long rectangular channel

Cross-waves in a long rectangular channel are parametrically excited standing surface gravity waves that oscillate in a direction transverse to the wavemaker forcing. These basins have a horizontal bottom, rigid side walls, and a wavemaker at one end. A short channel generally has a vertical wall opposite the wavemaker, while a long channel has a sloping beach far from the wavemaker that simulates a semi-infinite domain. Cross-waves in a short channel occur in addition to any standing longitudinal waves produced by the wavemaker, while cross-waves in a long channel occur in addition to the longitudinal progressive waves generated by the wavemaker. The term cross-wave is used here to specify a parametrically forced transverse wave, while a transverse wave generated by wavemaker motion antisymmetric about its midpoint is referred to as a sloshing wave.

The progressive wave frequency ω_p is equal to that of the wavemaker forcing and the deep water dispersion relation $\omega_p^2 = gk$ provides the wavenumber k associated with the frequency ω_p. The channel width determines the wavelengths $\lambda_c = 2(\text{basin width})/\text{n}$ of possible cross-wave modes where n is the mode number and is equal to the number of half-wavelengths across the tank. The cross-wave frequency ω_c is related to the wavelength by the deep water dispersion relation $\omega_c^2 = g\kappa$, $\kappa = 2\pi/\lambda_c$ where κ is the wavenumber of the cross-wave. Cross-waves generally have half the frequency of the wavemaker forcing $\left(\omega_c \approx \frac{1}{2}\omega_p\right)$, although additional resonances can occur. The following general discussion based on Bogoliubov and Mitropolsky [1961] illustrates the possible frequency relationships.

Assume the motion of a parametrically forced oscillator is described by Mathieu's equation

$$\ddot{x} + \sigma^2(1 - \varepsilon \cos \nu t)x = 0, \quad \varepsilon << 1. \tag{1.1}$$

Resonance occurs when the natural frequency σ is related to the parametric forcing frequency ν by $\sigma = N\nu/M$, N and M integers. Bogoliubov and Mitropolsky expand in perturbation series the displacement x, the time-derivative of the amplitude $\partial a/\partial t$, and the time derivative of the phase $\partial\theta/\partial t$, and solve by the method of successive approximations. An instability due to parametric resonance occurs for some range of parametric forcing frequency ν and for some values of the nonlinearity parameter ε. In the parameter space defined by ν as the abcissa and ε as the ordinate, the region in which the parametric resonance occurs is called the zone of instability and is delineated by a neutral stability curve. A typical neutral stability curve is somewhat V-shaped. The primary (fundamental) resonance of $N = 1$ and $M = 2$ has the largest zone of instability (the widest V-shape). If the forcing frequency lies within the interval described by the zone, the instability (such as a cross-wave) will occur. The zone of instability thus determines the bandwidth of the resonance. Letting N vary and carrying out the perturbations, Bogoliubov and Mitropolsky show that the bandwidth of the zone of instability diminishes with order N as ε^N. They also show that the neutral stability curve minimum (the bottom of the V-shape) occurs at $\varepsilon = 0$ without damping and at higher values of ε when damping is included. This minimum value increases as N increases. Thus the primary resonance case $\sigma = \nu/2$ is of the most practical interest.

Laboratory experiments have shown that the amplitude of the cross-wave can be much larger than both the wavemaker forcing amplitude and the progressive wave amplitude. The wavemaker forcing will parametrically generate a cross-wave in the lab when two conditions are met: 1) some minimum amplitude of wavemaker forcing is exceeded, and 2) the wavemaker (and progressive wave) frequency ω_p is in some narrow bandwidth about $M\omega_c/N$. These two conditions are the same as those described in the discussion from

Bogoliubov and Mitropolsky above. The primary resonance is for $N = 1$ and $M = 2$, which is the general case explored in the cross-wave literature.

Garrett [1970] showed that the amplitude of cross-waves in a short channel was governed by a form of Mathieu's equation and that their growth was due to the rate of working of the wavemaker against the transverse stresses associated with the cross-waves. Garrett is the only one to review resonance cases other than the primary. Mahony [1972] obtained similar results for cross-waves in a long channel. Jones [1984] determined that the order ε interactions between the cross-wave with the progressive wave and the cross-wave with itself contributed to the parametric resonance effect, but that the order ε interaction of the progressive wave with itself did not contribute. Miles [1988] and Miles and Becker [1988] applied a Lagrangian formulation to cross-waves in both short and long channels and applied classical perturbation theory.

Of the various experiments on cross-waves in long channels, two are of particular note. Shemer and Lichter [1987] defined a neutral stability curve for cross-waves that indicated boundaries between steady, quasi-periodic, and chaotic behavior. Underhill, Lichter, and Bernoff [1991] found three prominent frequencies present: the primary subharmonic and two slow temporal modulations. Their stability diagrams were divided very precisely into regions where the cross-wave motion was periodic, quasi-periodic, or chaotic. Quasi-periodic motion consists of two or more incommensurate frequencies while chaotic motion is sensitive to initial conditions.

Here, parametrically generated cross-waves in a long channel are formulated in terms of a Hamiltonian that is used to apply a mathematical technique called the Melnikov method to predict the chaotic behavior of cross-waves. The Melnikov method is a global perturbation technique that is used to prove the existence of chaos in dynamical systems [Melnikov, 1963; Guckenheimer and Holmes, 1983; Wiggins, 1988]. The method has been applied to numerous mechanical systems and has been successfully applied to a fluid continuum by Holmes [1986] and Allen, Samelson, and Newberger [1991]. Holmes [1986] applied the

Melnikov method to surface waves in a cylindrical basin generated by vertical oscillations of the basin and found chaos. Allen, Samelson, and Newberger [1991] applied the Melnikov method to quasi-geostrophic flow over a variable topography and also found chaos.

The original planar method of Melnikov [1963] was a technique applied to a system of first order ordinary differential equations of two phase space variables. The first step in the technique was to characterize the unperturbed (unforced and undamped) system by determining the fixed points that were saddles and finding the homoclinic or heteroclinic orbits. The method cannot be applied without a homoclinic or heteroclinic orbit. Melnikov then defined a function, which has since been called the Melnikov function, that described the distance between the stable and unstable manifolds near the homoclinic orbit when the perturbation is applied. A distance of zero indicates the manifolds intersect transversely, and an infinite number of intersections indicates chaotic motion.

Wiggins and Holmes [1987] extended the planar method to a system with three phase space variables. The basic procedure remained the same, but the Melnikov function contained additional terms and there was a requirement that the averaged third equation contain at least one simple zero (see Proposition 2.2, Wiggins and Holmes, 1987) in order for an orbit to survive the perturbation. Wiggins [1988 & 1990] further generalized the method to apply to systems having more than three degrees of freedom.

Since the Melnikov method is applied to a system of first order ordinary differential equations, the general approach to obtaining these equations is through a Hamiltonian formulation. The evolution equations are derivatives of the Hamiltonian and describe the motion of a system in terms of first order ODEs. This approach is such a natural way of obtaining the appropriate system that most forms of the Melnikov function now include the Hamiltonian [Guckenheimer and Holmes, 1983; Wiggins and Holmes, 1987; Wiggins, 1988; Wiggins, 1990; and Moon, 1987].

The global perturbation technique of the Melnikov method is used to show that cross-waves parametrically excited in a long wave channel are chaotic. The application of the method requires a great deal of preparatory work to formulate the mathematical model in an appropriate way. The approach used is to obtain the Hamiltonian formulation in terms of classical mechanics. The Lagrangian is expressed in terms of progressive and cross-wave velocity potentials in §2. The conjugate momenta are calculated from a Legendre transformation. The Hamiltonian is obtained in §3 from the Lagrangian. A sequence of seven canonical transformations follow in order to simplify the Hamiltonian and provide evolution equations which can be integrated to calculate the homoclinic orbits. A complete analysis of the unperturbed phase space is given in §4; this section also includes the Melnikov function calculations showing chaos. Cross-wave experiments were performed at the O. H. Hinsdale-Wave Research Laboratory (OHH-WRL) at Oregon State University to support the theoretical conclusions (Chapter III). The most intriguing observation from the experiment was the simultaneous excitation of two cross-wave modes of different resonance cases: the primary resonance, where the mode 1 cross-wave had half the forcing frequency, and a secondary resonance, where the mode 4 cross-wave frequency equaled the forcing frequency. Poincaré maps obtained from the data showed strange attractors that also indicate chaos.

2. Lagrangian formulation

All dependent and independent dimensional variables are denoted with a prime to distinguish them from nondimensional variables. The fluid is assumed to be incompressible and inviscid and the flow to be irrotational. The fluid particle velocities $\boldsymbol{u}'$ and the pressure in the fluid P' are defined by

$$\boldsymbol{u}' = -\overline{\nabla}'\phi', \qquad \frac{P'}{\rho'} = -g'z' + \dot{\phi}' - \tfrac{1}{2}\left|\overline{\nabla}'\phi'\right|^2, \tag{2.1a,b}$$

where ϕ' is the dimensional velocity potential, $\overline{\nabla}'$ is the three-dimensional gradient operator, and the over-dot indicates the partial derivative with respect to time, $\partial/\partial t'$. The Bernoulli function is assumed to be incorporated into the velocity potential. The fluid domain shown in Figure 1 is a rectangular channel with $x' = 0$ the equilibrium vertical position of the wavemaker, $y' = 0$ the centerline of the channel, and $z' = 0$ the still water level. The channel is semi-infinite (although Figure 1 shows the channel to be of finite length) so the length extends to $x' \to \infty$, the side walls are vertical at $y' = \pm b'$, and the horizontal bottom is $z' = -h'$. The free surface position of the water is defined as $z' = \eta'(x', y', t')$ and the wavemaker displacement from equilibrium is defined as $x' = \chi'(z', t')$, which does not allow for any variation in wavemaker amplitude across the channel.

The dimensional boundary value problem for ϕ', where subscripts denote partial differentiation, is described by the following:

$$\nabla'^2\phi' = 0 \qquad (\chi' < x' < \infty, -b' < y' < b', -h' < z' < \eta'), \tag{2.2a}$$

$$g'\eta' - \dot{\phi}' + \tfrac{1}{2}\left|\overline{\nabla}'\phi'\right|^2 = 0 \qquad (z' = \eta'), \tag{2.2b}$$

$$\dot{\eta}' = \eta'_{x'}\phi'_{x'} + \eta'_{y'}\phi'_{y'} - \phi'_{z'} \qquad (z' = \eta'), \tag{2.2c}$$

$$\phi'_{z'} = 0 \qquad (z' = -h'), \tag{2.2d}$$

$$\dot{\chi}' = -\phi'_{x'} + \chi'_{z'}\phi'_{z'} \qquad (x' = \chi'), \tag{2.2e}$$

$$a'\phi'_{x'} + c'\phi' = 0 \qquad (x' \to \infty), \tag{2.2f}$$

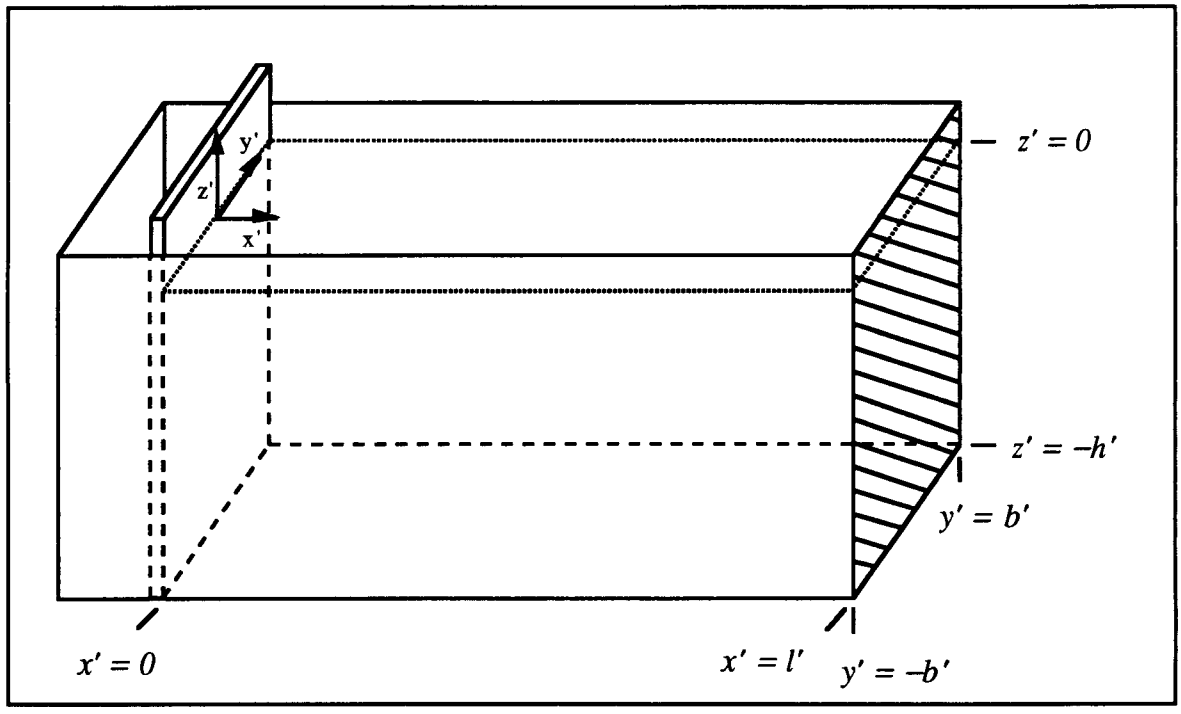

Figure 1. Definition sketch of the rectangular wave channel.

$$\phi'_{y'} = 0 \qquad (y' = \pm b'), \tag{2.2g}$$

where the boundary condition (2.2f) is a generic linear radiation condition. For outgoing waves at infinity, condition (2.2f) has $a' = 1$ and $c' = \mp ik'$, k' the wavenumber, for a time dependence of $e^{\pm i\omega t'}$ [Mei, 1989]. Equation (2.2f) may also be used for the null condition (no motion), $a' = 1$ and $c' = 0$, which was used by Miles and Becker [1988]. Mahony [1972], Jones [1984], and Lichter and Chen [1987] do not explicity state the radiation condition used.

The Hamiltonian is found from the Lagrangian. Luke [1967] determined that the Lagrangian $\overline{L'}$ for a free surface wave is given by

$$\overline{L'} = \iiint_{V'} \left[\tfrac{1}{2} \left| \overline{\nabla' \phi'} \right|^2 - \dot{\phi}' + g' z' \right] dV', \tag{2.3}$$

where the volume V' is the fluid domain and the integrand is the Lagrangian density $\overline{L'_V}$. Luke proved that this Lagrangian is correct for an unbounded fluid by applying Hamilton's principle (the first variation of the time-integrated Lagrangian is zero) and obtained the boundary value problem (2.2a-d) for deep water waves. Luke also pointed out that this Lagrangian is not the classical kinetic minus potential energies. A classical mechanics approach would normally follow by calculating the conjugate momentum density from $p' = \partial \overline{L'_V}/\partial \dot{\phi}'$, with the Hamiltonian density determined from a Legendre transformation. However, this result does not yield a set of evolution equations for the canonical variables because the momentum density p' is constant. This problem is avoided by following Miles [1988] and writing $\overline{L'}$ in terms of surface integrals. Using Green's First Identity

$$\iiint_{V'} \left[\phi' \nabla'^2 \phi' + \overline{\nabla'} \phi' \cdot \overline{\nabla'} \phi'\right] dV' = \iint_{S'} \phi' \frac{\partial \phi'}{\partial n} dS', \tag{2.4}$$

the transport theorem

$$\frac{\partial}{\partial t'} \iiint_{V'} \phi' \, dV' = \iiint_{V'} \dot{\phi}' \, dV' + \iint_{S'} \phi' (\boldsymbol{u}' \cdot \hat{\mathbf{n}}) \, dS', \tag{2.5}$$

and the divergence theorem

$$\iiint_{V'} [g' z'] \, dV' = \iiint_{V'} \left[\overline{\nabla'} \cdot \tfrac{1}{2} g' z'^2 \hat{\mathbf{k}}\right] dV' = \iint_{S'} \left[\tfrac{1}{2} g' z'^2 \hat{\mathbf{k}} \cdot \hat{\mathbf{n}}\right] dS', \tag{2.6}$$

where $\hat{\mathbf{k}}$ is the unit normal in the z' direction and all unit normals point out of the fluid domain, the Lagrangian (2.3) can also be written as

$$\begin{aligned} \overline{L'} = &- \iiint_{V'} \tfrac{1}{2} \phi' \nabla'^2 \phi' \, dV' + \tfrac{1}{2} \iint_{S'_{\eta'}} \left[\phi' \dot{\eta}' + g' \eta'^2\right]_{z'=\eta'} dS'_{\eta'} - \tfrac{1}{2} \iint_{S'_{l'}} \left[\phi' \phi'_{x'}\right]_{x'=l'} dS'_{l'} \\ &+ \tfrac{1}{2} \iint_{S'_{\chi'}} \left[g' z'^2 \chi'_{z'} - \phi' \dot{\chi}'\right]_{x'=\chi'} dS'_{\chi'} - \tfrac{1}{2} \iint_{S'_{h'}} g' h' \, dS'_{h'} - \frac{\partial}{\partial t'} \iiint_{V'} \phi' \, dV', \end{aligned} \tag{2.7}$$

where $x' = l' > 3h'$ is a distance down the channel which is assumed to be large but not infinite and is at least three water depths away from the wavemaker to avoid contaminating the radiation condition with the evanescent eigenmodes. Note that the integral of the fluid domain is to $x' = l'$ and not to $x' = +\infty$; the integrand $\left[\phi' \phi'_{x'}\right]_{x'=l'}$ cannot be replaced by any

form of the radiation condition (2.2f). Also note that since deep water is assumed, $k'h' > \pi$, so that $l' > 3h' > 3\pi/k'$.

Again following Miles [1988], the terms with zero variation are identified as

$$\overline{L}^o = \tfrac{1}{2}\iint_{S'_{\chi'}} \left[g' z'^2 \chi'_{z'}\right]_{x'=\chi'} dS'_{\chi'} - \tfrac{1}{2}\iint_{S'_{h'}} g'h'\, dS'_{h'} - \frac{\partial}{\partial t'}\iiint_{V'} \phi'\, dV', \tag{2.8}$$

and a new Lagrangian, $L' = \overline{L}' - \overline{L}^o$, which has the zero variation terms subtracted out, is given by

$$\begin{aligned} L' = &-\iiint_{V'} \tfrac{1}{2}\phi' \nabla'^2 \phi'\, dV' + \tfrac{1}{2}\iint_{S'_{\eta'}} \left[\phi'\dot{\eta}' + g'\eta'^2\right]_{z'=\eta'} dS'_{\eta'} \\ &-\tfrac{1}{2}\iint_{S'_{l'}} \left[\phi'\phi'_{x'}\right]_{x'=l'} dS'_{l'} - \tfrac{1}{2}\iint_{S'_{\chi'}} \left[\phi'\dot{\chi}'\right]_{x'=\chi'} dS'_{\chi'}, \end{aligned} \tag{2.9}$$

which still yields the boundary value problem (2.2) when Hamilton's principle is applied. From here the formulation departs from Miles.

In order to proceed further with the classical mechanics approach, the Lagrangian must be expressed in terms of a generalized coordinate or field variable, which may be either ϕ' or η'. Miles [1977] and Milder [1977] suggest the use of η' as the field variable because it is analogous to using the particle displacement as the coordinate in classical mechanics problems. They further define ϕ' on the surface as the conjugate momentum. However, Miles and Milder were using only integrals over the free surface; the surface integrals over the wavemaker and the far x' position (and the volume integral) in (2.9) further complicates the problem. The velocity potential ϕ' is chosen as the field variable, and η' and $\dot{\eta}'$ are written in terms of ϕ' by using both free surface boundary conditions (2.2b,c). The Lagrangian (2.9) is decomposed into the following integral terms:

$$L' = L'_{V'} + L'_{\chi'} + L'_{\xi'} + L'_{\eta'_1} + L'_{\eta'_2}, \tag{2.10}$$

$$L'_{V'} = -\iiint_{V'} \tfrac{1}{2}\phi' \nabla'^2 \phi'\, dV', \tag{2.11a}$$

$$L'_{\chi'} = -\tfrac{1}{2}\int_{-b'}^{b'}\int_{-h'}^{z'_o} \left[\phi'\dot{\chi}'\right]_{x'=\chi'} dz'\, dy', \tag{2.11b}$$

$$L'_{\xi'} = -\tfrac{1}{2}\int_{-b'}^{b'}\int_{-h'}^{z'_l}\left[\phi'\phi'_{x'}\right]_{x'=l'}dz'\,dy', \tag{2.11c}$$

$$L'_{\eta'_1} = \tfrac{1}{2}\int_{-b'}^{b'}\int_{x'_o}^{l'}\phi'\left[-\phi'_{z'} + \tfrac{1}{g'}\overline{\nabla}'_2\phi'\cdot\overline{\nabla}'_2\left(\dot{\phi}' - \tfrac{1}{2}\left|\overline{\nabla}'\phi'\right|^2\right)\right]_{z'=\eta'}dx'\,dy', \tag{2.11d}$$

$$L'_{\eta'_2} = \tfrac{1}{2}\int_{-b'}^{b'}\int_{x'_o}^{l'}\tfrac{1}{g'}\left[\dot{\phi}'^2 - \dot{\phi}'\left|\overline{\nabla}'\phi'\right|^2 + \tfrac{1}{4}\left|\overline{\nabla}'\phi'\right|^4\right]_{z'=\eta'}dx'\,dy'. \tag{2.11e}$$

The term z'_o is the free surface position at the wavemaker, $\eta'(x'=\chi',y',t')$, x'_o is the wavemaker displacement at the instantaneous free surface, $\chi'(z'=\eta',t')$, and z'_l is the free surface position at the far field x' location, $\eta' = (x'=l',y',t')$.

The velocity potential is assumed to be a linear sum of a progressive wave potential and a cross-wave potential, $\phi' = \phi'_p + \phi'_c$. The progressive wave potential ϕ'_p will not have any y' dependence, and the cross-wave potential ϕ'_c will not have any x' dependence. The dimensional (primed) variables are related to the nondimensional (unprimed) variables by the following scales:

$$x' = \frac{x}{k'},\quad y' = \frac{y}{\kappa'},\quad z' = \frac{z}{\kappa'},\quad t' = \frac{t}{\sqrt{g'\kappa'}}, \tag{2.12a-d}$$

$$\phi'_p = \phi_p a'_p\sqrt{\frac{g'}{k'}},\quad \phi'_c = \phi_c a'_c\sqrt{\frac{g'}{\kappa'}}, \tag{2.13a,b}$$

$$\eta' = a'_c\eta,\quad \chi' = a'_w\chi,\quad L' = \frac{La'^2_c g'}{k'\kappa'}, \tag{2.14a-c}$$

where k' and a'_p are the respective wavenumber and amplitude of the progressive wave, κ' and a'_c are the respective wavenumber and amplitude of the cross-wave, and a'_w is the amplitude of the wavemaker motion. The time scale used in (2.12d) is the cross-wave frequency for linear waves in deep water. The following dimensionless parameters are defined:

$$\varepsilon = \kappa' a'_c,\ \beta = \sqrt{\kappa'/k'} = \omega_c/\omega_p,\ \gamma = k'a'_w,\ \Gamma = a'_p/a'_c, \tag{2.15a-d}$$

$$\alpha = \kappa' h',\ \xi = k'l',\ b = \kappa' b', \tag{2.15e-h}$$

where ε is an the ordering parameter, β is a frequency ratio, γ is a perturbation (forcing) parameter, and α and ξ are large but not infinite. The parameter $\gamma < \varepsilon$ because

experiments show the cross-wave amplitude is larger than the forcing amplitude. The parameter order is then

$$0<\gamma^2<\varepsilon\gamma<\varepsilon^2<\gamma<\varepsilon<1, \quad \text{or} \quad 0<\frac{\gamma^2}{\varepsilon}<\gamma<\frac{\gamma}{\varepsilon}<1. \tag{2.16a,b}$$

The higher order terms to be neglected are $O(\varepsilon^2)$, $O(\varepsilon\gamma)$, and $O(\gamma^2)$.

Ignoring these higher order terms, the nondimensional Lagrangian is then given by the following components:

$$L = L_v + L_\chi + L_\xi + L_{\eta_1} + L_{\eta_2}, \tag{2.17}$$

$$L_v = -\tfrac{1}{2}\iiint_V \left(\Gamma\beta\phi_p + \phi_c\right)\left(\frac{\Gamma}{\beta^3}\phi_{p_{xx}} + \phi_{c_{yy}} + \Gamma\beta\phi_{p_{zz}} + \phi_{c_{zz}}\right) dx\,dy\,dz, \tag{2.18a}$$

$$L_\chi = -\tfrac{1}{2}\int_{-b}^{b}\int_{-\alpha}^{\varepsilon z_o}\left[\frac{\gamma}{\varepsilon}\left(\Gamma\beta\phi_p + \phi_c\right)\right]_{x=\gamma\chi} dz\,dy, \tag{2.18b}$$

$$L_\xi = -\tfrac{1}{2}\int_{-b}^{b}\int_{-\alpha}^{\varepsilon z_\xi}\left[\frac{\Gamma}{\beta^3}\left(\Gamma\beta\phi_p + \phi_c\right)\phi_{p_x}\right]_{x=\xi} dz\,dy, \tag{2.18c}$$

$$\begin{aligned} L_{\eta_1} = \tfrac{1}{2}\int_{-b}^{b}\int_{\gamma\chi_o}^{\xi}\Big[&-\left(\Gamma\beta\phi_p + \phi_c\right)\left(\Gamma\beta\phi_{p_z} + \phi_{c_z}\right) \\ &+\varepsilon\beta\left(\Gamma\beta\phi_p + \phi_c\right)\left(\frac{\Gamma^2}{\beta^2}\phi_{p_x}\dot{\phi}_{p_x} + \phi_{c_y}\dot{\phi}_{c_y}\right)\Big]_{z=\varepsilon\eta} dx\,dy, \end{aligned} \tag{2.18d}$$

$$\begin{aligned} L_{\eta_2} = \tfrac{1}{2}\int_{-b}^{b}\int_{\gamma\chi_o}^{\xi}\Big[&\left(\Gamma^2\beta^2\dot{\phi}_p^2 + \dot{\phi}_c^2 + 2\Gamma\beta\dot{\phi}_p\dot{\phi}_c\right) \\ &-\varepsilon\left(\Gamma\beta\dot{\phi}_p + \dot{\phi}_c\right)\left|\frac{\Gamma}{\beta}\phi_{p_x}\hat{\mathbf{i}} + \phi_{c_y}\hat{\mathbf{j}} + \Gamma\beta\phi_{p_z}\hat{\mathbf{k}} + \phi_{c_z}\hat{\mathbf{k}}\right|^2\Big]_{z=\varepsilon\eta} dx\,dy. \end{aligned} \tag{2.18e}$$

where $z_o = \eta(x=\chi, y, z, t)$, $z_\xi = \eta(x=\xi, y, t)$, and $x_o = \chi(z=0, t)$.

The integrands of L_{η_1} and L_{η_2} are to be evaluated on the unknown surface $z = \varepsilon\eta$, so a Taylor series approximation will be used,

$$f(z=\varepsilon\eta) \approx f(z=0) + \varepsilon\eta\frac{\partial f}{\partial z}(z=0) + O(\varepsilon^2), \tag{2.19}$$

where η is found from the nondimensionalized, linearized boundary condition (2.2b) by

$$\eta = \left(\Gamma\beta\dot{\phi}_p + \dot{\phi}_c\right)\Big|_{z=0}. \tag{2.20}$$

The integrand of L_χ is evaluated on the surface $x = \gamma\chi$ and is also expanded so that separation of variables and eigenfunction expansions can be used later,

$$f(x=\gamma\chi) \approx f(x=0) + \gamma\chi \frac{\partial f}{\partial x}(x=0) + O(\gamma^2). \tag{2.21}$$

After these approximations, (2.18b,d,e) become

$$L_\chi = -\tfrac{1}{2}\int_{-b}^{b}\int_{-\alpha}^{\varepsilon z_o}\left[\frac{\gamma}{\varepsilon}\left(\Gamma\beta\phi_p + \phi_c\right)\right]_{x=0} dz\, dy, \tag{2.22a}$$

$$\begin{aligned} L_{\eta_1} = \tfrac{1}{2}\int_{-b}^{b}\int_{\gamma\chi_o}^{\xi}\Big[& -\left(\Gamma\beta\phi_p + \phi_c\right)\left(\Gamma\beta\phi_{p_z} + \phi_{c_z}\right) \\ & +\varepsilon\beta\left(\Gamma\beta\phi_p + \phi_c\right)\left(\frac{\Gamma^2}{\beta^2}\phi_{p_x}\dot{\phi}_{p_x} + \phi_{c_y}\dot{\phi}_{c_y}\right) \\ & -\varepsilon\Gamma\beta\left(\dot{\phi}_c\phi_p\phi_{c_{zz}} + 2\dot{\phi}_c\phi_{p_z}\phi_{c_z} + \dot{\phi}_c\phi_c\phi_{p_{zz}} + \dot{\phi}_p\phi_c\phi_{c_{zz}} + \dot{\phi}_p\phi_{c_z}^2\right) \\ & -\varepsilon\Gamma^2\beta^2\left(\dot{\phi}_c\phi_p\phi_{p_{zz}} + \dot{\phi}_c\phi_{p_z}^2 + \dot{\phi}_p\phi_p\phi_{c_{zz}} + 2\dot{\phi}_p\phi_{p_z}\phi_{c_z} + \dot{\phi}_p\phi_c\phi_{p_{zz}}\right) \\ & -\varepsilon\left(\dot{\phi}_c\phi_c\phi_{c_z} + \dot{\phi}_c\phi_{c_z}^2 + \Gamma^3\beta^3\dot{\phi}_p\phi_p\phi_{p_{zz}} + \Gamma^3\beta^3\dot{\phi}_p\phi_{p_z}^2\right)\Big]_{z=0} dx\, dy, \end{aligned} \tag{2.22b}$$

$$\begin{aligned} L_{\eta_2} = \tfrac{1}{2}\int_{-b}^{b}\int_{\gamma\chi_o}^{\xi}\Big[& \left(\Gamma^2\beta^2\dot{\phi}_p^2 + \dot{\phi}_c^2 + 2\Gamma\beta\dot{\phi}_p\dot{\phi}_c\right) \\ & -\varepsilon\left(\Gamma\beta\dot{\phi}_p + \dot{\phi}_c\right)\left|\frac{\Gamma}{\beta}\phi_{p_x}\hat{\mathbf{i}} + \phi_{c_y}\hat{\mathbf{j}} + \Gamma\beta\phi_{p_z}\hat{\mathbf{k}} + \phi_{c_z}\hat{\mathbf{k}}\right|^2 \\ & +2\varepsilon\left(\dot{\phi}_c^2\dot{\phi}_{c_z} + \Gamma\beta\left(\dot{\phi}_c^2\dot{\phi}_{p_z} + 2\dot{\phi}_p\dot{\phi}_c\dot{\phi}_{c_z}\right)\right) \\ & +2\varepsilon\left(\Gamma^2\beta^2\left(\dot{\phi}_p^2\dot{\phi}_{c_z} + 2\dot{\phi}_p\dot{\phi}_c\dot{\phi}_{p_z}\right) + \Gamma^3\beta^3\dot{\phi}_p^2\right)\Big]_{z=0} dx\, dy. \end{aligned} \tag{2.22c}$$

The surface integral limits are also approximated by

$$\int_{-\alpha}^{\varepsilon z_o}[\ ]\,dz \approx \int_{-\alpha}^{0}[\ ]\,dz + \varepsilon z_o[\ ]_{z=0} + O(\varepsilon^2), \tag{2.23a}$$

$$\int_{-\alpha}^{\varepsilon z_\xi}[\ ]\,dz \approx \int_{-\alpha}^{0}[\ ]\,dz + \varepsilon z_\xi[\ ]_{z=0} + O(\varepsilon^2), \tag{2.23b}$$

$$\int_{\gamma\chi_o}^{\xi}[\ ]\,dx \approx \int_{0}^{\xi}[\ ]\,dx - \gamma\chi_o[\ ]_{x=0} + O(\gamma^2), \tag{2.23c}$$

where $z_o = \left(\Gamma\beta\dot{\phi}_p + \dot{\phi}_c\right)\Big|_{x=0}$, $z_\xi = \left(\Gamma\beta\dot{\phi}_p + \dot{\phi}_c\right)\Big|_{x=\xi}$, and $x_o = \chi(z=0,t)$.

The Lagrangian (2.17) now has terms approximated by:

$$L_\chi = -\tfrac{1}{2}\int_{-b}^{b}\int_{-a}^{0}\left[\frac{\gamma}{\varepsilon}\left(\Gamma\beta\phi_p + \phi_c\right)\dot{\chi}\right]_{x=0} dz\, dy$$
$$-\tfrac{1}{2}\int_{-b}^{b}\left[\gamma z_o\left(\Gamma\beta\phi_p + \phi_c\right)\dot{\chi}\right]_{x,z=0} dy, \tag{2.24a}$$

$$L_{\eta_1} = \tfrac{1}{2}\int_{-b}^{b}\int_{0}^{\xi}\left[\text{integrand of (2.35)}\right]_{z=0} dx\, dy$$
$$+\tfrac{1}{2}\int_{-b}^{b}\left[\gamma x_o\left(\Gamma\beta\phi_p + \phi_c\right)\left(\Gamma\beta\phi_{p_z} + \phi_{c_z}\right)\right]_{x,z=0} dy, \tag{2.24b}$$

$$L_{\eta_2} = \tfrac{1}{2}\int_{-b}^{b}\int_{0}^{\xi}\left[\text{integrand of (2.36)}\right]_{z=0} dx\, dy$$
$$-\tfrac{1}{2}\int_{-b}^{b}\left[\gamma x_o\left(\Gamma^2\beta^2\dot{\phi}_p^2 + \dot{\phi}_c^2 + 2\Gamma\beta\dot{\phi}_p\dot{\phi}_c\right)\right]_{x,z=0} dy, \tag{2.24c}$$

$$L_\xi = -\tfrac{1}{2}\int_{-b}^{b}\int_{-a}^{0}\left[\frac{\Gamma}{\beta^3}\left(\Gamma\beta\phi_p + \phi_c\right)\phi_{p_x}\right]_{x=\xi} dz\, dy$$
$$-\tfrac{1}{2}\int_{-b}^{b}\left[\varepsilon z_\xi \frac{\Gamma}{\beta^3}\left(\Gamma\beta\phi_p + \phi_c\right)\phi_{p_x}\right]_{x=\xi,z=0} dy. \tag{2.24d}$$

The forms of the velocity potentials are now to be specified. The cross-wave potential ϕ_c will be described by a deep water standing wave in the basin width, and the progressive wave potential ϕ_p will be described by a deep water traveling wave. As the chaos is assumed to be temporal, rather than spatial, the time dependencies of the potentials will remain unspecified variables. The deep water velocity potentials are

$$\phi_c = q(t)\cos(y-b)e^z, \qquad \phi_p = \left[Q_1(t)\cos x + Q_2(t)\sin x\right]e^{z/\beta^2}, \tag{2.25a,b}$$

where the variables q, Q_1, and Q_2 are the generalized coordinates.

A note on the progressive wave potential is in order here. A wave traveling in the positive x direction would normally be described by

$$\cos(x-t) \text{ or } (\cos x\cos t + \sin x\sin t). \tag{2.26}$$

However, this form of a traveling wave does not allow for any slow modulation of the traveling wave. Both Jones [1984] and Miles and Becker [1988] allow for a slow temporal modulation. By replacing the functions $\cos t$ and $\sin t$ with the generalized coordinates

$Q_1(t)$ and $Q_2(t)$, the system is expressed in a more general form and the progressive wave is allowed to vary according to the evolution equations obtained from the Hamiltonian. The system described in this way will contain the full richness of dynamics possible. This is also analogous to the whirling pendulum example in Wiggins [1988, p.440], where specifying a rotation rate is just a limiting case of allowing the rotation rate to be described by the equation governing the angular momentum. Furthermore, any assumed relationship between Q_1 and Q_2, such as

$$Q_1 = Q, Q_2 = -\dot{Q}, \quad \text{or} \quad Q_1 = Q, Q_2 = P, \tag{2.27a,b}$$

where P would be the conjugate momentum of Q, would also further diminish the full dynamical system. Except for the most simple dynamical systems, an assumed form for the conjugate momentum would probably be wrong.

Before substituting the forms of the potentials into the Lagrangian, (2.18a) and (2.24) are simplified considerably by making both an assumption and an observation. The assumption follows from Jones [1984], where the cross-wave resonance effect was found to be independent of $O(\varepsilon)$ interactions of the progressive wave with itself. Accordingly, all $O(\varepsilon)$ interactions containing only progressive wave potential terms will be ignored. (If this assumption were not made, the Lagrangian would contain cubic $\dot{\phi}_p$ terms that would contribute to the calculation of conjugate momenta, and greatly complicate the expression for the Hamiltonian expressed in terms of the canonical variables.) The observation that simplifies the Lagrangian components (2.24) follows from the form of the cross-wave potential specified in (2.25a). The cross-wave potential is a standing wave, with y-dependence given by $\cos(y-b)$, which means that any term containing an odd-power of ϕ_c and time or spatial derivatives of ϕ_c will be zero when integrated over the width of the basin. Furthermore, the potentials (2.25) satisfy Laplace's equation, so (2.18a) is zero. The surface integrals in the Lagrangian (2.17) may now be simplified to

$$L_\chi = -\tfrac{1}{2}\int_{-b}^{b}\int_{-\alpha}^{0}\left[\frac{\gamma}{\varepsilon}\left(\Gamma\beta\phi_p\right)\dot{\chi}\right]_{x=0} dz\, dy - \tfrac{1}{2}\int_{-b}^{b}\left[\gamma\left(\Gamma^2\beta^2\dot{\phi}_p\phi_p + \dot{\phi}_c\phi_c\right)\dot{\chi}\right]_{x,z=0} dy, \tag{2.28a}$$

$$L_\xi = -\tfrac{1}{2}\int_{-b}^{b}\int_{-\alpha}^{0}\left[\frac{\Gamma^2}{\beta^2}\left(\phi_p\phi_{p_x}\right)\right]_{x=\xi} dz\,dy - \tfrac{1}{2}\int_{-b}^{b}\left[\frac{\varepsilon\Gamma}{\beta^3}\left(\dot\phi_c\phi_c\phi_{p_x}\right)\right]_{x=\xi,z=0} dy, \tag{2.28b}$$

$$\begin{aligned} L_{\eta_1} = \tfrac{1}{2}\int_{-b}^{b}\int_{0}^{\xi}\Big[&\left(-\Gamma^2\beta^2\phi_p\phi_{p_z} - \phi_c\phi_{c_z}\right) + \varepsilon\Gamma\beta^2\left(\phi_{c_y}\dot\phi_{c_y}\right) \\ &-\varepsilon\Gamma\beta\left(\dot\phi_c\phi_p\phi_{c_{zz}} + \dot\phi_c\phi_c\phi_{p_{zz}} + 2\dot\phi_c\phi_{c_z}\phi_{p_z} + \dot\phi_p\phi_c\phi_{c_{zz}} + \dot\phi_p\phi_{c_z}^2\right)\Big]_{z=0} dx\,dy \\ &+\tfrac{1}{2}\int_{-b}^{b}\left[\gamma\chi_o\left(\Gamma^2\beta^2\phi_p\phi_{p_z} + \phi_c\phi_{c_z}\right)\right]_{x,z=0} dy, \end{aligned} \tag{2.28c}$$

$$\begin{aligned} L_{\eta_2} = \tfrac{1}{2}\int_{-b}^{b}\int_{0}^{\xi}\Big[&\left(\Gamma^2\beta^2\dot\phi_p^2 + \dot\phi_c^2\right) - \varepsilon\Gamma\beta\left(\phi_p\phi_{c_y}^2 + \phi_p\phi_{c_z}^2 + 2\dot\phi_c\phi_{p_z}\phi_{c_z}\right) \\ &+2\varepsilon\left(\Gamma\beta\dot\phi_c\dot\phi_p\dot\phi_{c_z} + \Gamma\beta\dot\phi_c^2\dot\phi_{p_z} + \dot\phi_c^2\dot\phi_{c_z}\right)\Big]_{z=0} dx\,dy \\ &-\tfrac{1}{2}\int_{-b}^{b}\left[\gamma\chi_o\left(\Gamma^2\beta^2\dot\phi_p^2 + \dot\phi_c^2\right)\right]_{x,z=0} dy. \end{aligned} \tag{2.28d}$$

It is convenient to rewrite the Lagrangian (2.17) by grouping terms according to their order rather than the surface over which each term is integrated. The ordering terms will be: L_o which are all $O(1)$ terms in (2.28); L_ε which are all $O(\varepsilon)$ terms in (2.28); and L_γ which contains all terms in (2.28) with the perturbation parameter γ. The Lagrangian (2.17) is given by the following components:

$$L = L_o + L_\varepsilon + L_\gamma, \tag{2.29}$$

$$\begin{aligned} L_o = \tfrac{1}{2}\int_{-b}^{b}\int_{0}^{\xi}\Big[&\left(-\Gamma^2\beta^2\phi_p\phi_{p_z} - \phi_c\phi_{c_z}\right) + \left(\Gamma^2\beta^2\dot\phi_p^2 + \dot\phi_c^2\right)\Big]_{z=0} dx\,dy \\ &-\tfrac{1}{2}\int_{-b}^{b}\int_{-\alpha}^{0}\left[\frac{\Gamma^2}{\beta^2}\left(\phi_p\phi_{p_x}\right)\right]_{x=\xi} dz\,dy, \end{aligned} \tag{2.30a}$$

$$\begin{aligned} L_\varepsilon = &-\frac{\varepsilon}{2}\int_{-b}^{b}\left[\frac{\Gamma}{\beta^3}\left(\dot\phi_c\phi_c\phi_{p_x}\right)\right]_{x=\xi,z=0} dy \\ &+\frac{\varepsilon}{2}\int_{-b}^{b}\int_{0}^{\xi}\Big[-\Gamma\beta\left(\dot\phi_c\phi_p\phi_{c_{zz}} + \dot\phi_c\phi_c\phi_{p_{zz}} + 2\dot\phi_c\phi_{c_z}\phi_{p_z} + \dot\phi_p\phi_c\phi_{c_{zz}} + \dot\phi_p\phi_{c_z}^2\right) \\ &+\Gamma\beta^2\left(\phi_{c_y}\dot\phi_{c_y}\right) - \Gamma\beta\left(\phi_p\phi_{c_y}^2 + \phi_p\phi_{c_z}^2 + 2\dot\phi_c\phi_{p_z}\phi_{c_z}\right) \\ &+2\left(\Gamma\beta\dot\phi_c\dot\phi_p\dot\phi_{c_z} + \Gamma\beta\dot\phi_c^2\dot\phi_{p_z} + \dot\phi_c^2\dot\phi_{c_z}\right)\Big]_{z=0} dx\,dy, \end{aligned} \tag{2.30b}$$

$$L_\gamma = -\frac{\gamma}{2\varepsilon}\int_{-b-a}^{b}\int^{0}\left[\left(\Gamma\beta\phi_p\right)\dot{\chi}\right]_{x=0} dz\,dy - \frac{\gamma}{\varepsilon}\int_{-b}^{b}\left[\left(\Gamma^2\beta^2\dot{\phi}_p\phi_p + \dot{\phi}_c\phi_c\right)\dot{\chi}\right]_{x,z=0} dy$$
$$+\frac{\gamma}{2}\int_{-b}^{b}\left[x_o\left(\Gamma^2\beta^2\phi_p\phi_{p_z} + \phi_c\phi_{c_z} - \Gamma^2\beta^2\dot{\phi}_p^2 - \dot{\phi}_c^2\right)\right]_{x,z=0} dy. \tag{2.30c}$$

The potentials (2.25) are now substituted into the Lagrangian (2.29). The wavemaker forcing is specified as

$$\chi = f(z)\sin\frac{t}{\beta} \quad \begin{cases} f(z) = 1 - \dfrac{z}{\alpha} & \text{for a full draft hinge,} \\ f(z) = 1 & \text{for a full draft piston.} \end{cases}$$

A more generic planar wavemaker function is given by Hudspeth and Sulisz [1992]. Note that $f(z=0)=1$, since the wavemaker displacement was nondimensionalized by the displacement at the still water level. All integrals may now be evaluated since the spatial dependencies are known. Equations (2.31) below show the integrated forms of the Lagrangian components. All subscripted coefficients *a*, *b*, and *c* indicate integrals over *x*, subscripted coefficients *A*, *B*, and *d* indicate functions of *x* evaluated at $x = \xi$, and the coefficient f_1 indicates the integral over *z* of the wavemaker depth function *f(z)* times the *z*-dependence of ϕ_p. The subscripted coefficients μ are all functions of the frequency ratio parameter β. All coefficients are defined in Table 1 in the Appendix. The Lagrangian components of (2.29), assuming $O\left(e^{-\alpha}\right) << 1$ because of deep water, are now:

$$L_o = -\Gamma^2 b\left(a_2 - \tfrac{1}{2}d_{11}\right)Q_1^2 - \Gamma^2 b\left(b_2 + \tfrac{1}{2}d_{11}\right)Q_2^2 - \Gamma^2 b\left(2c_{11} + \tfrac{1}{2}d_2\right)Q_1Q_2$$
$$+\left(\Gamma^2\beta^2 ba_2\right)\dot{Q}_1^2 + \left(\Gamma^2\beta^2 bb_2\right)\dot{Q}_2^2 + \left(2\Gamma^2\beta^2 bc_{11}\right)\dot{Q}_1\dot{Q}_2 \tag{2.31a}$$
$$-\left(\frac{b\xi}{2}\right)q^2 + \left(\frac{b\xi}{2}\right)\dot{q}^2,$$

$$L_\varepsilon = -\varepsilon\left(2\Gamma\beta ba_1\right)q^2\dot{Q}_1 - \varepsilon\left(2\Gamma\beta bb_1\right)q^2\dot{Q}_2 + \varepsilon\left(\Gamma ba_1\mu_1\right)\dot{q}^2\dot{Q}_1 + \varepsilon\left(\Gamma bb_1\mu_1\right)\dot{q}^2\dot{Q}_2$$
$$-\varepsilon\Gamma b\left(a_1\mu_2 - \frac{B_1}{2\beta^3}\right)q\dot{q}Q_1 - \varepsilon\Gamma b\left(b_1\mu_2 + \frac{A_1}{2\beta^3}\right)q\dot{q}Q_2, \tag{2.31b}$$

$$L_\gamma = -\frac{\gamma}{\varepsilon}\left(\Gamma b f_1 \cos\frac{t}{\beta}\right)Q_1 - \gamma\left(\Gamma^2\beta b\cos\frac{t}{\beta}\right)\dot{Q}_1 Q_1 + \gamma\left(\Gamma^2 b\sin\frac{t}{\beta}\right)Q_1^2$$
$$-\gamma\left(\Gamma^2\beta^2 b\sin\frac{t}{\beta}\right)\dot{Q}_1^2 - \gamma\left(\frac{b}{2\beta}\cos\frac{t}{\beta}\right)q\dot{q} - \gamma\left(\frac{b}{2}\sin\frac{t}{\beta}\right)\dot{q}^2 \qquad (2.31c)$$
$$+\gamma\left(\frac{b}{2}\sin\frac{t}{\beta}\right)q^2.$$

The Lagrangian components $L_o + L_\varepsilon$ represent the free oscillations of the system. The perturbed component L_γ is the forcing. Each generalized coordinate has an associated conjugate momentum determined from the free oscillation components of L by a Legendre transformation [Goldstein, 1980]. These conjugate momenta are:

$$p = \frac{\partial(L_o + L_\varepsilon)}{\partial\dot{q}} = (b\xi)\dot{q} + \varepsilon(2\Gamma b a_1\mu_1)\dot{q}\dot{Q}_1 + \varepsilon(2\Gamma b b_1\mu_1)\dot{q}\dot{Q}_2$$
$$-\varepsilon\Gamma b\left(a_1\mu_2 - \frac{B_1}{2\beta^3}\right)qQ_1 - \varepsilon\Gamma b\left(b_1\mu_2 + \frac{A_1}{2\beta^3}\right)qQ_2 \qquad (2.32a)$$

$$P_1 = \frac{\partial(L_o + L_\varepsilon)}{\partial\dot{Q}_1} = (2\Gamma^2\beta^2 b a_2)\dot{Q}_1 + (2\Gamma^2\beta^2 b c_{11})\dot{Q}_2 - \varepsilon(2\Gamma\beta b a_1)q^2$$
$$+\varepsilon(\Gamma b a_1\mu_1)\dot{q}^2 \qquad (2.32b)$$

$$P_2 = \frac{\partial(L_o + L_\varepsilon)}{\partial\dot{Q}_2} = (2\Gamma^2\beta^2 b b_2)\dot{Q}_2 + (2\Gamma^2\beta^2 b c_{11})\dot{Q}_1 - \varepsilon(2\Gamma\beta b b_1)q^2$$
$$+\varepsilon(\Gamma b b_1\mu_1)\dot{q}^2 \qquad (2.32c)$$

The Hamiltonian must be written in terms of the three pairs of canonical variables, (q,p), (Q_1,P_1), and (Q_2,P_2). This requires that the variables $\dot{q}$, $\dot{Q}_1$, and $\dot{Q}_2$ be expressed only in terms of the six canonical variables. The first step is to invert (2.32) to obtain

$$\dot{q} = \frac{p + \varepsilon\Gamma b\left(a_1\mu_2 - \frac{B_1}{2\beta^3}\right)qQ_1 + \varepsilon\Gamma b\left(b_1\mu_2 + \frac{A_1}{2\beta^3}\right)qQ_2}{b\xi + \varepsilon 2\Gamma b\left(a_1\mu_1\dot{Q}_1 + b_1\mu_1\dot{Q}_2\right)}, \qquad (2.33a)$$

$$\dot{Q}_1 = \frac{P_1}{2\Gamma^2\beta^2 b a_2} - \frac{c_{11}\dot{Q}_2}{a_2} + \varepsilon\left(\frac{a_1 q^2}{\Gamma\beta a_2}\right) - \varepsilon\left(\frac{a_1\mu_1\dot{q}^2}{2\Gamma\beta^2 a_2}\right), \qquad (2.33b)$$

$$\dot{Q}_2 = \frac{P_2}{2\Gamma^2\beta^2 b b_2} - \frac{c_{11}\dot{Q}_1}{b_2} + \varepsilon\left(\frac{b_1 q^2}{\Gamma\beta b_2}\right) - \varepsilon\left(\frac{b_1\mu_1\dot{q}^2}{2\Gamma\beta^2 b_2}\right). \qquad (2.33c)$$

The variable $\dot{q}$ contains an $O(\varepsilon)$ expression in the denominator and will be approximated using the binomial expansion to obtain

$$\begin{aligned}\dot{q} \approx \frac{p}{b\xi} + \varepsilon\frac{\Gamma}{\xi}\left(a_1\mu_2 - \frac{B_1}{2\beta^3}\right)qQ_1 + \varepsilon\frac{\Gamma}{\xi}\left(b_1\mu_2 + \frac{A_1}{2\beta^3}\right)qQ_2 \\ -\varepsilon\frac{2\Gamma}{b\xi^2}\left(a_1\mu_1\dot{Q}_1 + b_1\mu_1\dot{Q}_2\right)p + O\left(\varepsilon^2\right).\end{aligned} \tag{2.34}$$

Equations (2.33b-c) and (2.34) are solved simultaneously to $O\left(\varepsilon^2\right)$ and give

$$\begin{aligned}\dot{q} = \frac{p}{b\xi} + \varepsilon\frac{\Gamma}{\xi}\left(a_1\mu_2 - \frac{B_1}{2\beta^3}\right)qQ_1 + \varepsilon\frac{\Gamma}{\xi}\left(b_1\mu_2 + \frac{A_1}{2\beta^3}\right)qQ_2 \\ -\varepsilon\frac{\mu_1}{\Gamma\beta^2b^2\xi^2}\left(\frac{a_1b_2 - b_1c_{11}}{a_2b_2 - c_{11}^2}\right)pP_1 - \varepsilon\frac{\mu_1}{\Gamma\beta^2b^2\xi^2}\left(\frac{a_2b_1 - c_{11}a_1}{a_2b_2 - c_{11}^2}\right)pP_2,\end{aligned} \tag{2.35a}$$

$$\begin{aligned}\dot{Q}_1 = \frac{P_1}{2\Gamma^2\beta^2b}\left(\frac{b_2}{a_2b_2 - c_{11}^2}\right) - \frac{P_2}{2\Gamma^2\beta^2b}\left(\frac{c_{11}}{a_2b_2 - c_{11}^2}\right) \\ +\varepsilon\frac{q^2}{\Gamma\beta}\left(\frac{a_1b_2 - b_1c_{11}}{a_2b_2 - c_{11}^2}\right) - \varepsilon\frac{\mu_1p^2}{2\Gamma\beta^2b^2\xi^2}\left(\frac{a_1b_2 - b_1c_{11}}{a_2b_2 - c_{11}^2}\right),\end{aligned} \tag{2.35b}$$

$$\begin{aligned}\dot{Q}_2 = -\frac{P_1}{2\Gamma^2\beta^2b}\left(\frac{c_{11}}{a_2b_2 - c_{11}^2}\right) + \frac{P_2}{2\Gamma^2\beta^2b}\left(\frac{a_2}{a_2b_2 - c_{11}^2}\right) \\ +\varepsilon\frac{q^2}{\Gamma\beta}\left(\frac{a_2b_1 - a_1c_{11}}{a_2b_2 - c_{11}^2}\right) - \varepsilon\frac{\mu_1p^2}{2\Gamma\beta^2b^2\xi^2}\left(\frac{a_2b_1 - a_1c_{11}}{a_2b_2 - c_{11}^2}\right).\end{aligned} \tag{2.35c}$$

Each equation (2.35) contains a term in the denominator (see Table 1)

$$\left(a_2b_2 - c_{11}^2\right) = \tfrac{1}{4}\left(\xi^2 - \sin^2\xi\right), \tag{2.36}$$

which is always greater than zero since the parameter ξ is some large $\left(\xi = k'l' >> 1\right)$ but finite distance down the channel.

3. Hamiltonian formulation

The Hamiltonian is determined from the Legendre transformation

$$H = p\dot{q} + P_1\dot{Q}_1 + P_2\dot{Q}_2 - L. \tag{3.1}$$

The Hamiltonian will also be written in component form with H_o the $O(1)$ terms, H_ε the $O(\varepsilon)$ terms, and H_γ the perturbed (forced) terms containing the parameter γ. The Hamiltonian written in component form is:

$$H = H_o + H_\varepsilon + H_\gamma + O(\varepsilon^2, \varepsilon\gamma, \gamma^2), \tag{3.2}$$

$$\begin{aligned} H_o = {} & \Gamma^2 b(a_2 - \tfrac{1}{2}d_{11})Q_1^2 + \Gamma^2 b(b_2 + \tfrac{1}{2}d_{11})Q_2^2 + \Gamma^2 b(2c_{11} + \tfrac{1}{2}d_2)Q_1Q_2 \\ & + \tfrac{1}{2}b\xi q^2 + \frac{p^2}{2b\xi} + \frac{b_2P_1^2 - 2c_{11}P_1P_2 + a_2P_2^2}{4\Gamma^2\beta^2 b(a_2b_2 - c_{11}^2)}, \end{aligned} \tag{3.3a}$$

$$\begin{aligned} H_\varepsilon = {} & \varepsilon\frac{\Gamma}{\xi}\left(a_1\mu_2 - \frac{B_1}{2\beta^3}\right)Q_1qp + \varepsilon\frac{\Gamma}{\xi}\left(b_1\mu_2 + \frac{A_1}{2\beta^3}\right)Q_2qp \\ & + \frac{\varepsilon}{\Gamma\beta}\left(\frac{a_1b_2 - b_1c_{11}}{a_2b_2 - c_{11}^2}\right)q^2P_1 + \frac{\varepsilon}{\Gamma\beta}\left(\frac{a_2b_1 - a_1c_{11}}{a_2b_2 - c_{11}^2}\right)q^2P_2 \\ & - \frac{\varepsilon\mu_1}{2\Gamma\beta^2b^2\xi^2}\left(\frac{a_1b_2 - b_1c_{11}}{a_2b_2 - c_{11}^2}\right)P_1p^2 - \frac{\varepsilon\mu_1}{2\Gamma\beta^2b^2\xi^2}\left(\frac{a_2b_1 - a_1c_{11}}{a_2b_2 - c_{11}^2}\right)P_2p^2, \end{aligned} \tag{3.3b}$$

$$\begin{aligned} H_\gamma = {} & \frac{\gamma}{\varepsilon}\Gamma bf_1Q_1\cos\frac{t}{\beta} + \frac{\gamma}{2\beta}\left(\frac{b_2Q_1P_1 - c_{11}Q_1P_2}{a_2b_2 - c_{11}^2}\right)\cos\frac{t}{\beta} \\ & - \gamma\Gamma^2bQ_1^2\sin\frac{t}{\beta} + \frac{\gamma}{4\Gamma^2\beta^2b}\left(\frac{b_2^2P_1^2 - 2b_2c_{11}P_1P_2 + c_{11}^2P_2^2}{(a_2b_2 - c_{11}^2)^2}\right)\sin\frac{t}{\beta} \\ & + \frac{\gamma}{2\beta\xi}qp\cos\frac{t}{\beta} - \frac{\gamma b}{2}q^2\sin\frac{t}{\beta} + \frac{\gamma}{2b\xi^2}p^2\sin\frac{t}{\beta}. \end{aligned} \tag{3.3c}$$

The $H_o + H_\varepsilon$ components represent the free oscillations of the system and are autonomous, while the perturbed (forced) terms are all nonautonomous.

The subscripted coefficients *a*, *b*, *c*, *d*, *A*, and *B* in (3.3) are all functions of the parameter $\xi = k'l'$, the nondimensional distance down the channel (see Table 1). The Hamiltonian may be simplified by approximating these terms according to their order of ξ.

All $\cos\xi$ and $\sin\xi$ terms are assumed to be $O(1)$, and recall that $\xi >> 1$. For example, the P_1^2 coefficient in H_o is approximated by:

$$\frac{b_2}{a_2 b_2 - c_{11}^2} = \frac{2(\xi - \cos\xi \sin\xi)}{(\xi^2 - \sin^2\xi)} = 2 \text{ times } O\left(\frac{1}{\xi}\right) \approx \frac{2}{\xi}. \tag{3.4}$$

This type of approximation is used only for determining the order of the coefficient for each variable grouping, not to rank the importance of different variable combinations. This means that the P_1^2 coefficient in H_o is $O(1/\xi)$, while the $P_1 P_2$ coefficient in H_o is $O(1/\xi^2)$, which is not neglected. This sort of approximation of coefficients by order of ξ will be used again later. Using these approximations, the Hamiltonian components are

$$\begin{aligned} H_o = {} & \tfrac{1}{2}\Gamma^2 b\xi Q_1^2 + \tfrac{1}{2}\Gamma^2 b\xi Q_2^2 + \tfrac{1}{2}\Gamma^2 b Q_1 Q_2 + \tfrac{1}{2} b\xi q^2 \\ & + \frac{p^2}{2b\xi} + \frac{P_1^2}{2\Gamma^2\beta^2 b\xi} + \frac{P_2^2}{2\Gamma^2\beta^2 b\xi} - \frac{P_1 P_2}{\Gamma^2\beta^2 b\xi^2}; \end{aligned} \tag{3.5a}$$

$$\begin{aligned} H_\varepsilon = {} & \varepsilon\frac{\Gamma\mu_5}{\xi} Q_1 qp + \varepsilon\frac{\Gamma(\mu_2 - \mu_5)}{\xi} Q_2 qp + \frac{2\varepsilon}{\Gamma\beta\xi} q^2 P_1 \\ & + \frac{2\varepsilon}{\Gamma\beta\xi} q^2 P_2 - \frac{\varepsilon\mu_1}{\Gamma\beta^2 b^2\xi^3} P_1 p^2 - \frac{\varepsilon\mu_1}{\Gamma\beta^2 b^2\xi^3} P_2 p^2, \end{aligned} \tag{3.5b}$$

$$\begin{aligned} H_\gamma = {} & \frac{\gamma}{\varepsilon}\Gamma b f_1 Q_1 \cos\frac{t}{\beta} + \frac{\gamma}{\beta\xi} Q_1 P_1 \cos\frac{t}{\beta} - \frac{\gamma}{\beta\xi^2} Q_1 P_2 \cos\frac{t}{\beta} - \gamma\Gamma^2 b Q_1^2 \sin\frac{t}{\beta} \\ & + \frac{\gamma}{\Gamma^2\beta^2 b\xi^2} P_1^2 \sin\frac{t}{\beta} - \frac{2\gamma}{\Gamma^2\beta^2 b\xi^3} P_1 P_2 \sin\frac{t}{\beta} + \frac{\gamma}{\Gamma^2\beta^2 b\xi^4} P_2^2 \sin\frac{t}{\beta} \\ & + \frac{\gamma}{2\beta\xi} qp\cos\frac{t}{\beta} - \frac{\gamma b}{2} q^2 \sin\frac{t}{\beta} + \frac{\gamma}{2b\xi^2} p^2 \sin\frac{t}{\beta}. \end{aligned} \tag{3.5c}$$

The Melnikov method requires first an analysis of the unperturbed $(\gamma = 0)$ system which involves calculating the first order evolution equations according to

$$\dot{q}_n = \frac{\partial(H_o + H_\varepsilon)}{\partial p_n}, \quad \dot{p}_n = \frac{\partial(H_o + H_\varepsilon)}{\partial q_n}. \tag{3.6a,b}$$

Next the fixed points of the system, which are the values of (q_n, p_n) such that

$$\dot{q}_n = 0 \quad \text{and} \quad \dot{p}_n = 0,$$

are computed. Finally, the fixed points are classified to determine the saddle points and then the homoclinic orbits are calculated about these saddles.

However, the above unperturbed system is very complicated, in part because it has three degrees of freedom, but also because of all the combinations of interactive terms. The beauty of formulating the problem in terms of the Hamiltonian is that any number of canonical transformations can be made, all of which preserve the dynamics of the evolution equations. Choosing canonical transformations that simplify the Hamiltonian will also simplify the calculation of the homoclinic orbits and the Melnikov function. Holmes [1986] used this property to great advantage to study chaotic waves in a cylindrical basin using two separate transformations. Cross-waves in a long channel are more complex and require seven transformations. The key to finding suitable transformations lies in concentrating on the $O(1)$ terms and simplifying H_o as much as possible. Each transformation will be discussed separately in the sections below.

All of the canonical transformations must satisfy the requirements of the Poisson brackets,

$$[u,v]_{q,p} = \sum_n \left(\frac{\partial u}{\partial q_n}\frac{\partial v}{\partial p_n} - \frac{\partial u}{\partial p_n}\frac{\partial v}{\partial q_n} \right), \tag{3.7a}$$

where the (q_n, p_n) are a complete set of canonical variables, and (u,v) are any two variables from another set [Fetter and Walecka, 1980; Goldstein, 1980]. The conditions on the Poisson brackets are shown below.

$$[u,v]_{q,p} = \begin{cases} 1 & \text{for } u,v \text{ a canonical pair} \\ 0 & \text{for } u,v \text{ not a canonical pair} \end{cases} \tag{3.7b}$$

3a. Rotation of axes transformation

$$\{(q,p),(Q_1,P_1),(Q_2,P_2)\} \Rightarrow \{(q',p'),(Q_1',P_1'),(Q_2',P_2')\}$$

The first canonical transformation puts the H_o terms into a more classical form. The component H_o contains the two product terms Q_1Q_2 and P_1P_2 which can be removed

following a rotation of axes transformation. This simplifies the action/angle transformations in §3b. The new canonical variables and the transformed Hamiltonian components are denoted with primes. The rotation transformations are:

$$q = q' \qquad p = p' \tag{3.8a,b}$$

$$Q_1 = Q_1'\cos\theta + Q_2'\sin\theta \qquad P_1 = P_1'\cos\theta + P_2'\sin\theta \tag{3.8c,d}$$

$$Q_2 = Q_1'\sin\theta - Q_2'\cos\theta \qquad P_2 = P_1'\sin\theta - P_2'\cos\theta \tag{3.8e,f}$$

The value of the axes rotation angle $\theta = \pi/4$ is chosen so that the new product terms, $Q_1'Q_2'$ and $P_1'P_2'$, in the new $O(1)$ component H_o' are zero. The transformed Hamiltonian and its components are:

$$H \Rightarrow H' = H_o' + H_\varepsilon' + H_\gamma' + O\left(\varepsilon^2, \varepsilon\gamma, \gamma^2\right), \tag{3.9}$$

$$H_o' = \tfrac{1}{2}\Gamma^2 b\xi Q_1'^2 + \tfrac{1}{2}\Gamma^2 b\xi Q_2'^2 + \tfrac{1}{2}b\xi q'^2 + \frac{p^2}{2b\xi} + \frac{P_1'^2 + P_2'^2}{2\Gamma^2\beta^2 b\xi}, \tag{3.10a}$$

$$\begin{aligned} H_\varepsilon' = {} & \varepsilon\frac{\Gamma\mu_2\sqrt{2}}{2\xi}Q_1'q'p' - \varepsilon\frac{\Gamma\sqrt{2}(\mu_2 - 2\mu_5)}{2\xi}Q_2'q'p' \\ & -\varepsilon\frac{\mu_1\sqrt{2}}{\Gamma\beta^2 b^2\xi^3}P_1'p'^2 + \varepsilon\frac{2\sqrt{2}}{\Gamma\beta\xi}P_1'q^2, \end{aligned} \tag{3.10b}$$

$$\begin{aligned} H_\gamma' = {} & \frac{\gamma\sqrt{2}\,\Gamma b f_1}{2\varepsilon}\left(Q_1' + Q_2'\right)\cos\frac{t}{\beta} + \frac{\gamma}{2\beta\xi}\left(Q_1'P_1' + Q_2'P_1' + Q_1'P_2' + Q_2'P_2'\right)\cos\frac{t}{\beta} \\ & + \frac{\gamma}{2\beta\xi}q'p'\cos\frac{t}{\beta} - \tfrac{1}{2}\gamma\Gamma^2 b\left(Q_1'^2 + Q_2'^2 + 2Q_1'Q_2'\right)\sin\frac{t}{\beta} - \tfrac{1}{2}\gamma b q'^2\sin\frac{t}{\beta} \\ & + \frac{\gamma}{2b\xi^2}p'^2\sin\frac{t}{\beta} + \frac{\gamma}{2\Gamma^2\beta^2 b\xi^2}\left(P_1'^2 + P_2'^2 + 2P_1'P_2'\right)\sin\frac{t}{\beta}. \end{aligned} \tag{3.10c}$$

The coefficients in H_o' and H_γ' are approximated according to their order of ξ as before. This approximation is not necessary for the H_ε' coefficients. For example, the $P_1'^2$ coefficient in H_o' includes the approximation

$$\left(\frac{1}{\xi} - \frac{1}{\xi^2}\right) \approx \frac{1}{\xi}. \tag{3.11}$$

The importance of using this type of approximation by order of ξ is as follows. The rotation of axes transformation was originally applied to the Hamiltonian without any

coefficient approximations. Without any approximations, the rotation angle θ was a complicated arc tangent function of various square roots of a_i, b_i, and c_{ij} combinations. This value of θ did not have a numerical value without either specifying a value of ξ or using an approximation of order ξ. This type of approximation by order of ξ as in (3.4) and (3.11) for the coefficients allows the Hamiltonian to be expressed more simply, and illuminates the physics and diminishes the algebra.

3b. Action/angle transformation

$$\left\{(q',p'),(Q_1',P_1'),(Q_2',P_2')\right\} \Rightarrow \left\{(\hat{q},\hat{p}),(\hat{Q}_1,\hat{P}_1),(\hat{Q}_2,\hat{P}_2)\right\}$$

The second canonical transformation is to action/angle variables. (This was Holmes' [1986] first transformation.) The goal is to eliminate the generalized coordinates from the $O(1)$ component. The transformations are given by the following:

$$q' = \sqrt{\frac{2\hat{p}}{b\xi}}\sin\hat{q} \qquad p' = \sqrt{2\hat{p}b\xi}\cos\hat{q} \qquad (3.12a,b)$$

$$Q_1' = \sqrt{\frac{2\hat{P}_1}{\Gamma^2\beta b\xi}}\sin\hat{Q}_1 \qquad P_1' = \sqrt{2\hat{P}_1\Gamma^2\beta b\xi}\cos\hat{Q}_1 \qquad (3.12c,d)$$

$$Q_2' = \sqrt{\frac{2\hat{P}_2}{\Gamma^2\beta b\xi}}\sin\hat{Q}_2 \qquad P_2' = \sqrt{2\hat{P}_2\Gamma^2\beta b\xi}\cos\hat{Q}_2 \qquad (3.12e,f)$$

The new momenta variables must all be nonnegative for the Hamiltonian to be real. The transformed Hamiltonian and its components are:

$$H' \Rightarrow \hat{H} = \hat{H}_o + \hat{H}_\varepsilon + \hat{H}_\gamma + O(\varepsilon^2, \varepsilon\gamma, \gamma^2), \qquad (3.13)$$

$$\hat{H}_o = \hat{p} + \frac{\hat{P}_1}{\beta} + \frac{\hat{P}_2}{\beta}, \qquad (3.14a)$$

$$\hat{H}_\varepsilon = -\frac{2\varepsilon\hat{p}\sqrt{\hat{P}_1}}{\beta^2\xi\sqrt{\beta b\xi}}\cos\hat{Q}_1 - \frac{\varepsilon(8+2/\beta^2)\hat{p}\sqrt{\hat{P}_1}}{\xi\sqrt{\beta b\xi}}\cos\hat{Q}_1\cos 2\hat{q}$$
$$+\frac{\varepsilon\mu_2\hat{p}\sqrt{\hat{P}_1}}{\xi\sqrt{\beta b\xi}}\sin\hat{Q}_1\sin 2\hat{q} - \frac{\varepsilon(\mu_2-2\mu_5)\hat{p}\sqrt{\hat{P}_2}}{\xi\sqrt{\beta b\xi}}\sin\hat{Q}_2\sin 2\hat{q}, \tag{3.14b}$$

$$\hat{H}_\gamma = \frac{\gamma f_1\sqrt{b\hat{P}_1}}{2\varepsilon\sqrt{\beta\xi}}\left[\sin\left(\hat{Q}_1+\frac{t}{\beta}\right)+\sin\left(\hat{Q}_1-\frac{t}{\beta}\right)\right]+\frac{\gamma\hat{P}_2}{4\beta\xi}\left[3\sin\left(2\hat{Q}_2+\frac{t}{\beta}\right)-\sin\left(2\hat{Q}_2-\frac{t}{\beta}\right)\right]$$
$$+\frac{\gamma\hat{p}}{4\beta\xi}\left[(1+2\beta)\sin\left(2\hat{q}+\frac{t}{\beta}\right)+(1-2\beta)\sin\left(2\hat{q}-\frac{t}{\beta}\right)\right]$$
$$+\frac{\gamma\sqrt{\hat{P}_1\hat{P}_2}}{2\beta\xi}\left[3\sin\left(\hat{Q}_1+\hat{Q}_2+\frac{t}{\beta}\right)-\sin\left(\hat{Q}_1+\hat{Q}_2-\frac{t}{\beta}\right)\right] \tag{3.14c}$$
$$+\frac{\gamma\hat{P}_1}{4\beta\xi}\left[3\sin\left(2\hat{Q}_1+\frac{t}{\beta}\right)-\sin\left(2\hat{Q}_1-\frac{t}{\beta}\right)\right]+\frac{\gamma f_1\sqrt{b\hat{P}_2}}{2\varepsilon\sqrt{\beta\xi}}\left[\sin\left(\hat{Q}_2+\frac{t}{\beta}\right)+\sin\left(\hat{Q}_2-\frac{t}{\beta}\right)\right].$$

The $O(1)$ $\hat{H}_o$ component can now be used as a check on the physics of the problem. The action/angle transformation is used in classical mechanics problems to obtain the frequency of periodic motion without finding a complete solution to the motion of the system [Goldstein, 1980]. The frequency of the motion is given by the first evolution equation, $\dot{q}_i = \partial H/\partial p_i$, which is unity for the cross-wave angle coordinate $\hat{q}$ and $1/\beta = \omega_p/\omega_c$ for the progressive wave angle coordinates $\hat{Q}_1$ and $\hat{Q}_2$. Recall that the cross-wave frequency was used to scale time in (2.1d). This transformation provides a physical check on approximating the coefficients by their order of ξ.

3c. Hamilton-Jacobi transformation

$$\left\{(\hat{q},\hat{p}),(\hat{Q}_1,\hat{P}_1),(\hat{Q}_2,\hat{P}_2)\right\} \Rightarrow \left\{(q^*,p^*),(Q_1^*,P_1^*),(Q_2^*,P_2^*)\right\}$$

The next canonical transformation applies the Hamilton-Jacobi theory which is generally used in classical mechanics to obtain variables that are constant in time by

transforming the Hamiltonian to be identically zero [Goldstein, 1980]. This transformation will closely follow that of Holmes [1986]. The idea is to find a transformation that makes the $O(1)$ terms in the Hamiltonian zero when the system is exactly in resonance. This transformation will be nonautonomous, explicitly including the time variable in the transformations. A nonautonomous transformation requires the construction of a generating function because the transformed Hamiltonian depends on the time derivative of the generating function [Goldstein, 1980].

Since the transformed Hamiltonian H^* is

$$H^* = \hat{H} + \frac{\partial \hat{F}}{\partial t}, \tag{3.15}$$

the generating function

$$F = -\hat{p}t - \frac{\hat{P}_1 t}{\beta} - \frac{\hat{P}_2 t}{\beta} \tag{3.16}$$

would transform the $\hat{H}_o$ component to zero. However, following Holmes [1986], this transformation is adapted to include *near* resonance cases by defining a detuning parameter, which transforms the $O(1)$ $\hat{H}_o$ component to be $O(\varepsilon)$ rather than zero. Furthermore, Holmes included a mechanism to remove one of the canonical variables from the unperturbed Hamiltonian, which automatically makes one of the evolution equations zero and reduces the number of degrees of freedom. Another important aspect of Holmes' transformation was that some of the perturbed terms were transformed to be autonomous. This allowed Holmes to time average and greatly simplify his system. Note that without autonomous perturbed terms for the cross-wave system, averaging would remove all the perturbed terms and eliminate the possibility of applying the Melnikov method.

As mentioned in the §1, it is a goal to formulate the problem in terms of various integer frequency ratios between the forcing and the cross-wave. With this in mind, the transformations that satisfy the Poisson brackets, generating function $\hat{F}$, and detuning parameter Ω are defined as

$$\hat{q} = q^* + \frac{MQ_1^*}{2N} + \frac{Nt}{M\beta} \qquad \hat{p} = p^* - \frac{2NP_2^*}{M} \tag{3.17a,b}$$

$$\hat{Q}_1 = \frac{MQ_1^*}{N} + \frac{t}{\beta} \qquad \hat{P}_1 = \frac{NP_1^*}{M} - \frac{p^*}{2} \tag{3.17c,d}$$

$$\hat{Q}_2 = 2q^* + \frac{MQ_1^*}{N} + \frac{MQ_2^*}{N} + \frac{t}{\beta} \qquad \hat{P}_2 = \frac{NP_2^*}{M} \tag{3.17e,f}$$

$$\hat{F} = -\hat{p}q^* - \hat{P}_1Q_1^* - \hat{P}_2Q_2^* - \frac{N\hat{p}t}{M\beta} - \frac{\hat{P}_1t}{\beta} - \frac{\hat{P}_2t}{\beta} + \left(\hat{q}\hat{p} + \hat{Q}_1\hat{P}_1 + \hat{Q}_2\hat{P}_2\right) \tag{3.18}$$

$$\varepsilon\Omega = 1 - \frac{N}{M\beta} \tag{3.19}$$

The time-dependent terms in the angle coordinate transformations (3.17a,c,e) include the frequency of the motion. The time derivatives of $\hat{Q}_1$ and $\hat{Q}_2$ give the nondimensional progressive wave frequency $1/\beta$; the time derivative of $\hat{q}$ gives the nondimensional cross-wave frequency $N/M\beta$, which reflects the various possible frequency ratios between the forcing and the response [Bogoliubov and Mitropolsky, 1961]. The terms in parentheses in equation (3.18) are needed because this generating function $\hat{F}$ is of type three [Goldstein, 1980].

The Q_1^* variable may be eliminated from (3.14b) using the following angle sum identity:

$$\cos\left(\hat{Q}_1 - 2\hat{q}\right) = \cos\left(\frac{t}{\beta}\left[1 - \frac{2N}{M}\right] - 2q^*\right). \tag{3.20}$$

Equation (3.20) does not contain Q_1^*, which is how the Q_1^* coefficients in (3.17a,c) were chosen; however, it is an autonomous term only if $M = 2N$, which is the primary parametric resonance [Bogoliubov and Mitropolsky, 1961]. At present, only this primary parametric resonance contributes to autonomous $O(\varepsilon)$ nonlinear terms in the transformed Hamiltonian. This is a very important point because when the system is later averaged (again following Holmes [1986]), only the nonlinear autonomous terms contribute to homoclinic orbits. To include parametric resonances other than the primary, the problem should be reformulated to include higher order $O(\varepsilon^2)$ terms.

Considering only the primary parametric resonance $N=1$ and $M=2$, the Hamiltonian is written in the component form

$$\hat{H} \Rightarrow H^* = H_\varepsilon^* + H_\varepsilon^*(t) + H_\gamma^* + H_\gamma^*(t) + O\left(\varepsilon^2, \varepsilon\gamma, \gamma^2\right), \tag{3.21}$$

where H_ε^* are the autonomous $O(\varepsilon)$ components, $H_\varepsilon^*(t)$ the nonautonomous $O(\varepsilon)$ components, H_γ^* the autonomous perturbed components, and $H_\gamma^*(t)$ the nonautonomous perturbed components. The division into autonomous and nonautonomous components is useful because the nonautonomous components will average to zero. The nonautonomous components, in particular the perturbed component, are fairly long equations shown in Table 2 in Appendix I. The autonomous components are:

$$\begin{aligned} H_\varepsilon^* = {} & \varepsilon\Omega\left(p^* - P_2^*\right) + \varepsilon\frac{\left(\mu_2 - 8 - 2/\beta^2\right)}{2\xi\sqrt{2b\beta\xi}}\left(p^* - P_2^*\right)\sqrt{P_1^* - p^*}\cos 2q^* \\ & -\varepsilon\frac{\left(\mu_2 - 2\mu_5\right)}{2\xi\sqrt{2b\beta\xi}}\left(p^* - P_2^*\right)\sqrt{P_2^*}\cos 2Q_2^* \end{aligned} \tag{3.22a}$$

$$\begin{aligned} H_\gamma^* = {} & \gamma\left[\frac{f_1}{2\varepsilon}\sqrt{\frac{b\left(P_1^* - p^*\right)}{2\beta\xi}}\right]\sin 2Q_1^* + \gamma\frac{\left(1-2\beta\right)}{4\beta\xi}\left(p^* - P_2^*\right)\sin\left(2Q_1^* + 2q^*\right) \\ & +\gamma\left[\frac{f_1}{2\varepsilon}\sqrt{\frac{bP_2^*}{2\beta\xi}}\right]\sin\left(2Q_1^* + 2Q_2^* + 2q^*\right) \end{aligned} \tag{3.22b}$$

Note the linear term $\varepsilon\Omega\left(p^* - P_2^*\right)$ containing the detuning parameter from the $\hat{H}_o$ component. Since the action variables must be nonnegative, the condition on the new momenta variables is

$$P_1^* \geq p^* \geq P_2^* \geq 0. \tag{3.23}$$

3d. Shift transformation

$$\{(q^*,p^*),(Q_1^*,P_1^*),(Q_2^*,P_2^*)\} \Rightarrow \{(q'',p''),(Q_1'',P_1''),(Q_2'',P_2'')\}$$

Each term in the unperturbed Hamiltonian (3.22a) contains the common term $(p^* - P_2^*)$ which can be transformed to a single new variable with a shift transformation. The shift canonical transformations are:

$$q^* = q'' \qquad p^* = p'' + P_2'' \qquad \text{(3.24a,b)}$$

$$Q_1^* = Q_1'' \qquad P_1^* = P_1'' + P_2'' \qquad \text{(3.24c,d)}$$

$$Q_2^* = Q_2'' - q'' - Q_1'' \qquad P_2^* = P_2'' \qquad \text{(3.24e,f)}$$

The shift transformation preserves the time dependencies of each component, so that autonomous components remain autonomous after the transformation. The new set of Hamiltonian components is given by

$$H^* \Rightarrow H'' = H_\varepsilon'' + H_\varepsilon''(t) + H_\gamma'' + H_\gamma''(t) + O(\varepsilon^2, \varepsilon\gamma, \gamma^2), \qquad (3.25)$$

where the nonautonomous components $H_\varepsilon''(t)$ and $H_\gamma''(t)$ are shown in Table 3 in Appendix I. The autonomous components are:

$$\begin{aligned} H_\varepsilon'' = {} & \varepsilon\Omega p'' + \varepsilon\frac{(\mu_2 - 8 - 2/\beta^2)}{2\xi\sqrt{2b\beta\xi}} p''\sqrt{P_1'' - p''}\cos 2q'' \\ & -\varepsilon\frac{(\mu_2 - 2\mu_5)}{2\xi\sqrt{2b\beta\xi}} p''\sqrt{P_2''}\cos(2Q_2'' - 2Q_1'' - 2q'') \end{aligned} \qquad (3.26a)$$

$$\begin{aligned} H_\gamma'' = {} & \gamma\left[\frac{f_1}{2\varepsilon}\sqrt{\frac{b(P_1'' - p'')}{2\beta\xi}}\right]\sin 2Q_1'' + \gamma\frac{(1-2\beta)}{4\beta\xi} p''\sin(2Q_1'' + 2q'') \\ & +\gamma\left[\frac{f_1}{2\varepsilon}\sqrt{\frac{bP_2''}{2\beta\xi}}\right]\sin 2Q_2'' \end{aligned} \qquad (3.26b)$$

The condition (3.23) on the momenta variables is now:

$$P_1'' \geq p'' \geq P_2'' \geq 0. \qquad (3.27)$$

3e. Nonautonomous Q_2'' transformation

$$\{(q'',p''),(Q_1'',P_1''),(Q_2'',P_2'')\} \Rightarrow \{(\tilde{q},\tilde{p}),(\tilde{Q}_1,\tilde{P}_1),(\tilde{Q}_2,\tilde{P}_2)\}$$

This canonical transformation removes another variable from the autonomous components of the Hamiltonian by transforming them to nonautonomous components. The idea behind this transformation follows from Fetter and Walecka [1980, Chapter 6] that *any* generating function F generates *some* canonical transformation which guarantees that there will be a new Hamiltonian given by

$$\tilde{H} = H'' + \frac{\partial F''}{\partial t}, \tag{3.28}$$

and so provides the extraordinary flexibility of choosing an arbitrary generating function.

The motivation behind the following transformations is the application of the averaging theorem:

$$q'' = \tilde{q} \qquad p'' = \tilde{p} \tag{3.29a,b}$$

$$Q_1'' = \tilde{Q}_1 \qquad P_1'' = \tilde{P}_1 \tag{3.29c,d}$$

$$Q_2'' = \tilde{Q}_2 + \frac{t}{\beta} \qquad P_2'' = \tilde{P}_2 \tag{3.29e,f}$$

$$F'' = -\tilde{q}p'' - \tilde{Q}_1 P_1'' - \tilde{Q}_2 P_2'' - \frac{P_2'' t}{\beta} + (q''p'' + Q_1'' P_1'' + Q_2'' P_2'') \tag{3.30}$$

Note the appearance of the time variable t in (3.29e). The parenthetical terms in F'' in equation (3.30) indicate a generating function of type three [Goldstein, 1980].

The transformed Hamiltonian components are

$$\tilde{H} = \tilde{H}_o + \tilde{H}_\varepsilon + \tilde{H}_\varepsilon(t) + \tilde{H}_\gamma + \tilde{H}_\gamma(t) + O(\varepsilon^2, \varepsilon\gamma, \gamma^2), \tag{3.31}$$

where the nonautonomous components $\tilde{H}_\varepsilon(t)$ and $\tilde{H}_\gamma(t)$ are shown in Table 4 in Appendix I and the autonomous components are:

$$\tilde{H}_o = -\frac{\tilde{P}_2}{\beta} \tag{3.32a}$$

$$\tilde{H}_\varepsilon = \varepsilon\Omega\tilde{p} + \frac{\varepsilon\left(\mu_2 - 8 - 2/\beta^2\right)}{2\xi\sqrt{2b\beta\xi}}\,\tilde{p}\sqrt{\tilde{P}_1 - \tilde{p}}\,\cos(2\tilde{q}) \tag{3.32b}$$

$$\tilde{H}_\gamma = \gamma\left[\frac{f_1}{2\varepsilon}\sqrt{\frac{b\left(\tilde{P}_1 - \tilde{p}\right)}{2\beta\xi}}\right]\sin 2\tilde{Q}_1 + \gamma\frac{(1-2\beta)}{4\beta\xi}\,\tilde{p}\sin\left(2\tilde{Q}_1 + 2\tilde{q}\right) \tag{3.32c}$$

The momenta condition (3.27) is now:

$$\tilde{P}_1 \geq \tilde{p} \geq \tilde{P}_2 \geq 0. \tag{3.33}$$

3f. $\tilde{Q}_1$ transformation

$$\left\{(\tilde{q},\tilde{p}),\left(\tilde{Q}_1,\tilde{P}_1\right),\left(\tilde{Q}_2,\tilde{P}_2\right)\right\} \Rightarrow \left\{(\tilde{q}',\tilde{p}'),\left(\tilde{Q}_1',\tilde{P}_1'\right),\left(\tilde{Q}_2',\tilde{P}_2'\right)\right\}$$

Another transformation is needed in conjunction with the transformation in §3g in order to satisfy Proposition 4.1.17 from Wiggins [1988] discussed in detail in §4. These two transformations cannot be combined into one single transformation because they are of different types. The transformations are:

$$\tilde{q} = \tilde{q}' \qquad \tilde{p} = \tilde{p}' \tag{3.34a,b}$$

$$\tilde{Q}_1 = \frac{\tilde{Q}_1'}{2\tilde{P}_1'} \qquad \tilde{P}_1 = \tilde{P}_1'^2 \tag{3.34c,d}$$

$$\tilde{Q}_2 = \tilde{Q}_2' \qquad \tilde{P}_2 = \tilde{P}_2' \tag{3.34e,f}$$

The Hamiltonian is transformed to

$$\tilde{H} \Rightarrow \tilde{H}' = \tilde{H}_o' + \tilde{H}_\varepsilon' + \tilde{H}_\varepsilon'(t) + \tilde{H}_\gamma' + \tilde{H}_\gamma'(t) + O\left(\varepsilon^2, \varepsilon\gamma, \gamma^2\right), \tag{3.35}$$

where the nonautonomous components are shown in Table 5 in Appendix I. The autonomous Hamiltonian components are:

$$\tilde{H}_o' = -\frac{\tilde{P}_2'}{\beta} \tag{3.36a}$$

$$\tilde{H}'_{\varepsilon} = \varepsilon\Omega\tilde{p}' + \frac{\varepsilon\left(\mu_2 - 8 - 2/\beta^2\right)}{2\xi\sqrt{2b\beta\xi}}\,\tilde{p}'\sqrt{\tilde{P}_1'^2 - \tilde{p}'}\cos 2\tilde{q}' \tag{3.36b}$$

$$\tilde{H}'_{\gamma} = \gamma\left[\frac{f_1}{2\varepsilon}\sqrt{\frac{b\left(\tilde{P}_1'^2 - \tilde{p}'\right)}{2\beta\xi}}\right]\sin\frac{\tilde{Q}_1'}{\tilde{P}_1'} + \frac{\gamma(1-2\beta)}{4\beta\xi}\,\tilde{p}'\sin\left(\frac{\tilde{Q}_1'}{\tilde{P}_1'} + 2\tilde{q}'\right) \tag{3.36c}$$

The momenta condition (3.33) is now:

$$\tilde{P}_1'^2 \geq \tilde{p}' \geq \tilde{P}_2' \geq 0. \tag{3.37}$$

3g. Nonautonomous $\tilde{Q}_1'$ transformation

$$\left\{(\tilde{q}',\tilde{p}'),\left(\tilde{Q}_1',\tilde{P}_1'\right),\left(\tilde{Q}_2',\tilde{P}_2'\right)\right\} \Rightarrow \left\{(q,p),(Q_1,P_1),(Q_2,P_2)\right\}$$

The final canonical transformation is designed to satisfy the conditions of Proposition 4.1.17 in Wiggins [1988]. This transformation makes the autonomous perturbed component (3.36c) become nonautonomous and makes two of the terms in the nonautonomous perturbed component shown in Table 5 in Appendix I become autonomous. The generating function used is of type two from Goldstein [1980]. The transformations and generating function are:

$$\tilde{q}' = q \qquad \tilde{p}' = p \tag{3.38a,b}$$

$$\tilde{Q}_1' = Q_1 - \frac{2P_1 t}{\beta} \qquad \tilde{P}_1' = P_1 \tag{3.38c,d}$$

$$\tilde{Q}_2' = Q_2 \qquad \tilde{P}_2' = P_2 \tag{3.38e,f}$$

$$\tilde{F}' = p\tilde{q}' + P_1\tilde{Q}_1' + P_2\tilde{Q}_2' + \frac{P_1^2 t}{\beta} - \left(qp + Q_1P_1 + Q_2P_2\right) \tag{3.39}$$

The transformed Hamiltonian and its components are:

$$H = \tilde{H}' + \frac{\partial\tilde{F}'}{\partial t} = H_o + H_\varepsilon + H_\varepsilon(t) + H_\gamma + H_\gamma(t) + O\left(\varepsilon^2, \varepsilon\gamma, \gamma^2\right) \tag{3.40}$$

where the nonautonomous components $H_\varepsilon(t)$ and $H_\gamma(t)$ are shown in Table 6 in Appendix I and the autonomous components are:

$$H_o = -\frac{P_2}{\beta} + \frac{P_1^2}{\beta} \tag{3.41a}$$

$$H_\varepsilon = \varepsilon\Omega p + \frac{\varepsilon\left(\mu_2 - 8 - 2/\beta^2\right)}{2\xi\sqrt{2b\beta\xi}}\, p\sqrt{P_1^2 - p}\cos 2q \tag{3.41b}$$

$$H_\gamma = \gamma\left[\frac{f_1}{2\varepsilon}\sqrt{\frac{b\left(P_1^2 - p\right)}{2\beta\xi}}\right]\sin\frac{Q_1}{P_1} + \frac{\gamma(1-2\beta)}{4\beta\xi}\, p\sin\left(\frac{Q_1}{P_1} + 2q\right) \tag{3.41c}$$

The momenta condition (3.37) is now in final form:

$$P_1^2 \geq p \geq P_2 \geq 0. \tag{3.42}$$

3h. The averaged system

The Hamiltonian will now be time averaged following Holmes [1986]. [See also Wiggins, 1988, Guckenheimer and Holmes, 1983, and Grimshaw, 1993, for a detailed discussion of the averaging theorem.] The averaged system has hyperbolic and periodic solutions corresponding to those of the full system.

The Hamiltonian, averaged over the progressive wave period $2\pi\beta$, is then given by the following:

$$\begin{aligned}\overline{H} = &-\frac{P_2}{\beta} + \frac{P_1^2}{\beta} + \varepsilon\Omega p + \frac{\varepsilon\left(\mu_2 - 8 - 2/\beta^2\right)}{2\xi\sqrt{2b\beta\xi}}\, p\sqrt{P_1^2 - p}\cos 2q \\ &+\gamma\left[\frac{f_1}{2\varepsilon}\sqrt{\frac{b\left(P_1^2 - p\right)}{2\beta\xi}}\sin\frac{Q_1}{P_1} + \frac{(1-2\beta)}{4\beta\xi}\, p\sin\left(\frac{Q_1}{P_1} + 2q\right)\right]\end{aligned} \tag{3.43}$$

The evolution equations from the averaged Hamiltonian are:

$$\begin{aligned}\dot{q} = &\varepsilon\Omega - \frac{\varepsilon\Lambda\left(2P_1^2 - 3p\right)}{2\sqrt{\left(P_1^2 - p\right)}}\cos 2q \\ &+\gamma\left[\frac{(1-2\beta)}{4\beta\xi}\sin\left(\frac{Q_1}{P_1} + 2q\right) - \frac{f_1}{4\varepsilon}\sqrt{\frac{b}{2\beta\xi\left(P_1^2 - p\right)}}\sin\frac{Q_1}{P_1}\right]\end{aligned} \tag{3.44a}$$

$$\dot{p} = -2\varepsilon\Lambda\, p\sqrt{P_1^2 - p}\sin 2q + \gamma\left[\frac{(2\beta-1)}{2\beta\xi}\, p\cos\left(\frac{Q_1}{P_1} + 2q\right)\right] \tag{3.44b}$$

$$\dot{Q}_1 = \frac{2P_1}{\beta} - \frac{\varepsilon\Lambda p P_1}{\sqrt{P_1^2 - p}}\cos 2q + \gamma\left[\frac{(2\beta-1)}{4\beta\xi P_1^2}\, pQ_1\cos\left(\frac{Q_1}{P_1} + 2q\right)\right.$$
$$\left. + \frac{f_1 P_1}{2\varepsilon}\sqrt{\frac{b}{2\beta\xi\left(P_1^2 - p\right)}}\sin\frac{Q_1}{P_1} - \frac{f_1 Q_1}{2\varepsilon P_1^2}\sqrt{\frac{b\left(P_1^2 - p\right)}{2\beta\xi}}\cos\frac{Q_1}{P_1}\right] \tag{3.44c}$$

$$\dot{P}_1 = -\gamma\left[\frac{f_1}{2\varepsilon P_1}\sqrt{\frac{b\left(P_1^2 - p\right)}{2\beta\xi}}\cos\frac{Q_1}{P_1} + \frac{(1-2\beta)}{4\beta\xi P_1}\, p\cos\left(\frac{Q_1}{P_1} + 2q\right)\right] \tag{3.44d}$$

$$\dot{Q}_2 = -\frac{1}{\beta} \tag{3.44e}$$

$$\dot{P}_2 = 0 \tag{3.44f}$$

where

$$\Lambda = -\frac{\left(\mu_2 - 8 - 2/\beta^2\right)}{2\xi\sqrt{2b\beta\xi}}. \tag{3.45}$$

Note that all equations (3.44a-f) are independent of Q_2 and P_2.

4. The Melnikov calculation

Since the evolution equations (3.44) do not depend on either Q_2 or P_2, it suffices to analyze the four dimensional subsystem consisting of the $q - p - P_1 - Q_1$ components shown below:

$$\dot{q} = \varepsilon\Omega - \frac{\varepsilon\Lambda\left(2P_1^2 - 3p\right)}{2\sqrt{\left(P_1^2 - p\right)}}\cos 2q + \gamma\left[\frac{(1-2\beta)}{4\beta\xi}\sin\left(\frac{Q_1}{P_1} + 2q\right) - \frac{f_1}{4\varepsilon}\sqrt{\frac{b}{2\beta\xi\left(P_1^2 - p\right)}}\sin\frac{Q_1}{P_1}\right] \tag{4.1a}$$

$$\dot{p} = -2\varepsilon\Lambda\, p\sqrt{P_1^2 - p}\sin 2q + \gamma\left[\frac{(2\beta-1)}{2\beta\xi}\, p\cos\left(\frac{Q_1}{P_1} + 2q\right)\right] \tag{4.1b}$$

$$\dot{P}_1 = -\gamma\left[\frac{f_1}{2\varepsilon P_1}\sqrt{\frac{b\left(P_1^2 - p\right)}{2\beta\xi}}\cos\frac{Q_1}{P_1} + \frac{(1-2\beta)}{4\beta\xi P_1}\, p\cos\left(\frac{Q_1}{P_1} + 2q\right)\right] \tag{4.1c}$$

$$\dot{Q}_1 = \frac{2P_1}{\beta} - \frac{\varepsilon\Lambda p P_1}{\sqrt{P_1^2 - p}}\cos 2q + \gamma\left[\frac{(2\beta-1)}{4\beta\xi P_1^2}\, pQ_1\cos\left(\frac{Q_1}{P_1} + 2q\right) + \frac{f_1 P_1}{2\varepsilon}\sqrt{\frac{b}{2\beta\xi\left(P_1^2 - p\right)}}\sin\frac{Q_1}{P_1} - \frac{f_1 Q_1}{2\varepsilon P_1^2}\sqrt{\frac{b\left(P_1^2 - p\right)}{2\beta\xi}}\cos\frac{Q_1}{P_1}\right] \tag{4.1d}$$

(See Wiggins [1988, p. 442] for an analogous situation.) This is an example of the type described by System III from Wiggins [1988, Chapter 4], since the entire vector field is derived from a Hamiltonian. Note that the order of the $\dot{Q}_1$ and $\dot{P}_1$ equations (4.1c,d) has been reversed from that of (3.44c,d) in order to be consistent with the notation in Wiggins [1988]. Using Wiggins' notation,

$$\left(\boldsymbol{q} = (q,p), P_1, Q_1\right) \in \Re^{2n} \times \Re^m \times \Re^m, \tag{4.2}$$

where $n = 1$ and $m = 1$ for (4.1). In general, Wiggins approaches the study of the perturbed System III with KAM type arguments. However, his discussion provides for a special case with $n = 1$ and $m = 1$ for which KAM theory is not needed and intersections of the stable and unstable manifolds result in ordinary Smale horseshoes [Wiggins, 1988, p. 394]; equations (4.1) are analyzed without KAM theory.

4a. The unperturbed system

The averaged system without forcing is analyzed first. Setting the perturbation parameter $\gamma = 0$ in (3.43) and (4.1), the averaged unperturbed Hamiltonian and evolution equations are reduced to:

$$\overline{H}(\gamma = 0) = -\frac{P_2}{\beta} + \frac{P_1^2}{\beta} + \varepsilon \Omega p - \varepsilon \Lambda p \sqrt{P_1^2 - p}\, \cos 2q \tag{4.3}$$

$$\dot{q} = \varepsilon \Omega - \varepsilon \tfrac{1}{2} \Lambda \frac{(2P_1^2 - 3p)}{\sqrt{P_1^2 - p}} \cos 2q \tag{4.4a}$$

$$\dot{p} = -2\varepsilon \Lambda p \sqrt{P_1^2 - p}\, \sin 2q \tag{4.4b}$$

$$\dot{P}_1 = 0 \tag{4.4c}$$

$$\dot{Q}_1 = \frac{2P_1}{\beta} - \varepsilon \Lambda \frac{pP_1}{\sqrt{P_1^2 - p}} \cos 2q \tag{4.4d}$$

The unforced evolution equations (4.4) depend only on the variables (q,p,P_1). Since P_1 is constant by (4.4c), the (q,p) phase planes may be determined for fixed values of P_1. Figure 2 illustrates contours of the Hamiltonian function (4.3) on standard phase portraits for five different ranges of the detuning parameter Ω. These phase portraits are π-periodic in q and bounded by the line $p = P_1^2$, where $\dot{q}$ is undefined in (4.4a).

The fixed points. The saddle points (hyperbolic fixed points) are given by

$$(q,p) = \left(\tfrac{1}{2} \cos^{-1}\left[\frac{\Omega}{P_1 \Lambda} \right], 0 \right), \tag{4.5}$$

where the detuning parameter must lie within the range

$$-P_1 \Lambda < \Omega < P_1 \Lambda\,. \tag{4.6}$$

Outside of this range there are no saddles as shown in Figures 2a,e. When $\Omega = 0$ the system is precisely in resonance (Figure 2c); although saddle points exist, there are no closed orbits connecting them.

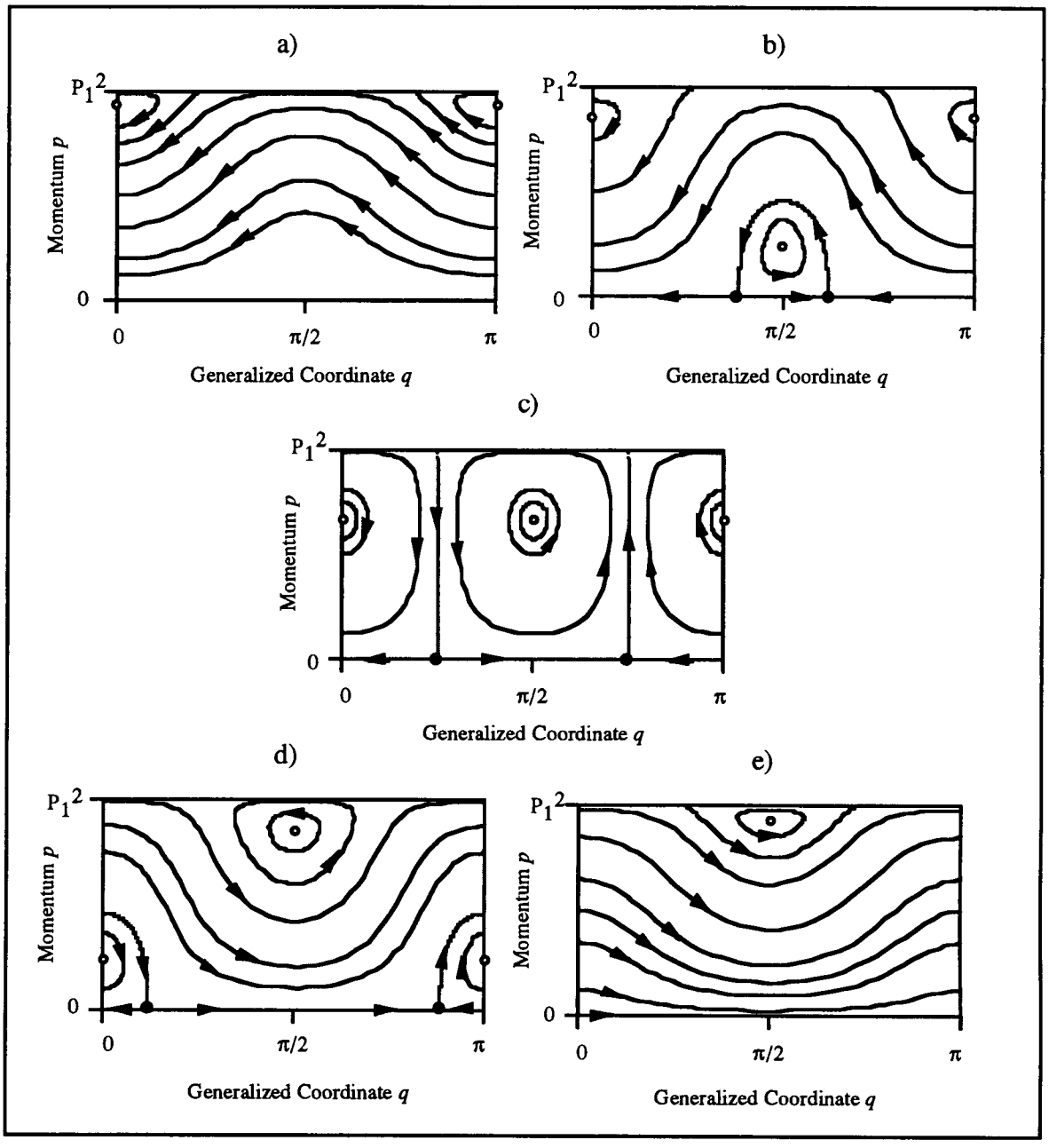

Figure 2. The (q,p) phase plane for the unperturbed system (4.4) for fixed P_1. For plotting purposes only, $\beta = 0.5$, $b = \pi$, $\xi = 24\pi$, $\varepsilon = 0.25$, $P_1 = 1$, and $\Lambda = 0.0034$. The detuning parameter range is: a) $\Omega \le -P_1\Lambda$ $(\Omega = -0.005)$; b) $-P_1\Lambda < \Omega < 0$ $(\Omega = -0.0025)$; c) $\Omega = 0$; d) $0 < \Omega < P_1\Lambda$ $(\Omega = 0.0025)$; and e) $P_1\Lambda < \Omega$ $(\Omega = 0.005)$.

It is the closed trajectories of the saddle points in Figures 2b,d that are important for the Melnikov method. There are two different values of q in each pair of saddle points

connected by the closed orbits because the arc cosine function in (4.5) is satisfied in two quadrants,

$$q = \tfrac{1}{2}\cos^{-1}(\alpha) = \begin{cases} \tfrac{1}{2}\theta_1 \\ \tfrac{1}{2}\theta_2 = \tfrac{1}{2}(2\pi - \theta_1). \end{cases} \tag{4.7}$$

Although the trajectory connecting the saddle points at different values of q is heteroclinic, the Melnikov function may be computed in the same manner as for a homoclinic trajectory [Wiggins, 1988, p.470]. Furthermore, the entire line $p = 0$ in the final canonical variables corresponds to the *(q,p)* origin in the original canonical variables; the saddle points connected by the heteroclinic trajectory in Figure 2b represent the same physical state, and the saddle points in Figure 2d represent the same physical state.

The unperturbed evolution equations (4.4) and the phase portraits in Figure 2 are similar to equations (2.13) and Figure 1 of Holmes [1986]. This is not surprising because Holmes' system of two modes in a vertically oscillating cylindrical basin was described by a Lagrangian given by Miles [1976] that differs from equation (2.3) only by the dynamic pressure component $\dot{\phi}'$.

The heteroclinic orbits. The heteroclinic trajectories lie on the level set

$$\overline{H}\left(\gamma = 0, q = \tfrac{1}{2}\cos^{-1}\left[\frac{\Omega}{P_1\Lambda}\right], p = 0\right) = -\frac{P_2}{\beta} + \frac{P_1^2}{\beta}. \tag{4.8}$$

Equation (4.3) for the unperturbed Hamiltonian can be solved for q in terms of p, P_1, P_2, and $\overline{H}$. Substituting in the value of $\overline{H}$ of the level set in (4.8) gives the relationship between q and p on the heteroclinic trajectory,

$$q_h = \tfrac{1}{2}\cos^{-1}\left[\frac{\Omega}{\Lambda\sqrt{P_1^2 - p}}\right], \tag{4.9}$$

where the subscript h refers to the heteroclinic orbit. On the heteroclinic trajectories

$$\cos 2q_h = \frac{\Omega}{\Lambda\sqrt{P_1^2 - p}}, \qquad \sin 2q_h = \pm\sqrt{1 - \frac{\Omega^2}{\Lambda^2(P_1^2 - p)}}. \tag{4.10a,b}$$

The equations (4.10) are substituted into the right hand side of the unperturbed evolution equations (4.4a,b,d) and integrated to obtain the solutions for q, p, and Q_1 on the heteroclinic trajectories:

$$p_h = \frac{1}{\Lambda^2}\left(\Lambda^2 P_1^2 - \Omega^2\right)\operatorname{sech}^2\left[\varepsilon t\sqrt{\Lambda^2 P_1^2 - \Omega^2}\right] \tag{4.11}$$

$$\begin{aligned} q_h &= \frac{\varepsilon\Omega}{2}\int_0^t \frac{p(\tau)}{P_1^2 - p(\tau)}\,d\tau \\ &= \pm\tfrac{1}{2}\tan^{-1}\left[\sqrt{\frac{\Lambda^2 P_1^2 - \Omega^2}{\Omega^2}}\,\tanh\left(\varepsilon t\sqrt{\Lambda^2 P_1^2 - \Omega^2}\right)\right] + \left(0, \pm\frac{\pi}{2}, \pm\pi, \ldots\right) \end{aligned} \tag{4.12}$$

$$Q_{1h} = \int_0^t \frac{2P_1}{\beta}\,d\tau - \varepsilon\Omega P_1\int_0^t \frac{p(\tau)}{P_1^2 - p(\tau)}\,d\tau = \frac{2P_1 t}{\beta} - 2P_1 q_h + Q_{10} \tag{4.13}$$

The sequence of constants of integration for q_h in (4.12) are required to obtain the repeated saddle point locations on the q-axis for Figures 2b and 2d. The constant of integration Q_{10} for Q_{1h} in (4.13) is unknown at this point but will be determined to have specific values for which the system is chaotic. The heteroclinic trajectory shown in Figure 2b will be the case analyzed by the Melnikov method and is shown in more detail in Figure 3. The positive sign for q_h in (4.12) is used to plot the trajectory backward in time from $t = 0$ and the negative sign to plot the trajectory forward in time from $t = 0$.

The heteroclinic trajectories, described by the two parametric equations (4.11) and (4.12) for p_h and q_h, are continuous functions of P_1 and form a surface in the three dimensional $q - p - P_1$ space shown in Figure 4. The manifold of the hyperbolic fixed points of the $q - p - P_1$ components of (4.4) is denoted as

$$\rho_o(P_1):\quad (q, p, P_1) = \left(\tfrac{1}{2}\cos^{-1}\left[\frac{\Omega}{P_1\Lambda}\right], 0, P_1\right), \tag{4.14}$$

which is the heavy line in Figure 4. This figure represents the same conditions as in Figures 2b and 3; the hyperbolic manifold is bounded below by the point $(\pi/2, 0, \Omega/\Lambda)$ and lies within the range $\frac{\pi}{4} < q < \frac{3\pi}{4}$; the arrows indicate the direction of motion on the heteroclinic trajectories.

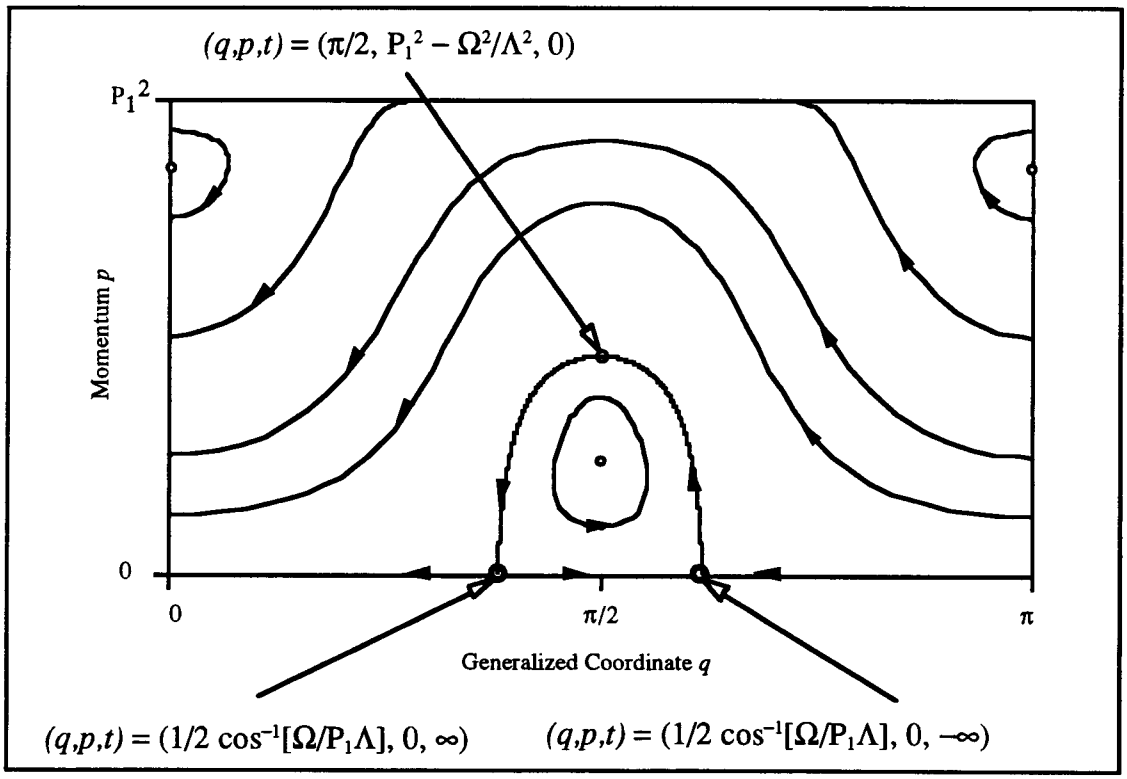

Figure 3. Details of the heteroclinic orbit of Figure 2b showing the (q,p) values at times $t=0$, $t=\infty$, and $t=-\infty$.

In the full $q-p-P_1-Q_1$ phase space, (4.4) has a two dimensional normally hyperbolic invariant manifold with boundary

$$\mathrm{M}=\left(\rho_o(P_1),Q_1\right), \quad P_1>\frac{\Omega}{\Lambda}. \tag{4.15}$$

M has three dimensional stable and unstable manifolds which coincide in the three dimensional heteroclinic manifold. (See Wiggins, 1988, Proposition 4.1.15.)

The unperturbed vector field restricted to M is given by

$$\dot{P}_1=0 \tag{4.16a}$$

$$\dot{Q}_1=\frac{\partial\overline{H}}{\partial P_1}\left(\gamma=0,\rho_o(P_1),P_1\right)=\frac{2P_1}{\beta} \tag{4.16b}$$

with flow given by

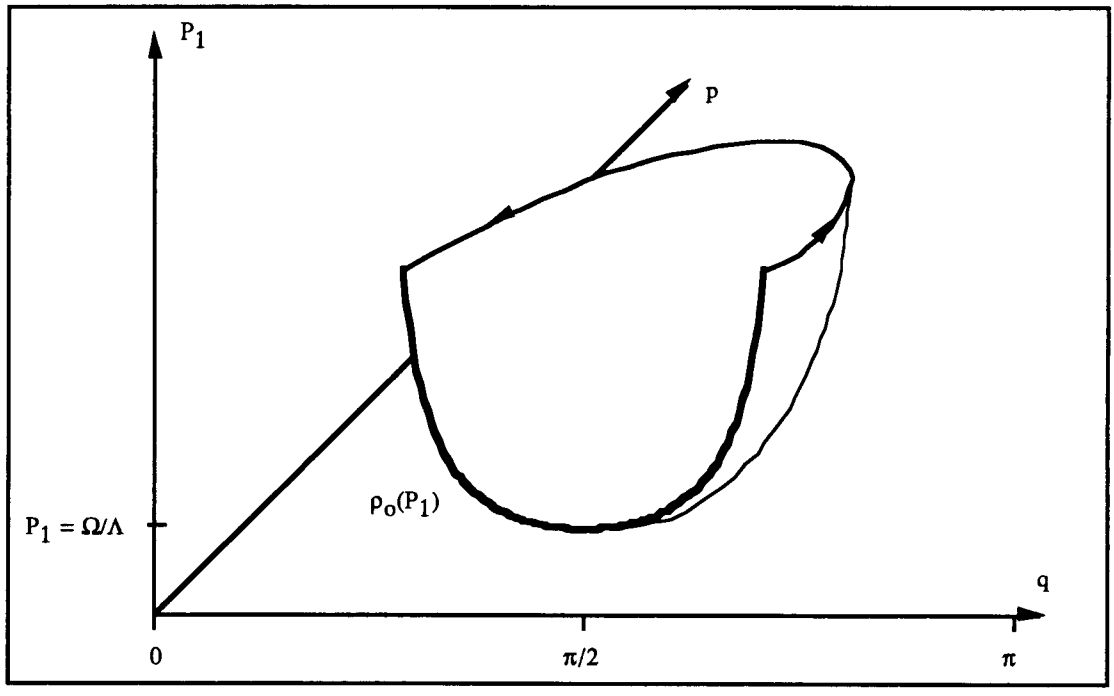

Figure 4. Schematic of the phase space structure of the unperturbed system (4.4a,b,c) for the same conditions as Figure 2b showing the one-dimensional manifold of hyperbolic fixed points $\rho_o(P_1)$ and the surface of separatrices containing the stable and unstable manifolds of ρ_o.

$$P_1(t) = P_1 = \text{ constant} \tag{4.17a}$$

$$Q_1(t) = \int \frac{\partial \overline{H}}{\partial P_1}\left(\gamma = 0, \rho_o(P_1), P_1\right) dt = \frac{2P_1 t}{\beta} + Q_{10}. \tag{4.17b}$$

So M has the structure of a one parameter family of one-tori. The tori on M for fixed $P_1 = \overline{P}_1$ are denoted as

$$\tau(\overline{P}_1) \equiv \left\{(\boldsymbol{q}, P_1, Q_1) \in \Re^2 \times P_1 \times \Re^1 \,|\, \boldsymbol{q} = \rho_o(P_1), P_1 = \overline{P}_1\right\}. \tag{4.18}$$

4b. The perturbed system

The perturbed system is studied next. By Proposition 4.1.16 [Wiggins, 1988], the perturbed system (4.1) possesses a two dimensional normally hyperbolic locally invariant manifold M_γ denoted as

$$M_\gamma = \left(\rho_\gamma(P_1), Q_1\right), \quad P_1 > \frac{\Omega}{\Lambda}, \quad \rho_\gamma(P_1) = \rho_o(P_1) + O(\gamma), \tag{4.19}$$

and M_γ has local stable and unstable two dimensional manilfolds. (Note that the dimensions of the stable and unstable manifolds of M and M_γ differ.) The procedure is to determine if M_γ contains any periodic orbits and then to determine whether or not the stable and unstable manifolds of these periodic orbits intersect by calculating the Melnikov function.

The flow on M_γ. There must be recurrent (periodic) motions on M_γ in order to apply the Melnikov method. For a dissipative system, which Wiggins [1988] denotes as his System I, the recurrent motions are found by averaging the perturbed $\dot{P}_1$ equation and finding its fixed point. [See Proposition 4.1.6, Wiggins, 1988 or Proposition 2.2, Wiggins and Holmes, 1987.] This procedure was followed by Allen, Samelson, and Newberger [1991] for their quasi-geostrophic flow problem which was of type System I. This procedure would need to be followed here if dissipation were included in the cross-wave problem. However, the perturbations in (4.1) are Hamiltonian since dissipation has not been included, and as mentioned earlier equations (4.1) are an example of System III [Wiggins, 1988]. Recurrent motions are guaranteed on M_γ if [Theorem 4.1.17, Wiggins, 1988]:

$$\det\left[\frac{\partial^2 \overline{H}}{\partial P_1^2}\left(\gamma = 0, \rho_o(P_1), P_1\right)\right] \neq 0. \tag{4.20}$$

Applying (4.20) to (4.3) and evaluating on the manifold of hyperbolic fixed points (where $p = 0$),

$$\frac{\partial^2 \overline{H}}{\partial P_1^2}\left(\gamma = 0, \rho_o(P_1), P_1\right) = \frac{2}{\beta}. \tag{4.21}$$

The nondegeneracy requirement is satisfied and recurrent motions exist on M_γ; the Melnikov function may be calculated.

Calculation of the Melnikov function. The Melnikov function is now calculated in order to determine if the two dimensional stable and unstable manifolds of the periodic orbits intersect in the three dimensional energy surfaces given by the level sets of (3.43). In this case the Melnikov function is a scalar and is given by

$$M(Q_{10}) = -\int_{-\infty}^{\infty} \left[\frac{\partial H^\gamma}{\partial Q_1}\right]_{q_h, p_h, Q_{1h}, \overline{P}_1} dt \tag{4.22}$$

[Wiggins, 1988, equations (4.1.92) and (4.1.85)] where

$$H^\gamma = \left[\frac{f_1}{2\varepsilon}\sqrt{\frac{b\left(P_1^2 - p\right)}{2\beta\xi}}\sin\frac{Q_1}{P_1} + \frac{(1-2\beta)}{4\beta\xi}\, p \sin\left(\frac{Q_1}{P_1} + 2q\right)\right]. \tag{4.23}$$

Equation (4.22) applies to System III and represents the measurement of the distance between the stable and unstable manifolds. Careful reading of Chapter 4 in Wiggins [1988] shows several forms of the Melnikov function that differ slightly for Systems I, II, and III with (4.22) applying only for System III. Furthermore, the Melnikov function may be a vector, depending on the dimensions of n and m in (4.2). For the case of System III, $n = 1$, and $m = 1$ the Melnikov function has only one component and may be computed by (4.22). (See examples 4.2ci, ii, and 4.2d in Wiggins, 1988 for uses of the above form of the Melnikov function.)

The Melnikov function (4.22) for the cross-wave problem is given by

$$M(Q_{10}) = -\int_{-\infty}^{\infty} \left[\frac{f_1}{2\varepsilon P_1}\sqrt{\frac{b\left(P_1^2 - p\right)}{2\beta\xi}}\cos\frac{Q_1}{P_1} + \frac{(1-2\beta)p}{4\beta\xi P_1}\cos\left(\frac{Q_1}{P_1} + 2q\right)\right]_{q_h, p_h, Q_{1h}, \overline{P}_1} dt. \tag{4.24}$$

Rather than substituting equations (4.11) and (4.12) into (4.24) to evaluate the Melnikov function on the heteroclinic orbit, equation (4.24) is evaluated first on Q_{1h} using (4.13) and then on $\overline{P}_1$,

$$M(Q_{10}) = -\int_{-\infty}^{\infty} \left[\frac{f_1}{2\varepsilon \overline{P}_1} \sqrt{\frac{b(\overline{P}_1^2 - p)}{2\beta\xi}} \cos\left(\frac{Q_{10}}{\overline{P}_1} - 2q + \frac{2t}{\beta} \right) + \frac{(1-2\beta)p}{4\beta\xi\overline{P}_1} \cos\left(\frac{Q_{10}}{\overline{P}_1} + \frac{2t}{\beta} \right) \right]_{q_h, p_h} dt. \tag{4.25}$$

Equation (4.25) is then expanded with various angle sum and multiple angle identities. The evaluation of $M(Q_{10})$ on q_h will then use (4.10a,b) for $\cos 2q_h$ and $\sin 2q_h$ rather than (4.12) for q_h. Analyzing Figure 3 for the cases $t = 0$ and the small time increments $t = \pm\delta t$, the signs of the square roots used in equations (4.10) are

$$\cos 2q_h = -\frac{\Omega}{\Lambda\sqrt{P_1^2 - p}} \quad \text{for} \quad -\infty \le t \le \infty, \tag{4.26a}$$

$$\sin 2q_h = +\sqrt{1 - \frac{\Omega^2}{\Lambda^2(P_1^2 - p)}} \quad \text{for} \quad 0 \le t \le \infty, \tag{4.26b}$$

$$\sin 2q_h = -\sqrt{1 - \frac{\Omega^2}{\Lambda^2(P_1^2 - p)}} \quad \text{for} \quad -\infty \le t \le 0. \tag{4.26c}$$

The Melnikov function is integrated in time from $-\infty$ to ∞, over which $\cos 2q_h$ is even and $\sin 2q_h$ is odd by (4.25). Recalling also that $\cos 2t/\beta$ is even and $\sin 2t/\beta$ odd, and keeping only even functions in (4.25), the Melnikov function is the sum of the following three components:

$$M(Q_{10}) = 2\cos\frac{Q_{10}}{\overline{P}_1}(I_1 + I_2 + I_3) \tag{4.27}$$

$$I_1 = -\frac{(1-2\beta)}{4\beta\xi\overline{P}_1} \int_0^{\infty} p_h \cos\frac{2t}{\beta}\, dt, \tag{4.28a}$$

$$I_2 = \frac{f_1\Omega}{2\varepsilon\overline{P}_1\Lambda}\sqrt{\frac{b}{2\beta\xi}} \int_0^{\infty} \cos\frac{2t}{\beta}\, dt, \tag{4.28b}$$

$$I_3 = -\frac{f_1}{2\varepsilon\overline{P}_1\Lambda}\sqrt{\frac{b}{2\beta\xi}} \int_0^{\infty} \sqrt{\Lambda^2(\overline{P}_1^2 - p_h) - \Omega^2}\, \sin\frac{2t}{\beta}\, dt. \tag{4.28c}$$

These components are evaluated explicitly in Appendix I and are:

$$I_1 = -(1-2\beta)\pi\left\{4\beta^2\xi\overline{P}_1\Lambda^2\varepsilon^2\sinh\left(\frac{\pi}{\beta\varepsilon\sqrt{\Theta}}\right)\right\}^{-1}, \tag{4.29a}$$

$$I_2 = 0. \tag{4.29b}$$

$$I_3 = -\frac{f_1\sqrt{\Theta}}{2\varepsilon\overline{P}_1\Lambda}\sqrt{\frac{b}{2\beta\xi}}\left[-\frac{\beta}{2}+\frac{\pi}{2\varepsilon\sqrt{\Theta}}\left(\sinh\frac{\pi}{\varepsilon\beta\sqrt{\Theta}}\right)^{-1}\right] \tag{4.29c}$$

for all $\overline{P}_1^2 > \Omega^2/\Lambda^2$ and where Θ is defined as

$$\Theta = \left(\Lambda^2\overline{P}_1^2 - \Omega^2\right). \tag{4.30}$$

Since all of the Melnikov components in (4.27) are bounded and do not sum to zero, the Melnikov function $M(Q_{10}) = 0$ when

$$\cos\frac{Q_{10}}{\overline{P}_1} = 0, \quad Q_{10} = \overline{P}_1\pi(2n+1)/2, \quad n = 0,\pm1,\pm2,... \tag{4.31}$$

for all $\overline{P}_1^2 > \Omega^2/\Lambda^2$. Furthermore, (4.31) represents simple zeroes of the Melnikov function since

$$\frac{\partial M}{\partial Q_{10}} = -\frac{2}{\overline{P}_1}\sin\frac{Q_{10}}{\overline{P}_1}\left(I_1 + I_2 + I_3\right) \tag{4.32}$$

is never zero when (4.31) is satisfied. The stable and unstable manifolds of the corresponding hyperbolic periodic orbit intersect transversely yielding Smale horseshoes on the appropriate three dimensional energy surface. (See Theorems 4.1.19 and 4.1.20 in Wiggins, 1988.)

5. Summary and concluding remarks

In the original formulation of the model, the variables $q(t)$, $Q_1(t)$, and $Q_2(t)$ represent the velocity potential amplitudes of eigenfunctions describing the cross-wave potential ϕ_c and the progressive wave potential ϕ_p, equations (2.5a,b). These generalized coordinates, along with their conjugate momenta $p(t)$, $P_1(t)$, and $P_2(t)$, were put through a series of seven canonical transformations that ultimately expressed the Hamiltonian and evolution equations in a form in which the Melnikov method could be applied. The results of §4 provide the theoretical predictive criteria from the Melnikov function that cross-waves can be chaotic. In order to understand the Melnikov function results, a reversal of the canonical transformations is necessary.

Recall that it was noted in §3g that both the final set of transformed variables and the original set of variables were denoted the same, without any overmarks. As this is no longer convenient, the original set of variables will now be designated as

$$\left(q_{orig}, p_{orig}, Q_{1orig}, P_{1orig}, Q_{2orig}, P_{2orig}\right). \tag{5.1}$$

The final set of transformed variables will still be referred to as

$$\left(q, p, Q_1, P_1, Q_2, P_2\right). \tag{5.2}$$

Beginning with the first canonical transformations in equations (3.8), the original variables are expressed in terms of the primed variables; the primed variables are then expressed in terms of the action/angle variables (3.12); the process continues using the successive canonical transformations (3.17), (3.24), (3.29), (3.34), and (3.38), until the original canonical variables are all written as functions of the final set of variables which were used to apply the Melnikov method. The original variables are then expressed as

$$q_{orig} = \sqrt{\frac{2p}{b\xi}} \sin\left(\frac{Q_1}{2P_1} + q + \frac{3t}{2\beta}\right), \tag{5.3a}$$

$$p_{orig} = \sqrt{2b\xi p} \cos\left(\frac{Q_1}{2P_1} + q + \frac{3t}{2\beta}\right), \tag{5.3b}$$

$$Q_{1orig} = \sqrt{\frac{P_1^2 - p}{2b\beta\xi\Gamma^2}}\sin\left(\frac{Q_1}{P_1} + \frac{3t}{\beta}\right) + \sqrt{\frac{2P_2}{4\Gamma^2 b\beta\xi}}\sin\left(2Q_2 + \frac{3t}{\beta}\right), \tag{5.3c}$$

$$P_{1orig} = \sqrt{\frac{P_1^2 - p}{2b\beta\xi\Gamma^2}}\cos\left(\frac{Q_1}{P_1} + \frac{3t}{\beta}\right) + \sqrt{\frac{2P_2}{4\Gamma^2 b\beta\xi}}\cos\left(2Q_2 + \frac{3t}{\beta}\right), \tag{5.3d}$$

$$Q_{2orig} = \sqrt{\frac{P_1^2 - p}{2b\beta\xi\Gamma^2}}\sin\left(\frac{Q_1}{P_1} + \frac{3t}{\beta}\right) - \sqrt{\frac{2P_2}{4\Gamma^2 b\beta\xi}}\sin\left(2Q_2 + \frac{3t}{\beta}\right), \tag{5.3e}$$

$$P_{2orig} = \sqrt{\frac{P_1^2 - p}{2b\beta\xi\Gamma^2}}\cos\left(\frac{Q_1}{P_1} + \frac{3t}{\beta}\right) - \sqrt{\frac{2P_2}{4\Gamma^2 b\beta\xi}}\cos\left(2Q_2 + \frac{3t}{\beta}\right). \tag{5.3f}$$

Note that q_{orig} and p_{orig} depend only on q, p, Q_1, and P_1 and not on Q_2 and P_2.

As mentioned in §4, the successive canonical transformations were applied to the system because the evolution equations obtained from the original Hamiltonian (3.5) were far too complicated to compute a homoclinic orbit; this separatrix may now be calculated.

A heteroclinic orbit in the final variables can be calculated using equations (4.11) - (4.13) for any constant value of $P_1 > \Omega/\Lambda$, and in the transformed system the heteroclinic orbit looks like an upside down letter "U" or the intersection mark "$\cap$" from set theory. Figure 5 shows that this $\cap$-shaped heteroclinic orbit becomes a homoclinic orbit in the (q_{orig}, p_{orig}) phase plane. The time zero point is indicated and corresponds to the time zero location at the top of the $\cap$-shaped orbit as noted in Figure 3. The trajectory shown in Figure 5 consists of two spirals; a counterclockwise spiral for negative time and a clockwise spiral for positive time. The origin represents the saddle points at $t = \pm\infty$. The parameter conditions used in Figure 5 are $\varepsilon = 0.25$, $\Omega = -.0025$, $P_1 = 1$, $b = 1$, and $\xi = 1.6441$. These values are similar to those used for Figures 2b and 3, except for b and ξ, which were chosen to better illustrate the spiral motion.

The homoclinic orbit shown in the (q_{orig}, p_{orig}) phase plane of Figure 5 actually occurs in the six dimensional phase space of all the original canonical variables, and in the full six dimensional space the trajectory would not cross itself. Figure 6 clarifies the trajectory of the homoclinic orbit since the time axis is added for perspective. Figure 6 also shows that the spiral is clockwise about the positive time axis and counterclockwise about the negative

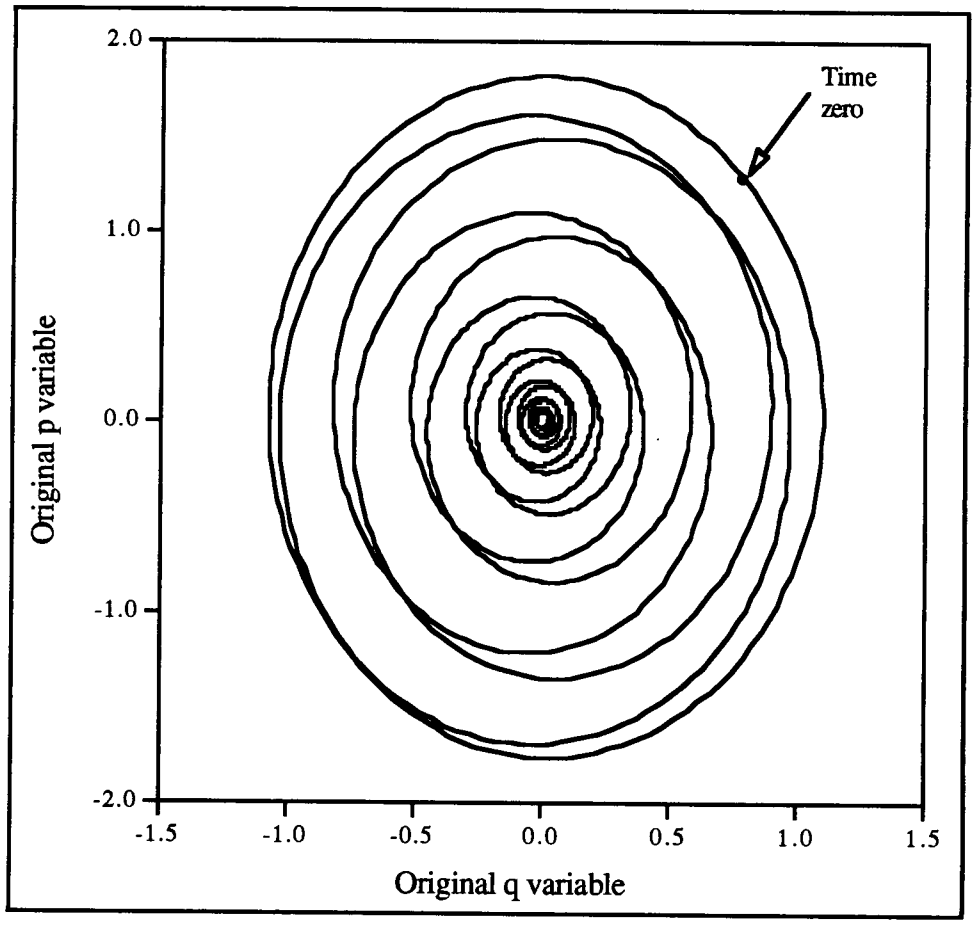

Figure 5. The heteroclinic orbit in the original (q,p) phase plane. $\Omega = -0.0025$, $\varepsilon = 0.25$, $P_1 = 1$, $b = 1$, and $\xi = 1.6441$.

time axis, and at $t = \pm\infty$ there are saddle points for $\left(q_{orig}, p_{orig}\right)$ = *(0,0)*. Figure 6 also graphically justifies the necessity of the canonical transformations; an equation describing the trajectory in Figure 6 would be very difficult to obtain.

Chaotic cross-wave motions occur about the homoclinic trajectory shown in Figure 6. Time series of these motion may also be calculated.

The final set of perturbed evolution equations (4.1) are integrated in time using a fourth-order Runge-Kutta technique, starting from a set of initial conditions on the heteroclinic orbit. The final variable Q_2 is also determined by integrating (3.44e),

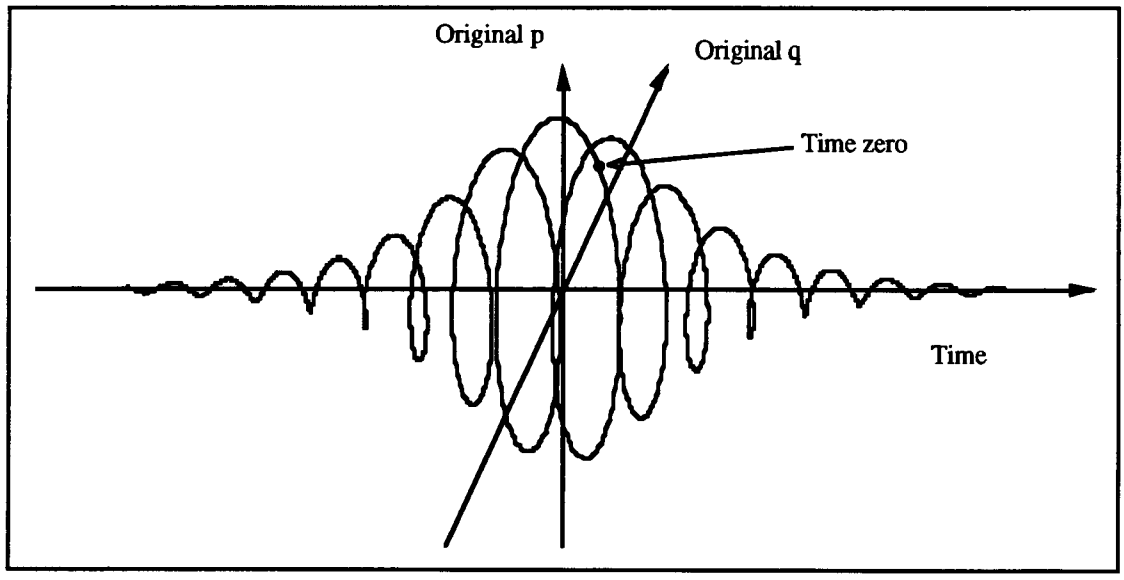

Figure 6. The heteroclinic orbit of Figure 5 with the time axis added for perspective.

$$Q_2 = -\frac{t}{\beta} + Q_{20}. \tag{5.4}$$

P_2 may be any value since $\dot{P}_2 = 0$ in (3.44f). Using the same parameters as in Figures 2b and 3 and a perturbation parameter $\gamma = 0.5$, $f_1 = 1$, $\Gamma = 1$, $P_2 = 1$, $Q_{20} = 0$, and the initial conditions of the time zero location at the top of the heteroclinic orbit in Figure 3, the time series of q_{orig} and Q_{1orig} are as plotted in Figure 7. The time series are calculated from equations (5.3a,c) after (4.1) are integrated. The time series indicate that for regular motion in Q_{1orig} (corresponding to periodic wavemaker forcing) the q_{orig} motion becomes irregular or chaotic.

Figure 8 is the time series of the sum of the cross-wave and progressive wave time dependencies. Recall that the velocity potentials from (2.25a,b) are

$$\phi_c = q_{orig}(t)\cos(y-b)e^z, \quad \phi_p = \left[Q_{1orig}(t)\cos x + Q_{2orig}(t)\sin x\right]e^{z/\beta^2}.$$

At the still water level $z = 0$, at a cross-wave crest location $\cos(y-b) = 1$, and at integer multiples of the progressive wave wavelength where $\cos x = 1$ and $\sin x = 0$, the total

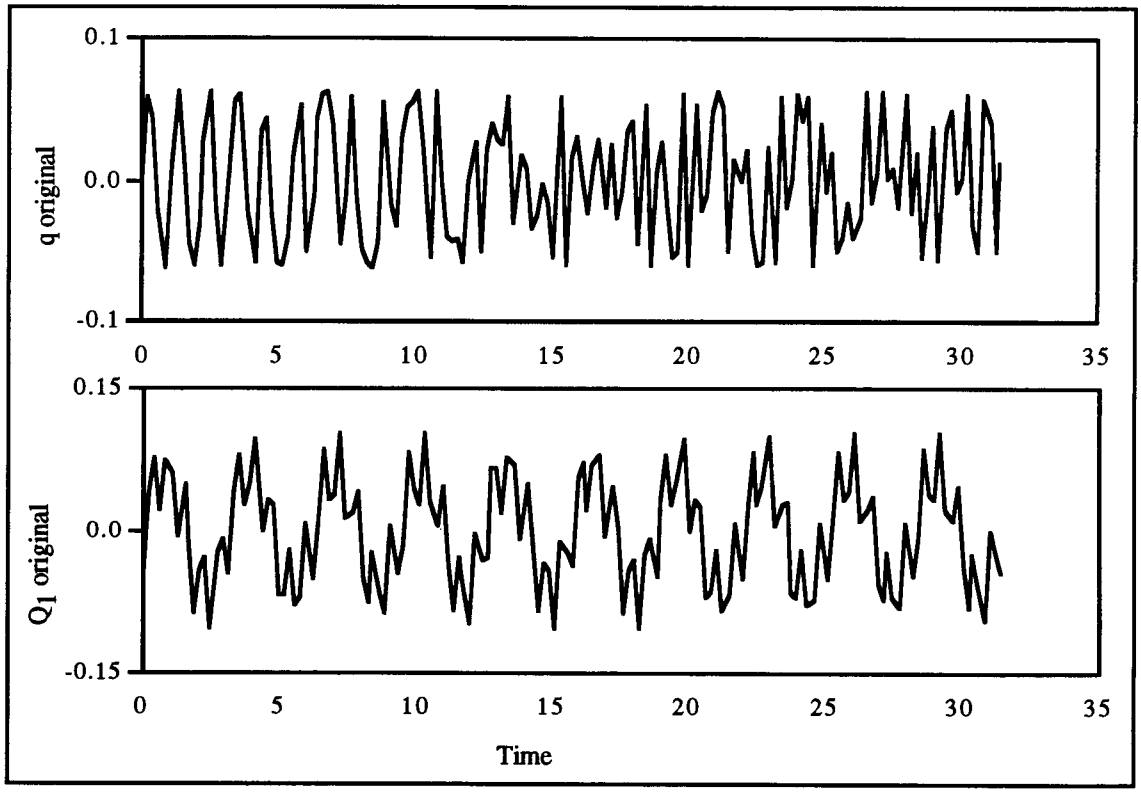

Figure 7. Time series of the original q and Q_1 variables showing chaotic behavior of the cross-wave variable q. Parameters used are the same as for Figures 2b and 3 with $\gamma = 0.5$, $f_1 = 1$, and $\Gamma = 1$. The initial conditions used for the final transformed variables are the time zero conditions on the heteroclinic orbit, $q = \pi/2$, $p = 0.4593$, $P_1 = 1$, and $Q_1 = 3\pi/2$.

velocity potential $\phi = \phi_c + \phi_p$ is the sum of q_{orig} and Q_{1orig}, as shown in Figure 8 for the two time series of Figure 7.

The phase portraits in Figure 2 and the solutions for p, q_1, and Q_1 on the heteroclinic trajectory, (4.11) - (4.13), were compared to Holmes' [1986] results in §4 and found to be similar. However, the heteroclinic trajectory of the original system, Figures 5 and 6, and the time series of q_{orig} and Q_{1orig} in Figure 8 do not agree with Holmes' results.

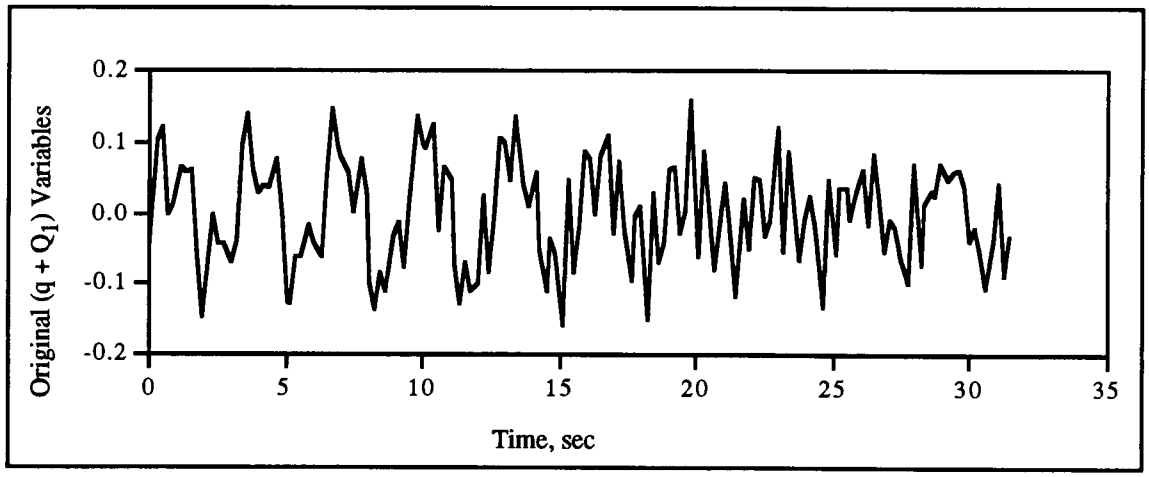

Figure 8. Time series of the sum of the original q and Q_1 variables. The sum is of the two time series shown in Figure 7.

Holmes [1986, p.379, Figure 2] shows the heteroclinic trajectory of his transformed system becoming the classical figure-eight homoclinic loop in his original system. Reversing Holmes' two canonical transformations for one pair (q_1, p_1) of his original coordinates results in their expression as functions of Holmes' final variables (Q_1, P_1, Q_2, P_2),

$$q_1 = \sqrt{\frac{2\omega_1 P_1}{g}} \cos(Q_1 + Q_2 + \tfrac{1}{2}\omega t), \tag{5.5a}$$

$$p_1 = -\sqrt{\frac{2gP_1}{\omega_1}} \sin(Q_1 + Q_2 + \tfrac{1}{2}\omega t). \tag{5.5b}$$

These equations are similar in form to the cross-wave equations (5.3a,b) above; these equations are not conducive to plotting a figure-eight. It appears that Holmes assumed the shape of the homoclinic orbit in his original system rather than calculating it. Furthermore, if the original system did contain a classical figure-eight homoclinic orbit, canonical transformations would be unnecessary since solutions to such orbits exist in the literature [Guckenheimer and Holmes, 1983, p.191, e.g.].

Holmes also plots time series of his two original coordinates q_1 and q_2 [Holmes, 1986, p.381, Figure 3]. His time series shows one mode oscillating at ω and the other at $\omega/2$, and a slowly varying envelope superimposed over both time series. Holmes describes this envelope as indicating an irregular exchange of energy between his two modes. Both of these time series differ significantly from those of Figure 8. As before, there is no clear evidence that Holmes actually computed these two time series.

Some specific remarks about the Melnikov function calculated in §4 are now in order.

1. It is important to remember that the Melnikov function is not valid exactly at resonance, $\Omega = 0$, because there is no heteroclinic orbit connecting saddle points under this condition.

2. The Melnikov function has an infinite number of zeroes for $\overline{P}_1^2 > \Omega^2/\Lambda^2$ as described in §4. However, as $\overline{P}_1^2 \to \Omega^2/\Lambda^2$, $\Theta \to 0$ from (4.30) and the Melnikov components I_1 and I_3 in (4.29a,c) approach infinity. The condition $\overline{P}_1^2 \to \Omega^2/\Lambda^2$ represents a case of weak chaos.

3. The type of wavemaker motion has no effect on whether or not the system is chaotic. The wavemaker type is characterized by the parameter f_1, defined in Table 1 of Appendix I as an integral of the wavemaker depth function *f(z)*,

$$f_1 = \int_{-\alpha}^{0} f(z)\, e^{z/\beta^2}\, dz. \tag{5.6}$$

As f_1 is finite for any physically realistic wavemaker, the Melnikov component I_3 (4.29c) which contains the parameter f_1 is finite. Furthermore, since I_3 is the only Melnikov component to contain the wavemaker parameter f_1, even if $f_1 = 0$ for some *f(z)*, chaos will still occur for the condition given by (4.31), $\cos\left(Q_{10}/\overline{P}_1\right) = 0$. The wavemaker parameter affects the time series obtained by integrating equations (4.1), but does not affect the zeroes of the Melnikov function and so does not determine if the cross-waves are chaotic.

4. Since damping was not included in the model, the Melnikov calculation allows for chaotic behavior for any non-zero forcing parameter γ. This result is not supported by experimental data (see §1), where a minimum wavemaker forcing (and thus a minimum progressive wave amplitude) must be exceeded to generate cross-waves. The parameter Γ, defined in (2.15d) as the ratio of the progressive wave amplitude to the cross-wave amplitude, does not appear in the Melnikov function; Γ ceased to appear in the Hamiltonian after the action/angle transformations. The Melnikov function results thus do not supply any information about the relative amplitudes of the cross-waves and progressive waves.

5. Finally, the Melnikov calculation provided no information on chaotic behavior for frequency ratios other than $\omega_p' : \omega_c' = 2:1$. This is because in the Hamilton-Jacobi transformation of §3c, the frequency ratio had to be specified as 2:1 in order to retain autonomous nonlinear terms. A frequency ratio of 1:1 requires that higher order terms be retained in the Taylor series expansions of §2. This result agrees with those of Holmes [1986] and Garrett [1970].

The results of new cross-wave experiments from the O. H. Hinsdale Wave Research Laboratory at Oregon State University will be compared to these theoretical results in a forthcoming paper.

Chapter III. Experimental Results

1. Cross-wave experiments in a long rectangular channel

Cross-waves are parametrically excited standing surface gravity waves that oscillate in a direction transverse to the wavemaker forcing. The cross-waves of interest here are generated in a long rectangular channel with rigid side walls, a horizontal flat bottom, a wavemaker at one end, and a sloping beach at the other. The cross-wave forms in addition to a progressive wave that travels down the channel from the wavemaker and dissipates on the beach.

The progressive wave frequency ω_p is equal to that of the wavemaker forcing and the deep water dispersion relation $\omega_p^2 = gk$ provides the wavenumber k associated with the frequency ω_p. The channel width determines the wavelengths $\lambda_{cn} = 2(\text{basin width})/n$ of possible cross-wave modes where n is the mode number and is equal to the number of half-wavelengths across the tank. The cross-wave frequency ω_{cn} is related to the wavelength by the deep water dispersion relation $\omega_{cn}^2 = g\kappa_n$, $\kappa_n = 2\pi/\lambda_{cn}$, where κ_n is the wavenumber of the cross-wave. The following general discussion based on Bogoliubov and Mitropolsky [1961] describes parametric resonance.

Assume the motion of a parametrically forced oscillator is described by Mathieu's equation

$$\ddot{x} + \sigma^2(1 - \varepsilon\cos\nu t)x = 0, \quad \varepsilon << 1. \tag{1.1}$$

Resonance occurs when the natural frequency σ is related to the parametric forcing frequency ν by $\sigma = N\nu/M$, N and M integers. Bogoliubov and Mitropolsky expand in perturbation series the displacement x, the time-derivative of the amplitude $\partial a/\partial t$, and the time derivative of the phase $\partial\theta/\partial t$, and solve by the method of successive approximations. An instability due to parametric resonance occurs for some range of parametric forcing

frequency ν and for some values of the nonlinearity parameter ε. In the parameter space defined by ν as the abcissa and ε as the ordinate, the region in which the parametric resonance occurs is called the zone of instability and is delineated by a neutral stability curve. A typical neutral stability curve is somewhat V-shaped. The primary (fundamental) resonance of $N = 1$ and $M = 2$ has the largest zone of instability (the widest V-shape). If the forcing frequency lies within the interval described by the zone, the instability (such as a cross-wave) will occur. The zone of instability thus determines the bandwidth of the resonance. Letting N vary and carrying out the perturbations, Bogoliubov and Mitropolsky show that the bandwidth of the zone of instability diminishes with order N as ε^N. They also show that the neutral stability curve minimum (the bottom of the V-shape) occurs at $\varepsilon = 0$ without damping and at higher values of ε when damping is included. This minimum value increases as N increases. Thus the primary resonance case $\sigma = \nu/2$ is of the most practical interest.

Laboratory experiments show that the amplitude of the cross-wave can be much larger than both the wavemaker forcing amplitude and the progressive wave amplitude. The wavemaker forcing will parametrically generate a cross-wave in the lab when two conditions are met: 1) some minimum amplitude of wavemaker forcing is exceeded, and 2) the wavemaker (and progressive wave) frequency ω_p is in some narrow bandwidth about $M\omega_{cn}/N$. Cross-waves generally have half of the frequency of the wavemaker forcing $\left(\omega_{cn} \approx \frac{1}{2}\omega_p\right)$, although additional resonances can occur. The general case explored in the cross-wave literature is that of the primary, $N = 1$ and $M = 2$.

Experimental studies of cross-waves in long channels began with Barnard and Pritchard [1972]. Stability diagrams were determined for various cross-wave modes; these diagrams indicate the regions in which cross-waves occur, each mode requiring some minimum amplitude of wavemaker forcing, and the cross-waves occur in a narrow band about a forcing frequency twice that of the cross-wave. Barnard and Pritchard also showed that the amplitude of the cross-wave varied with time, indicating a continual growth and

decay of the waves. Cross-wave amplitudes decreased with distance from the wavemaker. The channel used was 30.6 cm wide, the water depth was 16 cm, and the channel length was 270 cm; although the channel was long compared to its width and depth, it was also small enough that surface effects were important. In particular, an absorbent cotton bandage was placed on the wavemaker, the channel sides at the waterline, and on the beach to reduce the effects of uneven wetting. Water surface contamination was a crucial factor, necessitating skimming the water surface before each experimental run.

Lichter and Shemer [1986], Shemer and Lichter [1987], and Shemer and Kit [1989] all used a channel 1.2 m wide, 0.9 m deep, and 18 m long, where surface effects were negligible. All of these experiments studied the primary parametric resonance. Lichter and Shemer described the evolution of the wave energy spectrum with distance from the wavemaker. Shemer and Lichter classified different regions in the stability diagrams based on the presence or absence of an amplitude modulation. Shemer and Kit described the long-time modulation patterns of the cross-waves.

Underhill, Lichter, and Bernoff [1991] studied parametrically forced cross-waves and found three prominent frequencies present: the primary subharmonic and two slow temporal modulations. The stability diagrams were very precisely divided into regions where the cross-wave motion was periodic, quasi-periodic, or chaotic. As this channel was also fairly small (30.9 cm wide, 30 cm deep, and 121 cm long), surface tension effects were notable and a surfactant was added to the water. Shemer and Lichter [1987] also defined the neutral stability curve for a cross-wave with boundaries between steady, quasi-periodic, and chaotic behavior. Quasi-periodic behavior is motion that consists of two or more incommensurate frequencies. Chaotic behavior describes a motion that is sensitive to different initial conditions. Motion from one set of initial conditions cannot be used to predict the motion when the conditions are slightly varied.

A number of cross-wave experiments were performed in order to provide experimental evidence to support earlier theoretical results that cross-waves can be chaotic. The

theoretical analysis was an application of the Melnikov method to a model of cross-waves in a long rectangular channel [Chapter II]. Experimental evidence of chaos can be obtained by identifying five characteristics of chaotic motions [Moon, 1992]:

1) Sensitivity to initial conditions.

2) Broad Fourier spectrum from a single forcing frequency.

3) Fractal properties of the motion in phase space denoting a strange attractor.

4) Increasing complexity of regular motions as some experimental parameter is changed.

5) Transient or intermittent chaotic motions or nonperiodic bursts of irregular motion.

The fractal properties of the motion in the phase space (characteristic 3 above) are generally measured by the Poincaré map, which is a periodic sampling of the phase space variables. A single point in a Poincaré map indicates periodic motion; additional finite points show subharmonic oscillation; a closed curve indicates quasi-periodic motion; a fractal collection of points, or points filling a strange attractor, indicates chaotic motions. Underhill, Lichter, and Bernoff [1991] used the Fourier spectrum and the Poincaré map to identify chaotic motion in some of their experiments.

The experimental set-up is described in §2; the general results of the experiments are given in §3. Specific details of the experimental results are discussed as follows: §4 contains stability diagrams for primary resonances of modes 1, 2, and 4; §5 contains wave power spectra, Poincaré maps, and time series for some runs exploring the primary resonances of modes 2 and 4; §6 contains spectra and Poincaré maps for two runs looking for a secondary resonance for mode 2; §7 contains the results of the mode 1 primary resonance, which includes a case of simultaneous generation of modes 1 and 4.

2. Experimental set-up

The experiments were performed in the long wave channel at the O. H. Hinsdale-Wave Research Laboratory (OHH-WRL) at Oregon State University. The wave channel is 12 ft. wide, over 300 ft. long, and was filled to a water depth of 11.5 ft; surface tension effects were irrelevant. The end of the channel was a sloping beach. The wavemaker is full-draft, hinged at the bottom and operates with water on one side only. This channel is substantially larger than the ones used in any of the previous research mentioned. The most striking result of the cross-wave experiments was the simultaneous generation of cross-waves of the primary resonance $\omega_p:\omega_{cn} = 2:1$ and secondary resonance $\omega_p:\omega_{cn} = 1:1$, an effect which does not appear to have been reported previously.

Seven instruments recorded data for each run, located as shown in Figure 9. The first instrument recorded the wavemaker motion and the other six instruments recorded the water surface displacement. Three sonic profilers were located across the width of the channel near the wavemaker and three resistance wave gauges were located at various distances down the channel. There were 40 experimental runs each following the procedure below:

1. The water surface was allowed to settle to no motion.

2. The wavemaker motion would begin, holding a constant frequency and amplitude of motion.

3. Water surface displacement recordings began with the wavemaker motion.

4. There were 64 data points per wavemaker forcing period recorded for each instrument.

5. Wavemaker motion was stopped after a predetermined time, which was after 16384, 32768, or 65536 data points per instrument were recorded, corresponding to 256, 512, or 1024 forcing periods, respectively. Recording ceased when the wavemaker forcing ended.

6. The water surface was allowed to settle. This sometimes required two hours if a large cross-wave had been generated.

The initial conditions of the fluid domain are the water surface displacement and velocity at every location on the water surface. Although the water was allowed to settle between runs, it was not possible to obtain a perfectly motionless free surface. Each run was, by definition, begun with slightly different initial conditions; however, these initial conditions were never completely known. Sensitivity to initial conditions, characteristic 1 in §1, was not used as a diagnostic tool in these experiments since there is no way of knowing or specifying the entire set of displacements and velocities of the surface water particles.

The wavemaker forcing frequencies for the 40 experimental runs were chosen to study cross-waves of modes 1, 2, and 4. The frequencies of these modes were calculated from the deep water dispersion relation defined in §1:

$$\omega_{c1} = 2.903 \text{ s}^{-1}, \quad \omega_{c2} = 4.106 \text{ s}^{-1}, \quad \omega_{c4} = 5.807 \text{ s}^{-1}, \tag{2.1a,b,c}$$

$$f_{c1} = 0.462 \text{ Hz}, \quad f_{c2} = 0.653 \text{ Hz}, \quad f_{c4} = 0.924 \text{ Hz}. \tag{2.2a,b,c}$$

Note that

$$\omega_{c4} = 2\omega_{c1} \quad \text{and} \quad f_{c4} = 2f_{c1} \tag{2.3a,b}$$

because modes 1 and 4 are related by $\lambda_{c4} = \lambda_{c1}/4$ for any rectangular wave channel and for deep water

$$\omega_{c4} = \sqrt{g\kappa_4} = \sqrt{\frac{g2\pi}{\lambda_{c4}}} = \sqrt{\frac{g8\pi}{\lambda_{c1}}} = 2\sqrt{g\kappa_1} = 2\omega_{c1}. \tag{2.4}$$

In deep water the cross-wave mode frequencies are integer multiples of each other,

$$\omega_{c4} = 2\omega_{c1}, \quad \omega_{c8} = 2\omega_{c2}, \quad \omega_{c12} = 2\omega_{c3}, \quad \omega_{c16} = 2\omega_{c4}, \quad \ldots \tag{2.5a,b,c,d}$$

because the wavelengths are integer multiples of each other,

$$\lambda_{c1} = 4\lambda_{c4}, \quad \lambda_{c2} = 4\lambda_{c8}, \quad \lambda_{c3} = 4\lambda_{c12}, \quad \lambda_{c4} = 4\lambda_{c16}, \quad \ldots \tag{2.6a,b,c,d}$$

In intermediate depth water, where the dispersion relation is more complicated, the cross-wave mode frequency must be determined by

$$\omega_{cn} = \sqrt{g\kappa_n \tanh \kappa_n h} \tag{2.7}$$

where h is the water depth. In intermediate depth water, even though the cross-wave mode wavelengths are still related by (2.6), the cross-wave mode frequencies are not integer multiples of each other. Mode 1 has a wavelength of 24 ft., and in a water depth of 11.5 ft. does not quite meet the deep water condition $h > \lambda/2$. The mode 1 frequency calculated from (2.7) was $\omega_{c1} = 2.896\ s^{-1}$ and $f_{c1} = 0.461$ Hz, and so (2.3a) and (2.5a) are really $\omega_{c4} \approx 2\omega_{c1}$. All cross-wave modes other than $n = 1$ were strictly deep water waves.

As noted in §1, previous cross-wave experiments have concentrated on the primary resonance, $\omega_{cn} = \frac{1}{2}\omega_p$. These experiments include the secondary resonance, $\omega_{cn} = \omega_p$. A properly chosen single forcing frequency may excite one cross-wave mode as a primary resonance and an additional mode as a secondary resonance. For example, if

$$\omega_p = 2\omega_{c1} = \omega_{c4} \tag{2.8}$$

generates cross-waves of modes 1 and 4 simultaneously (as occurred in one of the experiments) then mode 1 is a primary resonance and mode 4 is a secondary resonance.

Each of the 40 experimental runs had a forcing (and progressive wave) frequency ω_p in some small bandwidth about one of the four conditions shown below:

1) $\omega_p \approx 2\omega_{c2}$,
2) $\omega_p \approx \omega_{c2}$,
3) $\omega_p \approx 2\omega_{c4}$,
4) $\omega_p \approx 2\omega_{c1} \approx \omega_{c4}$.

The placement of the measurement devices for each of the four conditions above are shown in Figure 9; Figure 9a for conditions 1) and 2); Figure 9b for condition 3); and Figure 9c for condition 4) above.

The gauges on the centerline of the channel shown in Figure 9a were positioned to measure peaks of mode 2; the other two locations near the wavemaker were positioned to record peaks of mode 8, should it occur. All locations shown in Figure 9b will record peaks of mode 4. Figure 9c shows a gauge 0.5 ft. from the side wall, which is as close as a gauge could be to the side, where mode 1 peaks occur. The gauges located 3 ft. from the

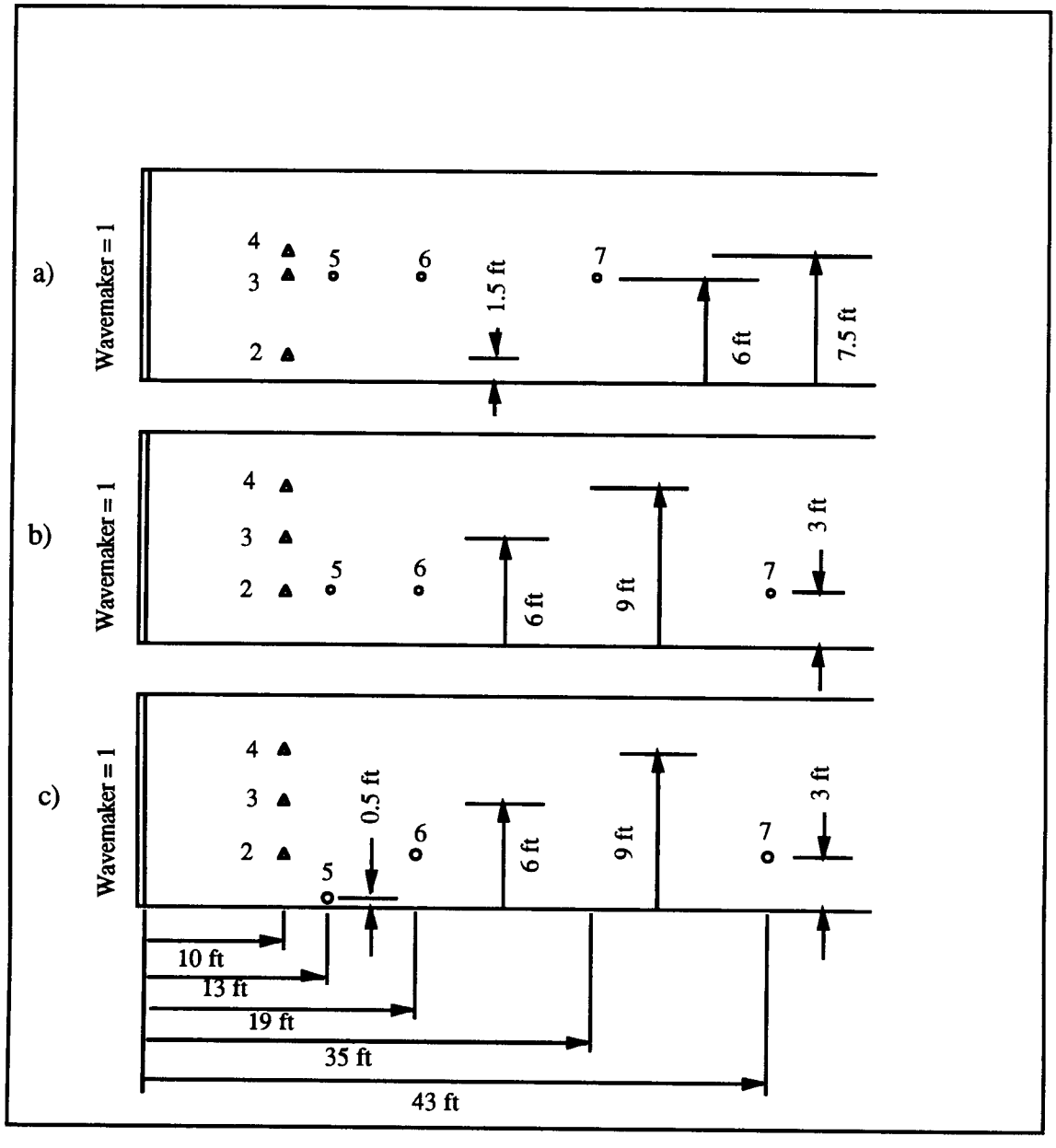

Figure 9. Wave gauge locations for sonic profilers (triangles) and resistance wave gauges (circles). a) Mode 2 runs, b) mode 4 runs, and c) mode 1 runs. Numbers refer to instrument numbers during data collection.

side in Figure 9c are at mode 4 peak locations and where mode 1 has an intermediate amplitude. The centerline location in 9c is a mode 1 node, but a mode 4 peak.

The sonic profilers were placed to determine if a secondary resonance cross-wave mode appeared. Since a secondary resonance cross-wave would have the same frequency as the forcing, its peak would be indistinguishable from that of the progressive wave in the wave power spectrum, and must be detected instead by comparing the water surface displacement measurements from the sonic profilers.

The transducers (sonic profilers and resistance wave gauges) were calibrated to convert volts to displacement. Signal conditioning adjusts the voltage to be in a -5.0 to +5.0 range. Rockland analog filters removed noise above the folding frequency. Analog signals from the sonic profilers were not filtered because of wild points. The analog voltage was converted to a digital value between 0 and 4095 using a PDP-11 with a 12 bit A/D converter.

Unfortunately, the data recorded from the sonic profilers, instruments 2, 3, and 4 shown as triangles in Figure 9, was extremely noisy. Most data files exceeded 90% bad points. The sonic profilers were positioned to detect secondary resonance cross-waves that may be superimposed on the primary resonance cross-wave and the progressive wave. The secondary resonance wave is of the same order amplitude as the progressive wave, both of which are an order of magnitude smaller than the primary resonance wave. Thus only subtle differences were expected in measurements between instruments 2, 3, and 4. While interpolation techniques exist to estimate values for bad data points, there were so many bad points that interpolating for subtle variations seemed suspect in a search for chaos. Therefore, the sonic profiler data was not used for any analyses. This means that there was no way to determine the amplitude of any secondary resonance cross-waves from these data.

Table 1 in Appendix II is a list of the wavemaker frequency and amplitude for each of the 40 runs. The table also includes comments of observations made during the experiments.

3. General results

The low numbered modes 1, 2, and 4 were studied because these modes can be easily generated in the long wave channel used at the OHH-WRL. Generating higher modes requires smaller waveboard strokes than for lower modes. The smallest waveboard stroke used to generate mode 4 was 0.3 in., a very small value for a water depth of 11.5 ft.

The cross-waves appearing as a primary resonance had amplitudes about an order of magnitude larger than the progressive wave amplitudes. This was a problem for mode 1 cross-waves. While the waveboard strokes used to produce mode 1 were well within the capabilities of the lab, the mode 1 cross-waves generated were so large that the wave resistance gauges were occasionally overtopped and some water sloshed over the side walls of the tank. This prevented a detailed analysis of the neutral stability curve for mode 1.

The cross-waves generated as a primary resonance contained a slow streamwise modulation which was also reported by Underhill, Lichter, and Bernoff [1991] and by Barnard and Pritchard [1972]. Underhill, Lichter, and Bernoff described this modulation as a 'standing wave whose amplitude envelope across the width of the tank was uniform, but grew and decayed with a low frequency'. Barnard and Pritchard described this modulation as a wave that detaches itself from the wavemaker and propagates along the wave channel. Photographs of this modulation for mode 2 are shown in Figure 10.

Underhill, Lichter, and Bernoff [1991] also discuss a second slow modulation that was spanwise. While no clean modulation of this type was seen in these experiments, the spanwise waves became less regular as the wavemaker forcing increased.

The amplitudes of the cross-waves generated as a secondary resonance were somewhat smaller than the progressive wave amplitudes and decreased in amplitude with distance from the waveboard. These secondary resonance waves could be seen for two runs for mode 2 and one run for mode 4. The presence of these waves could not be determined from the sonic profiler data because of noise, but photographs and observations made

during the experiments indicated their presence. Figure 11 shows a mode 2 cross-wave generated as a secondary resonance.

Primary resonances of cross-waves appeared much earlier as the wavemaker forcing amplitude increased. At large forcing amplitude the cross-waves appeared almost immediately. The run times of the experiments were limited in order to avoid very much contamination by any wave reflections from the beach.

a)

b)

Figure 10. Streamwise modulation for a mode 2 cross-wave generated as a primary resonance. The wavemaker frequency is $f_{wm} = 2f_{c2} = 1.307$ Hz. The cross-wave is seen superimposed over the crests of the progressive wave which has a significantly smaller amplitude than that of the cross-wave: a) towards wavemaker. b) away from wavemaker.

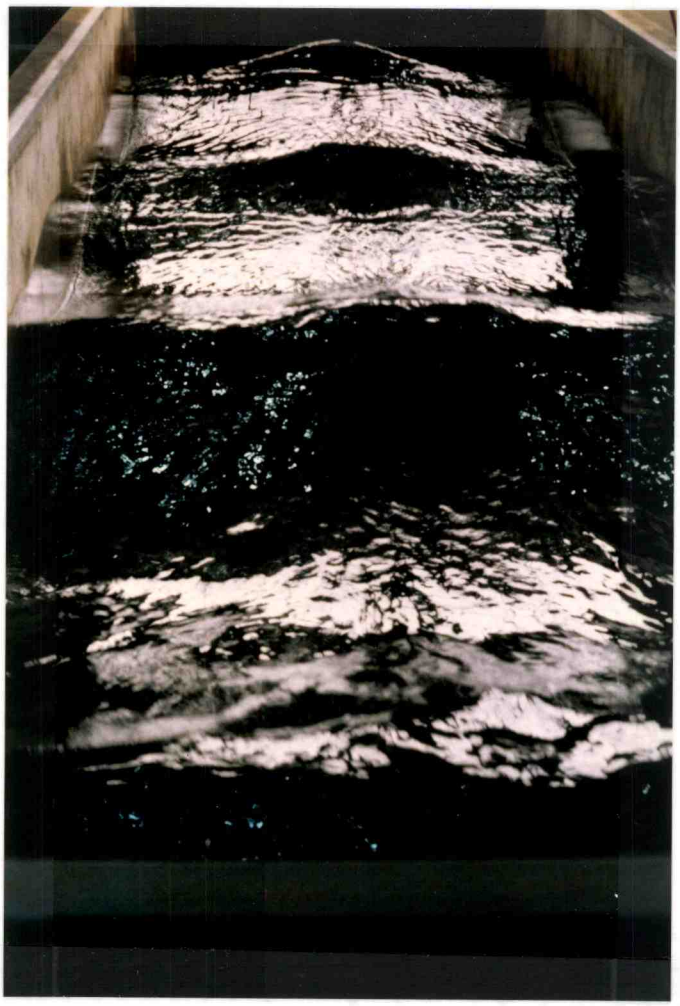

Figure 11. Mode 2 cross-wave generated as a secondary resonance. The wavemaker frequency is $f_{wm} = f_{c2} = 0.653$ Hz. The crests of the cross-wave can be seen superimposed over the progressive wave crests.

4. The cross-wave instability

Garrett [1970] showed that cross-waves may be modeled by a form of Mathieu's equation

$$\ddot{x} + \sigma^2(1 - \varepsilon \cos \upsilon t)x = 0, \quad \varepsilon << 1, \tag{3.1}$$

that allows for parametric resonance in some bandwidth about $\sigma = N\upsilon/M$, N and M integers with the primary resonance at $N = 1$, $M = 2$. The nonlinearity parameter ε in (3.1) is related to (but not equal to) the wavemaker forcing parameter, denoted as

$$\gamma = kS, \tag{3.2}$$

where k is the wavenumber of the progressive wave and S the amplitude of the wavemaker displacement.

If the forcing frequency lies within a narrow bandwidth about $\omega_{cn} = \frac{1}{2}\omega_p$, then cross-waves will appear in the system. The bandwidth over which cross-waves occur is the zone of instability. The wavemaker forcing frequency and amplitude are specified parameters. Changing either parameter only slightly can greatly affect the complexity of the motion if a cross-wave is generated. Thus the stability diagrams can be used to identify chaotic characteristic 4 listed in §1.

Before the 40 experimental runs were recorded, there was about a week of laboratory time spent video taping and photographing various cross-waves in order to determine the best set of parameters (wavemaker forcing frequency and amplitude) to use for the 40 runs. During the course of this pre-run testing it was noted that experimental repeatability was difficult in the vicinity of the neutral stability curve.

Figures 12, 13, and 14 are the stability diagrams obtained from the experimental runs for modes 1, 2, and 4. The dotted line is an estimate of the neutral stability curve; the numbers beside each data point indicate the run number of the experiment.

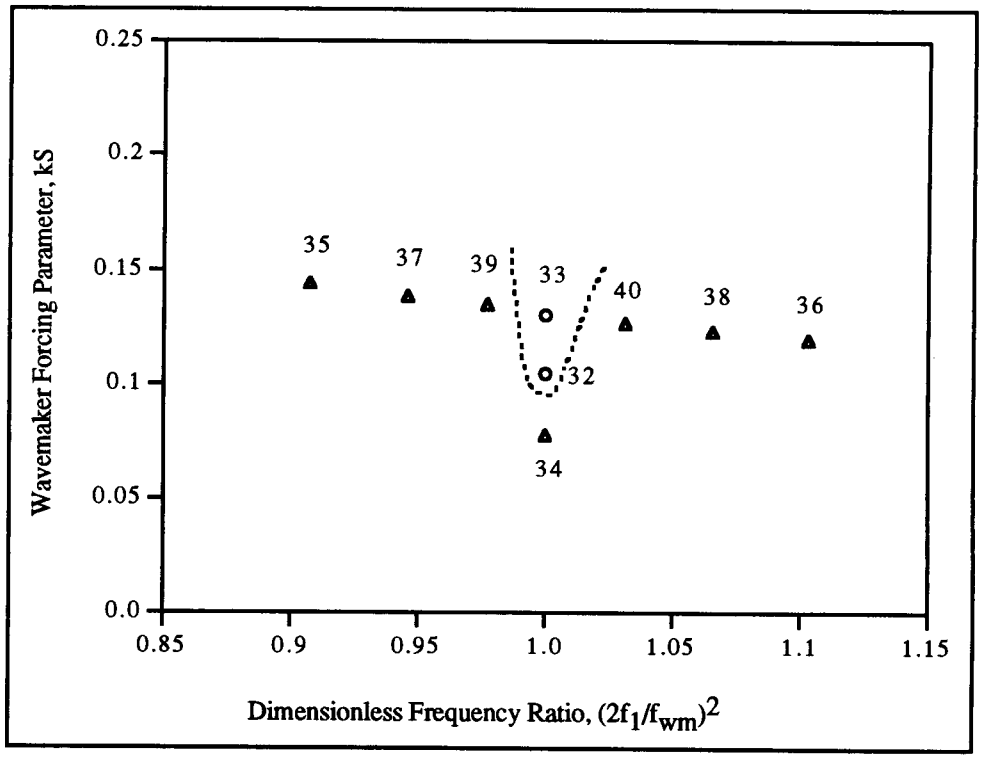

Figure 12. Stability diagram for mode 1 cross-waves. Numbers refer to the experiment run numbers for mode 1 (circles) and no cross-waves (triangles).

Increasing the wavemaker forcing parameter γ for mode 1 was not possible because then the cross-wave overtopped the walls of the channel. The curve in Figure 12 is only the lower portion of the neutral stability curve for mode 1 in this channel. The curve in Figure 12 indicates that the neutral stability curves are somewhat pointed and no rounded at the minimum.

The stability diagram for mode 2 shown in Figure 13 indicates how difficult it is to determine the neutral stability curve. For example, run 5 generated a cross-wave but run 6 did not; this makes it difficult to determine where the curve should actually be drawn between these two points.

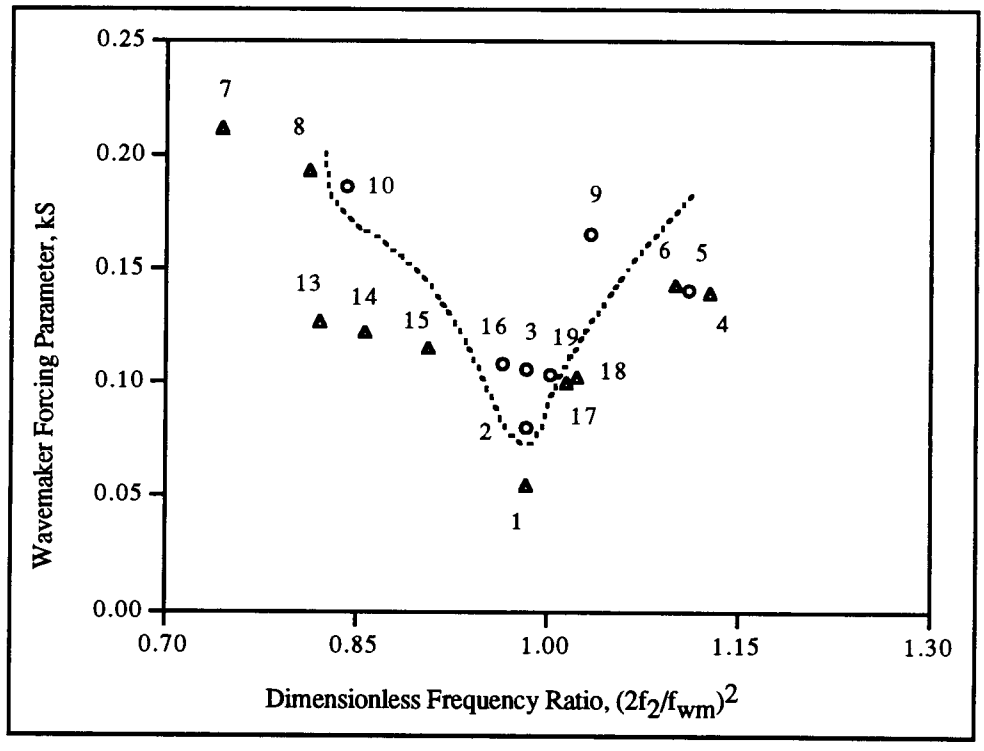

Figure 13. Stability diagram for mode 2 cross-waves. Numbers refer to the experiment run numbers for mode 2 (circles) and no cross-waves (triangles).

These were additional difficulties in determining the neutral stability curve in the vicinity of run 1 (Figure 13) and run 21 (Figure 14). These conditions were not consistently stable during the aforementioned pre-run testing, although no cross-waves developed for these runs during experimental recordings.

Underhill, Lichter, and Bernoff [1991] also reported an uncertainty in the location of the neutral stability curve. Their neutral stability curve had a hysteresis effect due to a different experimental procedure. They conducted each experiment run with a constant frequency but with a varying amplitude. The beginning eamplitude was very small, increased slowly to some maximum, and then decreased slowly to zero. Amplitudes were recorded when cross-waves first appeared as the amplitude increased and when cross-

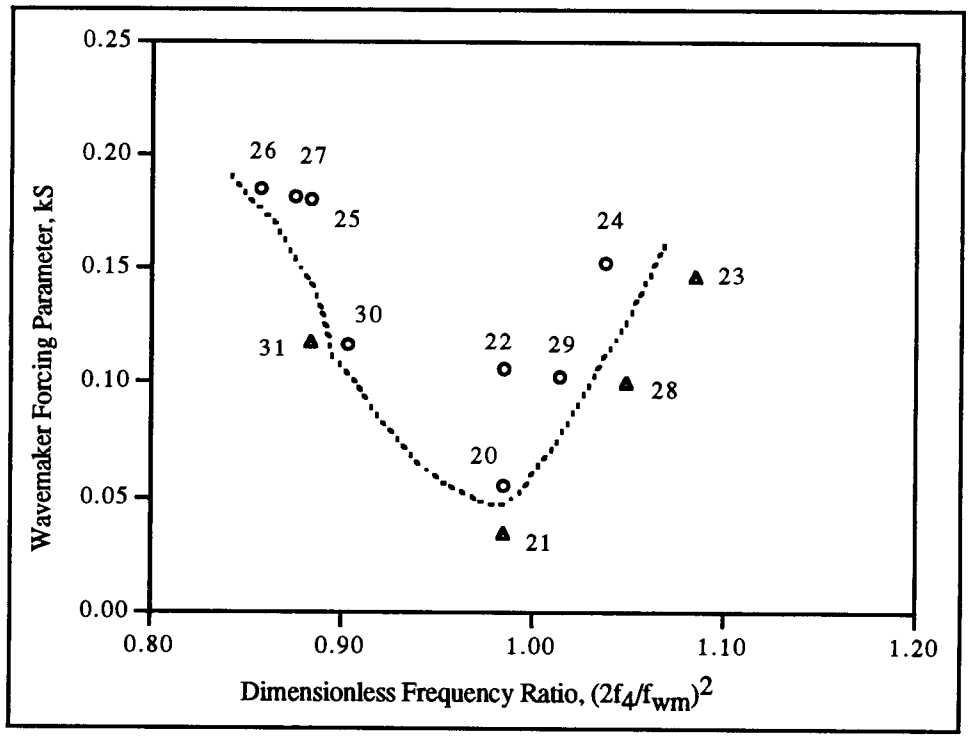

Figure 14. Stability diagram for mode 4 cross-waves. Numbers refer to experiment run numbers for mode 4 (circles) and no cross-waves (triangles).

waves disappeared as the amplitude decreased. The neutral stability curve had hysteresis; the cross-waves disappeared at lower amplitudes than for which they had appeared.

5. Primary resonances of modes 2 and 4

Figure 15 shows a portion of the time series of run 3 obtained from instrument 5. This is a primary resonance condition for mode 2 cross-waves, $(2f_{c2}/f_{wm})^2 = 0.983$. The progressive wave traveled to the location of instrument 5 in about 10 seconds. The cross-wave first appeared at about 100 seconds and by 130 seconds is the dominant wave present in the channel. The slow modulation of the cross-wave amplitude is visible from 130 seconds on. This modulation corresponds to the slow streamwise modulation described by Underhill, Lichter, and Bernoff [1991] and can be seen in Figure 10.

The modulation or beat pattern appears at a later time for instrument 6 (farther down the tank) than for 5, and also later in instrument 7 than for 6. This is clearly not due to wave reflections from the beach. If this modulation is assumed to be a beat frequency of the progressive wave frequency (1.317 Hz for run 3) and twice the cross-wave frequency, then the beat frequency and period would be

$$f_{beat} = f_{wm} - 2f_{c2} = 1.317 - 2(0.653) = 0.011\,\text{Hz} \rightarrow T_{beat} \approx 90\,\text{sec}, \qquad (5.1)$$

which is longer than the time between beat maxima at 150 and 220 seconds and longer than between maxima at 220 and 260 seconds.

A portion of the time series from instrument 5 during run 19 is shown in Figure 16. This is another primary resonance condition for mode 2, $(2f_{c2}/f_{wm})^2 = 1.002$. The cross-wave begins to develop at about 120 seconds. This time series does not have as regular a pattern of amplitude modulation as the time series in Figure 15.

The time series shown in Figures 15 and 16 do not clearly indicate irregular or chaotic motion (characteristic 5 in §1). The time series do show an increasing complexity of regular motion (the entire run 1 looked like the first 100 seconds in Figure 15) as the experimental parameters of wavemaker forcing frequency and amplitude were changed (characteristic 4 from §1).

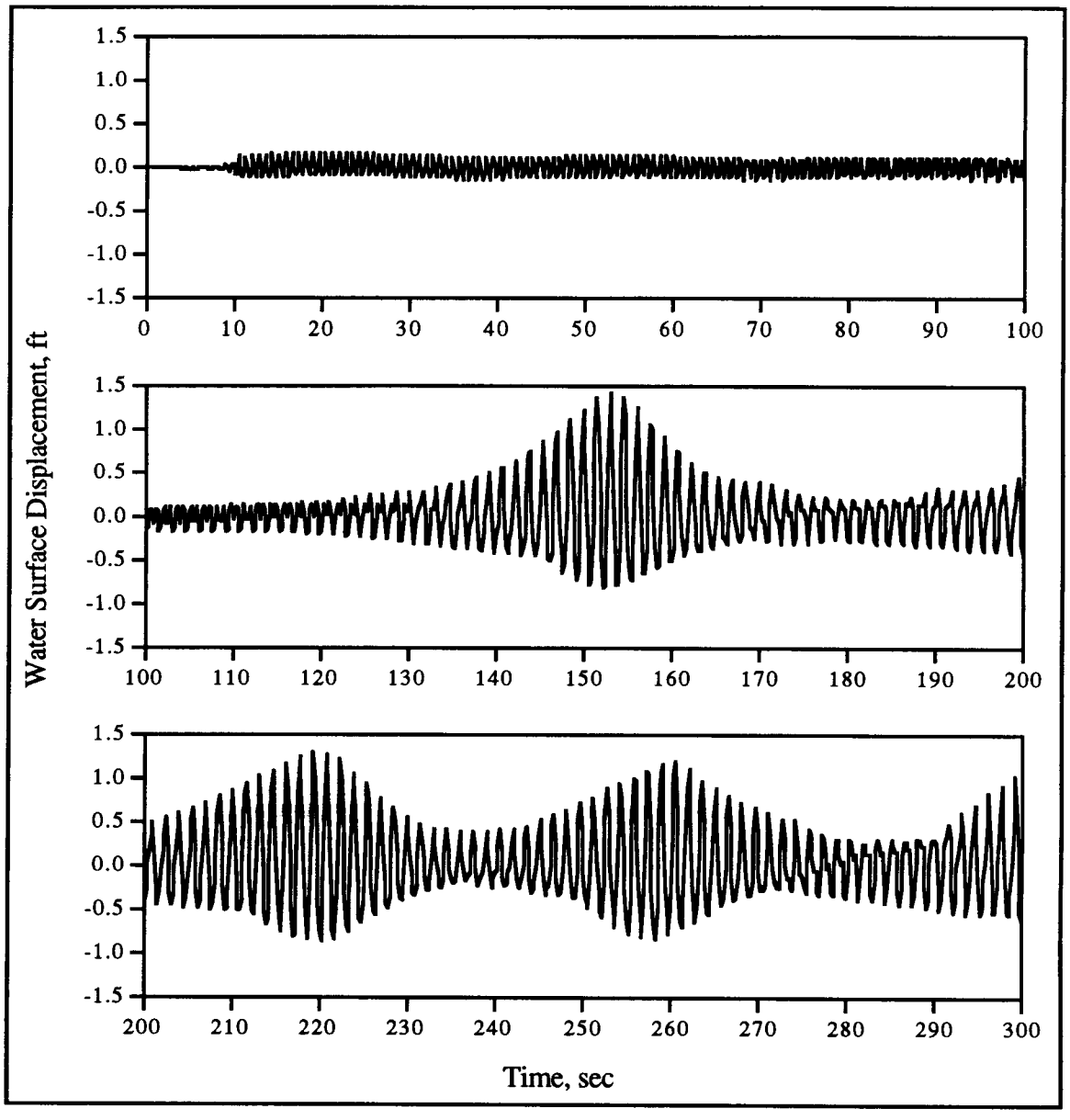

Figure 15. Time series of a mode 2 primary resonance cross-wave at instrument 5 for run 3.

Chaotic characteristics 2 (broad-banded spectra) and 3 (fractal properties in the phase space) were evident in the primary resonances of modes 2 and 4. Wave power spectra from five runs are shown in Figure 17 for mode 2 waves with corresponding Poincaré

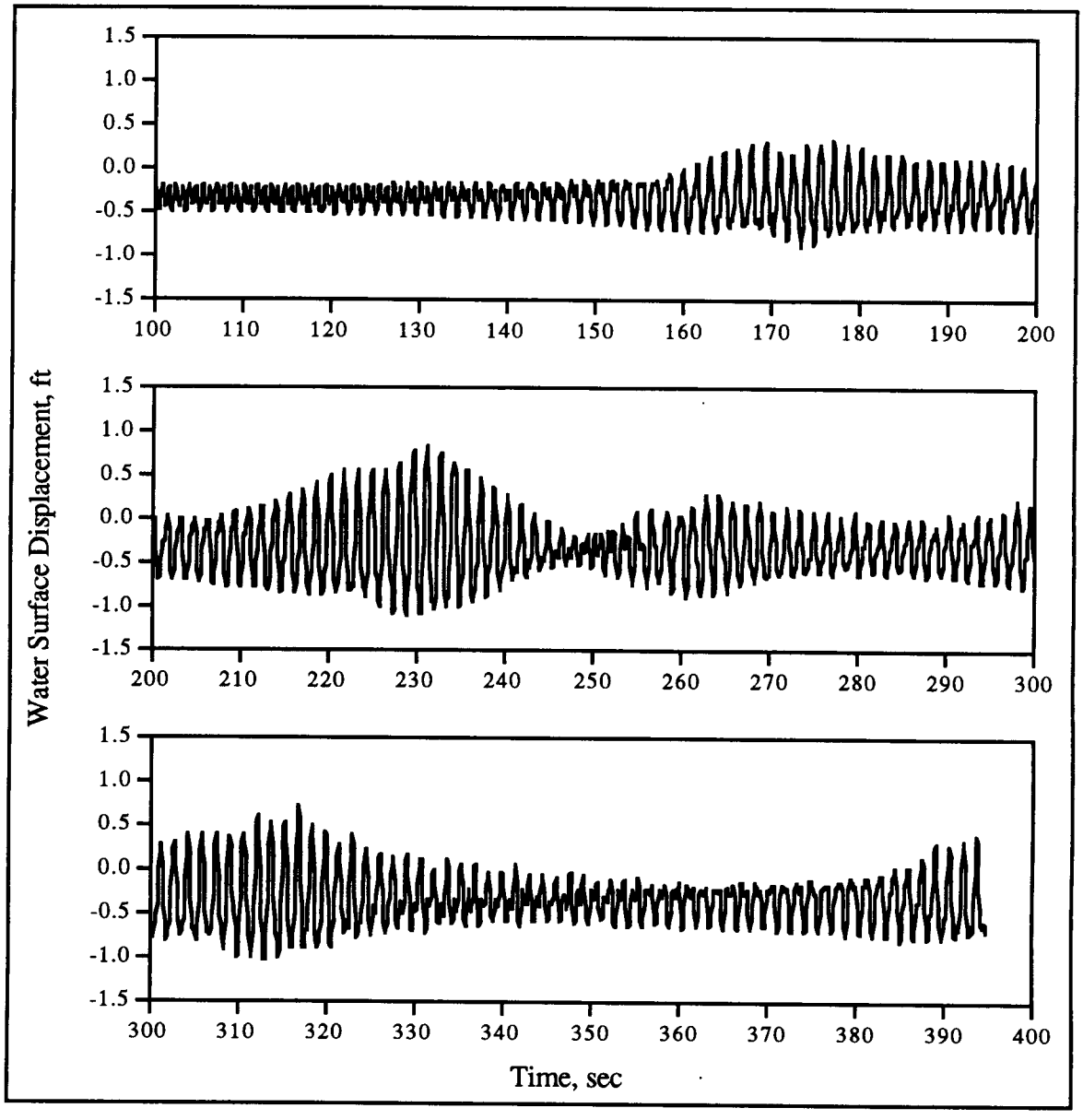

Figure 16. Time series of a mode 2 primary resonance cross-wave at instrument 5 for run 19.

maps shown in Figure 18. Figures 19 and 20 are spectra and Poincaré maps for mode 4 waves.

Each time series was subdivided into four records of equal length and the Fourier components were computed by FFT . The four one-sided spectra were ensemble averaged.

All Poincaré maps were obtained from instrument 5 data by first computing the water surface velocity from a finite difference,

$$\dot{\eta}(t_2) = \frac{\eta(t_2) - \eta(t_1)}{t_2 - t_1}, \tag{5.2}$$

and then plotting every 64th data pair $(\eta, \dot{\eta})$.

Figure 17 spectra are for five runs near the primary resonance of mode 2. Two runs (Figures 17a,b) did not develop cross-waves, and three runs (Figures 17c-e) had mode 2 develop.

All spectra in Figure 17 have peaks at the progressive wave/wavemaker frequency f_{wm} and harmonics of f_{wm}. The spectra in Figures 17c-e also have peaks at the mode 2 frequency and harmonics of f_{c2}. Figure 17a is clearly not broad-banded. The spectra in Figures 17c-e are more broad-banded than 17a or b, but not as broad-banded as the spectra discussed by Moon [1987, 1992] as evidence of chaotic motion.

The Poincaré maps in Figure 18 correspond to the experiment runs with spectra shown in Figure 17. The Poincaré map of a single periodic signal is a single point; a quasi-periodic signal maps to a closed loop; a chaotic signal maps to a fractal collection of points denoting a strange attractor. In Figure 18a, the data from run 1 mapped into a small cluster rather than the idealized single point because of nonlinear harmonics. The data from run 6 mapped as a wide loop in Figure 18b rather than the idealized smooth curve of a quasi-periodic signal. The quasi-periodic loop indicates two or more incommensurate frequencies were present.

The Poincaré maps of Figures 18c-e from run 3, 9, and 19, respectively, generated mode 2 cross-waves that are clearly neither points nor closed loops, but rather fit into the fractal category. These fractal collection of points denote strange attractors and are evidence of chaos. The map in Figure 18c has more points because run 3 was twice as long as the other run shown.

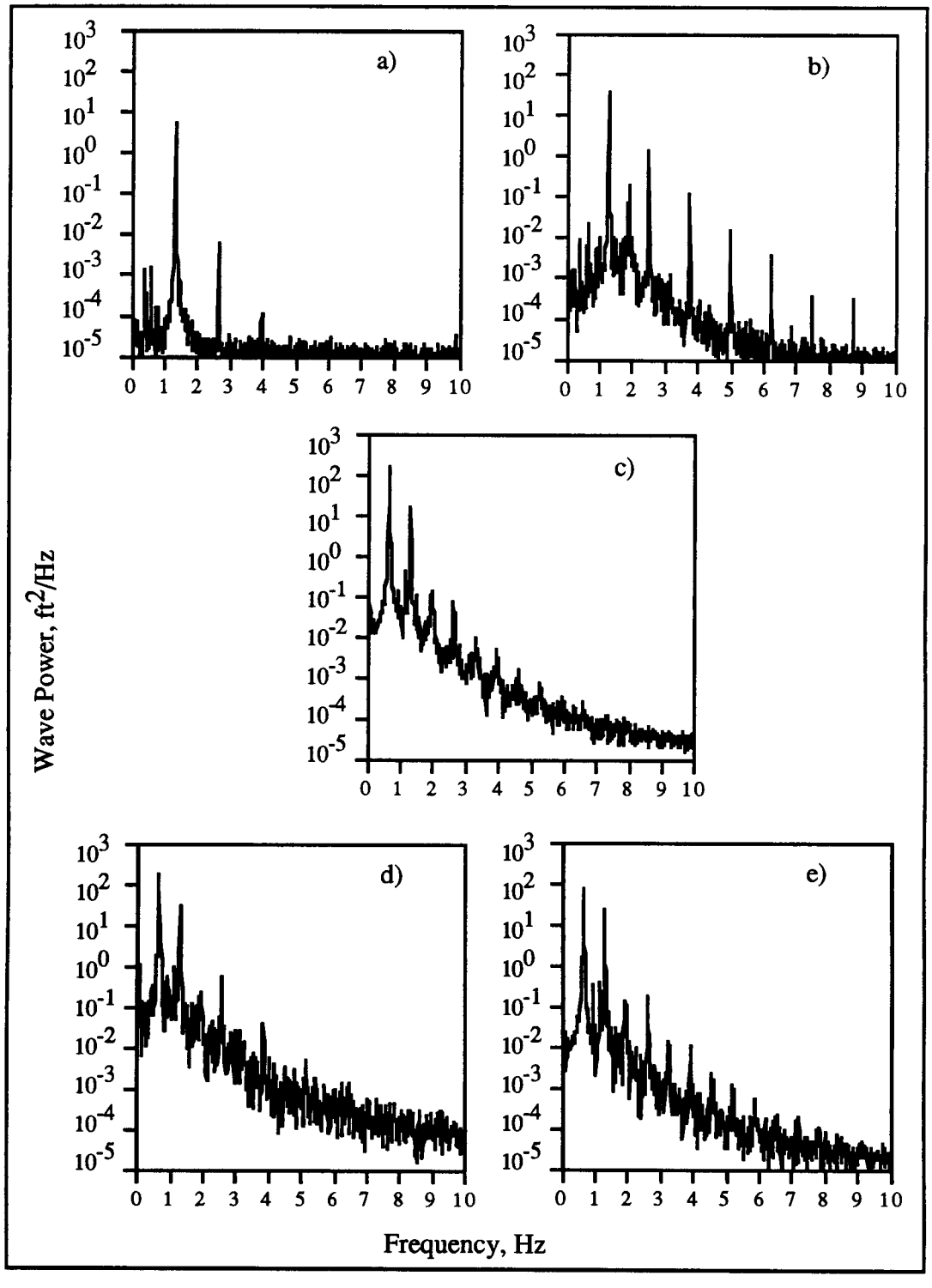

Figure 17. Power spectra for mode 2 cross-waves. a) Run 1 and b) run 6: no mode 2 cross-waves. c) Run 3, d) run 9, and e) run 19: mode 2 cross-waves developed.

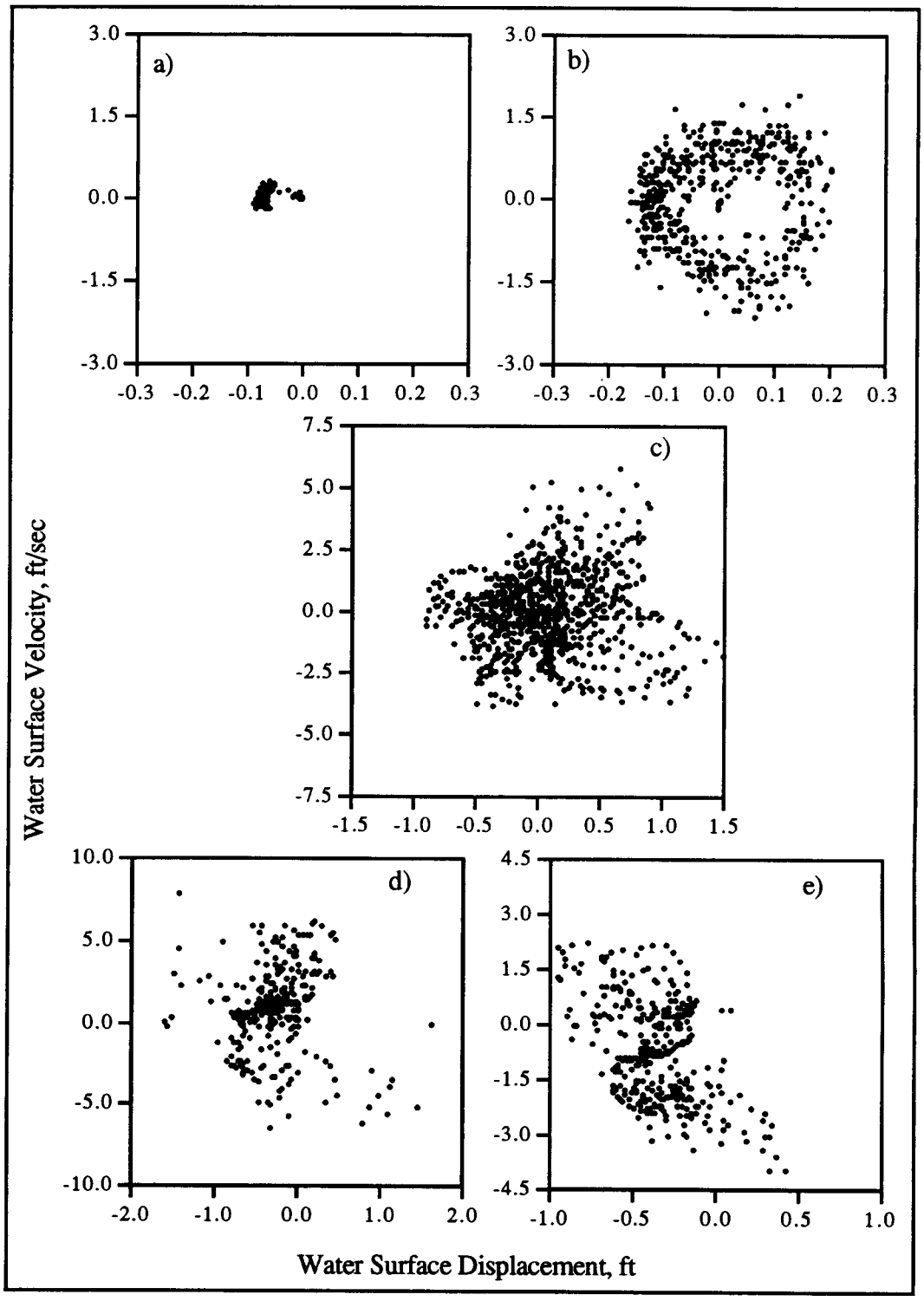

Figure 18. Poincaré maps for mode 2 cross-waves. a) Run 1 and b) run 6: no mode 2 cross-waves. c) Run 3, d) run 9, and e) run 19: mode 2 cross-waves developed.

These Poincaré maps cannot be compared with Underhill, Lichter, and Bernoff [1991] because they actually used 'pseudo' Poincaré plots, phase space maps of $\eta(t)$ versus $\eta(t+\tau)$ where τ is some time shift. Their data was sampled at the cross-wave frequency, and their time shift τ is not specified, only listed as being somewhere between 1/3 to 1/6 of the streamwise modulation period.

Figure 19 has spectra for four runs near the primary resonance of mode 4. One run (Figure 19a) did not have a cross-wave. Three runs (Figures 19b-d) contained mode 4 cross-waves.

The spectrum in Figure 19a is not at all broad-banded. The main spectral peak is at the progressive wave/wavemaker frequency; a small peak appears at the mode 4 frequency, although this wave was not visible to the eye. A mode 4 cross-wave would have probably become visible if the run had been longer.

The spectrum in Figure 19b has multiple harmonics for both f_{wm} and f_{c4}. It is both broad-banded and peaked. The spectra in Figures 19c and d are broad-banded but not very peaked. These fit more closely the broad-banded spectrum characteristic of chaotic motion described by Moon [1992].

The Poincaré maps corresponding to the data in Figure 19 are shown in Figure 20. Figure 20a for the case where no mode 4 was generated mapped as a small cluster of points rather than the idealized single point. Figure 20b could perhaps be labeled as a fractal collection of points, but Figures 20c and d seem to be more a collection of fuzzy points. According to Moon [1987], a fuzzy collection of points may indicate any of the following: i) too much random or noisy input; ii) strange attractor but very little dissipation; iii) strange attractor in phase space with more than three dimensions; iv) quasi-periodic motion with three or more dominant incommensurate frequencies. It is likely that case i) above pertains to these runs since the progressive waves generated were less than 0.005 ft (0.6 in) in amplitude.

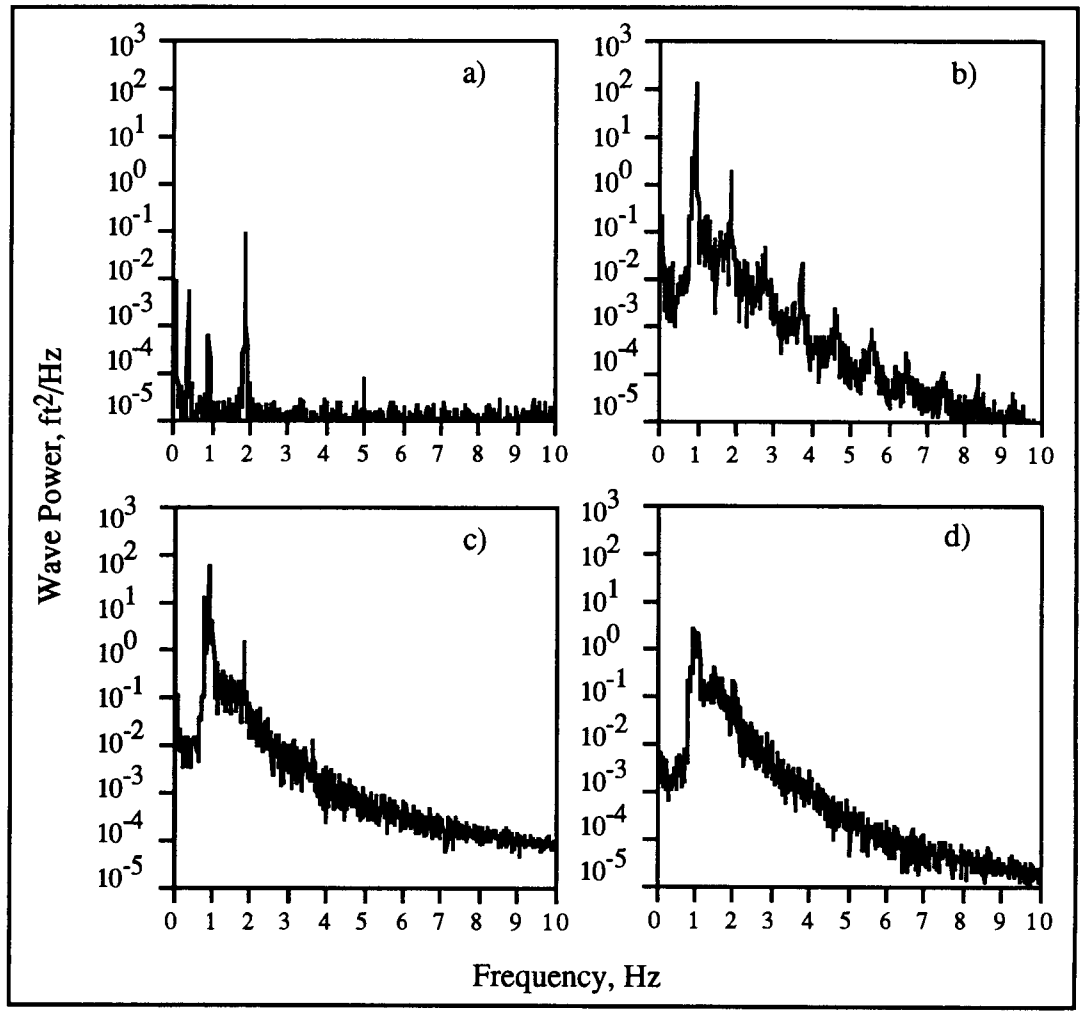

Figure 19. Power spectra for mode 4 cross-waves. a) Run 21: no cross-waves. b) Run 22, c) run 24, and d) run 26: mode 4 cross-waves developed.

The slow streamwise modulation shown in Figure 10 is not apparent in the wave power spectra of Figures 17 and 19. The ensemble averaging technique of using four records from the original time series of each run did not allow for a record length long enough to detect this modulation. Figure 21 shows the low frequency components of the wave spectrum obtained from run 3 without any averaging. There is no discernibly large peak indicating the slow streamwise modulation, and in particular no large peak at the

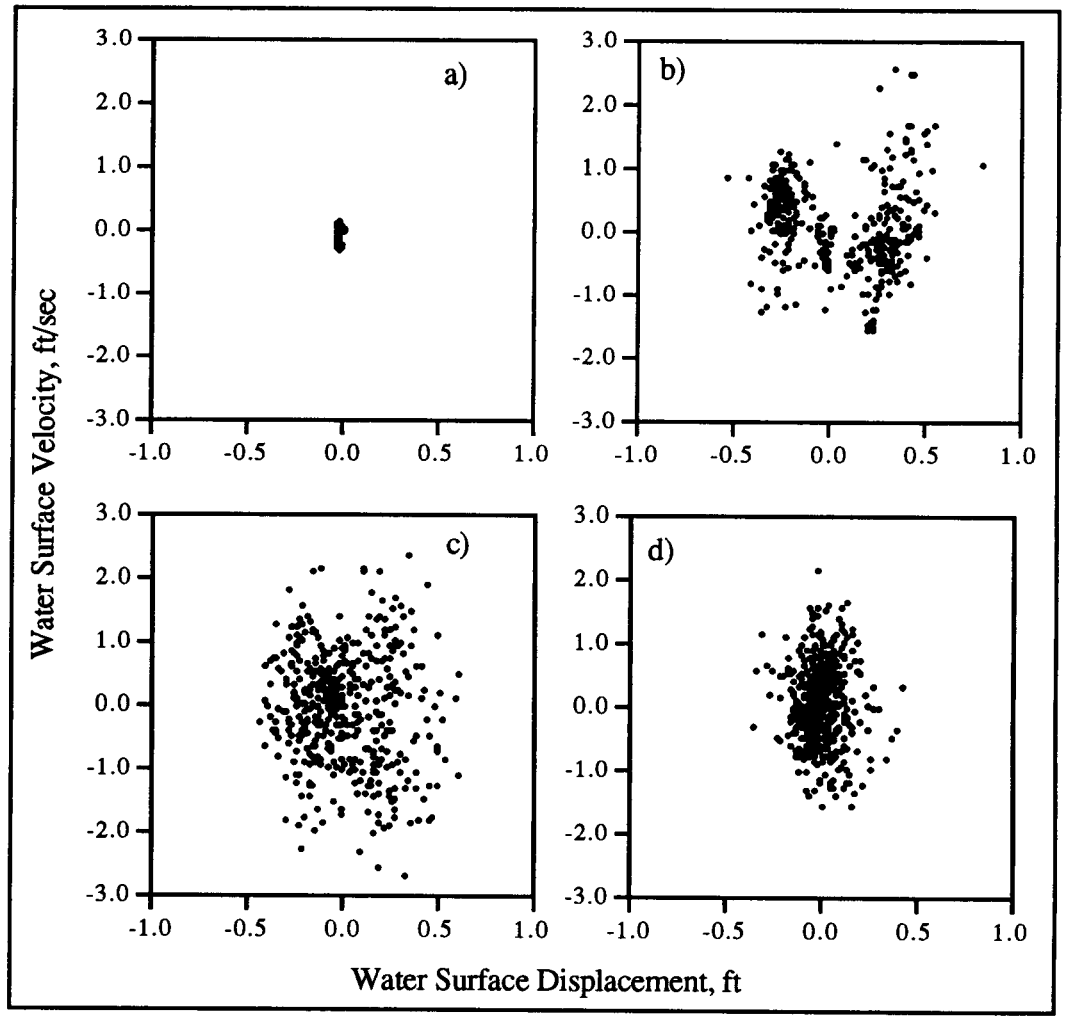

Figure 20. Poincaré maps for mode 4 cross-waves. Cases are the same as for Figure 19. a) run 21: no cross-waves. b) Run 22, c) run 24, and d) run 26: mode 4 cross-waves developed.

hypothesized beat frequency from (5.1). The experiment runs would need to be longer to obtain a spectral peak of the slow modulation.

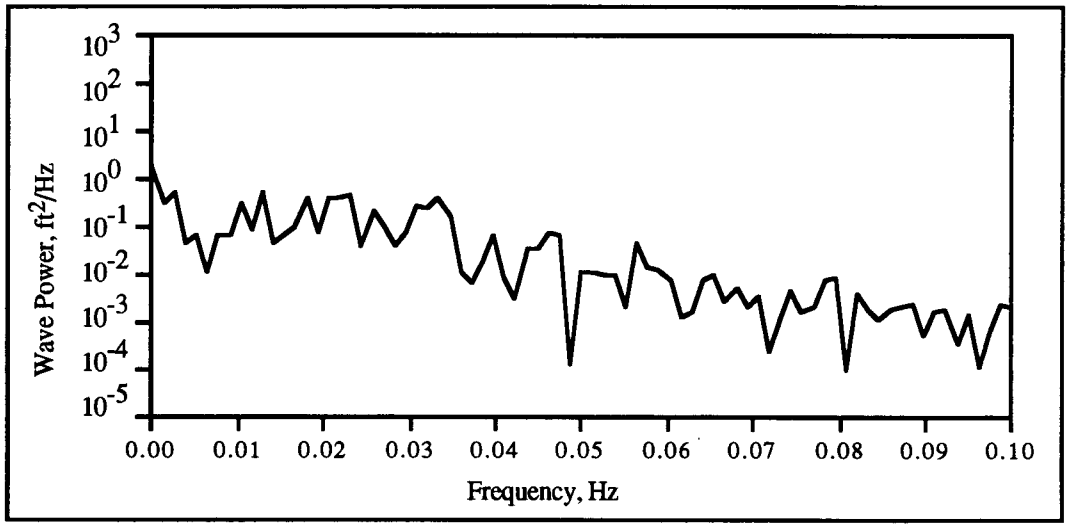

Figure 21. Low frequency components of Run 3 spectrum without averaging. No large peak exists at the hypothesized beat frequency of 0.011 Hz.

6. Secondary resonance of mode 2

A secondary resonance occurs when the forcing frequency equals a cross-wave mode frequency, $\omega_p = \omega_{cn}$. Figure 11 shows mode 2 as a secondary resonance for the same wavemaker frequency and amplitude as for run 11. A mode 4 secondary resonance also developed during run 33 and will be discussed in §7.

Only runs 11 and 12 were designed to detect mode 2 as a secondary resonance. Run 11 had a visible mode 2 and run 12 did not (see comments in Table 7). Fourier spectra and Poincaré maps for these two runs are shown in Figures 22 and 23,.

The spectra and Poincaré maps show no evidence of chaos in either run. Both spectra contain peaks at harmonics of f_{wm} and are not broad-banded; both maps show quasi-periodic loops.

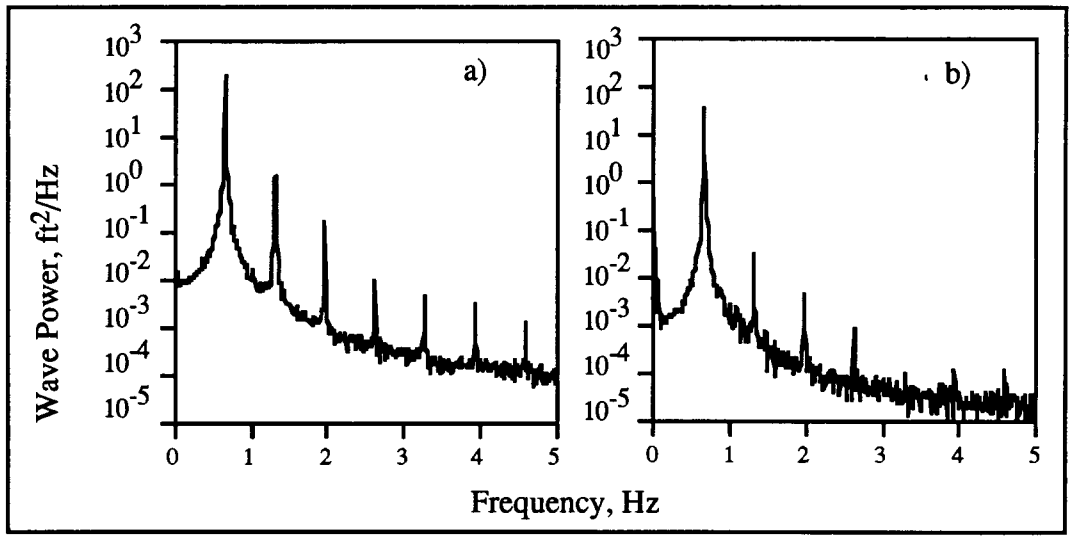

Figure 22. Power spectra for mode 2 secondary resonance conditions. a) Run 11: mode 2 cross-waves developed. b) Run 12: no mode 2 cross-waves.

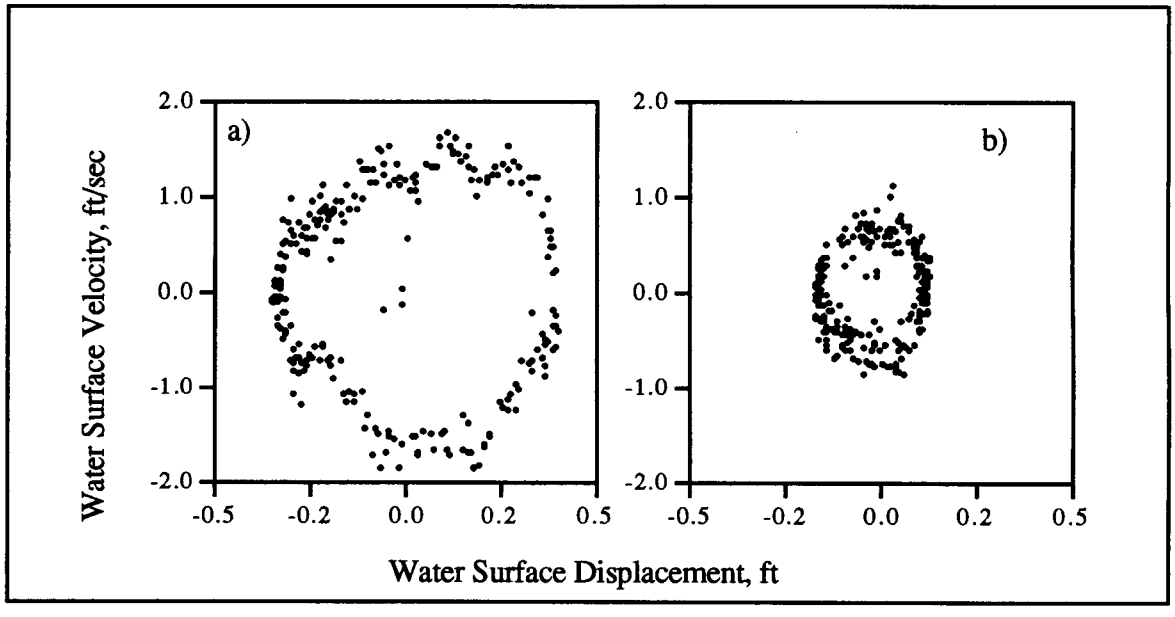

Figure 23. Poincaré maps for mode 2 secondary resonance cross-waves. a) Run 11: mode 2 cross-waves developed. b) Run 12: no mode 2 cross-waves.

7. Simultaneous primary and secondary resonances: modes 1 and 4

The most exciting experiment run was that of 33 in which two cross-wave modes were simultaneously generated: mode 1 as a primary resonance $\left(\omega_p = 2\omega_{c1}\right)$ and mode 4 as a secondary resonance $\left(\omega_p = \omega_{c4}\right)$. A series of four photographs in Figure 24 shows these cross-waves for the wavemaker frequency and amplitude in run 33. Figure 24a was near the beginning of the run and shows the mode 4 cross-wave superimposed on the progressive wave. A slight tilt of the water surface upwards on the left side of the channel indicates mode 1 was beginning to develop. Figure 24b taken at a slightly later time shows the mode 4 cross-wave had a streamwise modulation. The water surface still shows the tilt of mode 1 developing. In Figure 24c, mode 1 had developed. The mode 4 crests are visible on the left side of the channel and the progressive wave can still be clearly seen. The mode 1 wave was fully developed in Figure 24d. The mode 1 streamwise modulation and the progressive wave are visible but the mode 4 cross-wave is no longer visible.

The wave power spectrum and Poincaré map for run 33 are shown in Figure 25. The spectrum in Figure 25a shows peaks at harmonics of f_{c1} and $f_{wm} = f_p$. As was the case with the spectra for mode 2 in Figure 17, this spectrum is too peaked to label as broad-banded, and so does not convincingly indicate chaos. The Poincaré map in Figure 25b, however, seems to be a fractal collection of points denoting a strange attractor.

Runs 32 through 40, n the stability diagram for mode 1 in Figure 12, were designed to be in the bandwidth of $\omega_p \approx 2\omega_{c1}$. Only run 32 developed a mode 1 cross-wave, and only near the end of the run. No other runs were observed to have mode 4 generated. No spectra were broad-banded, and Poincaré maps for runs other than 33 showed quasi-periodic loops.

a)

b)

Figure 24. Cross-wave modes 1 and 4 for run 33. a) Secondary resonance of mode 4 cross-wave superimposed over the progressive wave. The small tilt of the water surface indicates mode 1 is growing. b) Streamwise modulation of secondary resonance mode 4. Tilted water surface indicates that mode 1 is still growing.

c)

d)

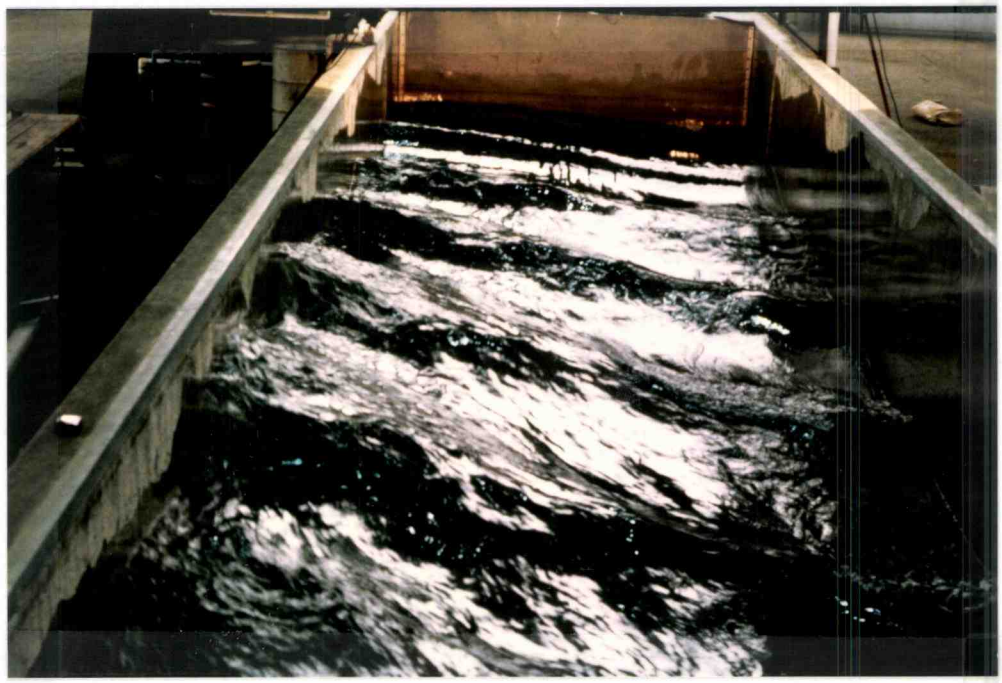

c) Primary resonance of mode 1 fully developed. Mode 4 crests are still visible on the left side of the channel. d) Streamwise modulation of primary resonance mode 1 visible. Progressive waves are still apparent, but there is no longer any visible mode 4 secondary resonance waves.

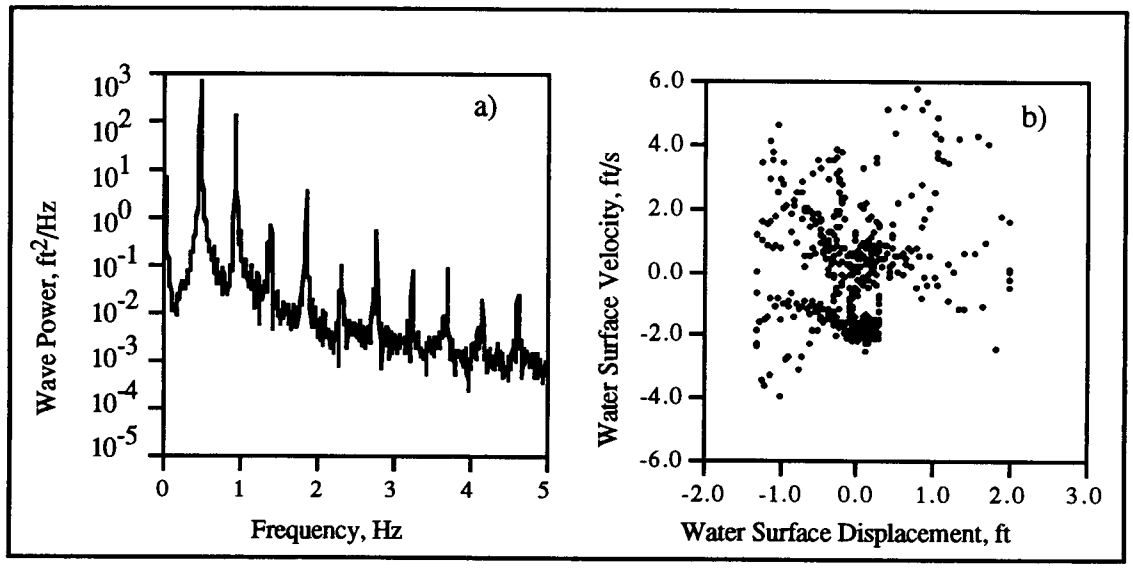

Figure 25. Power spectrum and Poincaré map for run 33 with mode 1 as a primary resonance and mode 4 as a secondary resonance.

8. Summary and concluding remarks

The experiments at the OHH-WRL were designed to provide experimental evidence to support the theoretical analysis showing that cross-waves may be chaotic. Five characteristics of chaotic motions [Moon, 1992] were discussed for the experimental data.

1) *Sensitivity to initial conditions.* This characteristic could not be evaluated. The initial conditions are the water surface displacement and velocity at every point on the water surface. While each experiment run began after allowing the water in the channel to settle, there was no guarantee that the surface was completely motionless everywhere for every run. Testing for sensitivity to initial conditions in a fluid continuum is inherently more difficult than for simple mechanical systems because of the infinite number of water particles on the free surface.

2) *Broad spectrum of Fourier transform from a single frequency input.* A precursor to chaos is the appearance of subharmonics and harmonics of some dominant frequency component [Moon, 1992]. The analogous dominant frequency component here is the progressive wave frequency f_p which is also equal to the wavemaker forcing frequency f_{wm}. All spectra shown exhibited harmonics of f_p. The spectra for runs of primary resonance cross-waves also showed multiple harmonics of the subharmonic cross-wave frequency $f_{cn} = \frac{1}{2} f_p$. Moon cautions against assuming that all multiharmonic output implies the presence of chaos because the system may have many hidden degrees of freedom. In addition, for systems having many degrees of freedom the use of the Fourier spectra is not of much help in detecting chaos unless changes in spectra with parameter changes are observed. A fluid continuum is a system with many large degrees of freedom.

While the spectra for runs generating primary resonance cross-waves are too peaked to describe as broad-banded, these spectra are at least broader than those for runs without cross-waves. For example, spectra in Figures 17c-e are broader than spectra in Figures

17a,b. It is noteworthy that the only subharmonic present in the spectra is $\frac{1}{2}f_p$. The spectra neither confirm or deny the presence of chaotic motions for cases with primary resonance cross-waves.

3) *Fractal properties of the motion in phase space denoting a strange attractor.* The Poincaré maps of primary resonances of mode 1 and 2 cross-waves showed fractal properties (Figures 18c, e, and e and 25b). The Poincaré maps of primary resonance mode 4 cross-waves (Figures 20b, c, and d) were a little too 'fuzzy' to label as fractal, probably due to too much noisy input. The case of the secondary resonance mode 2 cross-wave (Figure 23a) showed no evidence of chaos, but rather the classic quasi-periodic loop.

4) *Increasing complexity of regular motions as some experimental parameter is changed.* This chaotic characteristic is evident in the stability diagrams of Figures 12, 13, and 14. Outside of the neutral stability curve, the motion is a regular progressive wave. Crossing the neutral stability curve by slightly varying the wavemaker amplitude or frequency results in a more complex system when the cross-wave develops.

5) *Transient or intermittent chaotic motions.* This characteristic of chaotic motion is determined by observing the time series. Figures 15 and 16 are time series from primary resonances of mode 2 cross-waves. No irregular motion is visible in Figure 15, although Figure 16 has some slight irregularities. There were no time series from any of the 40 experiment runs that confirmed conclusively that cross-waves were chaotic.

The experimental results indicating that cross-waves generated as a primary resonance are chaotic are limited. Poincaré maps show fractal properties and regular motions become complex upon varying the forcing frequency and amplitude parameters. Fourier spectra were only somewhat broad; only a few time series show slightly irregular motions.

Run 11 generated a secondary resonance cross-wave only and exhibited no evidence of chaos. Perhaps comprehensive testing of secondary resonances would provide some evidence of chaos.

One last comment on the experimental results is in order. The experiment runs in the vicinity of the neutral stability curves were not always repeatable. Sometimes wavemaker frequency and amplitude conditions near the neutral stability curve would generate a cross-wave and sometimes would not. This may have depended on the initial stillness of the water, the duration of the forcing, or slight differences in the forcing amplitude and frequency. The neutral stability curve should perhaps be considered a transition zone with an as yet undetermined structure.

Chapter IV. Recommendations for Future Research

There are quite a few directions that future research could take to further explore chaotic cross-waves both theoretically and experimentally. Each suggestion is discussed separately below, beginning with theoretical research ideas and ending with experimental research ideas.

1) *Add dissipative terms.* Dissipative forces could be included in the Lagrangian as a perturbation, just as the wavemaker forcing terms are. As such, they would not be used to calculate the conjugate momenta variables. Miles [1976] and Holmes [1986] assumed that dissipation was proportional to the square of the vertical velocity of the free surface, $\dot{\eta}^2$.

Including dissipation would result in evolution equations of the type System I from Wiggins [1988] and would require the application of an averaging theorem to the perturbations [Wiggins, 1988, p. 358, Proposition 4.1.6] to determine the orbits that survive the perturbation. Additionally, a different form for the Melnikov function would be required because equation (4.22) in Chapter II applied only to System III.

2) *Include higher order terms.* The Melnikov method predicted chaotic behavior for primary resonance cross-waves when the wavemaker forcing frequency and the cross-wave frequency have the ratio 2:1. Calculating the Melnikov function for the secondary resonance (1:1) cross-waves would require that $O(\varepsilon^2)$ terms be retained in the Taylor series expansions of the integrals (Chapter II, §3) in order to obtain autonomous nonlinear terms from the Hamilton-Jacobi theory.

Several difficulties are anticipated with inclusion of higher order terms. First, the perturbations, which are $O(\gamma)$, must be of lower order that the unperturbed terms. In the analysis of Chapter II, the ordering assumption was

$$\gamma^2 < \varepsilon^2 < \gamma < \varepsilon < 1.$$

Simply including $O(\varepsilon^2)$ terms would violate the assumption that the perturbations are smaller than the nonlinearities. This problem might be overcome by applying scales different from those of equations (2.12)-(2.14) in Chapter II.

The second difficulty is Jones' [1984] assumption (Chapter II, §2) that progressive wave/progressive wave $O(\varepsilon)$ interactions could be ignored because they do not contribute to cross-wave resonance at $O(\varepsilon)$. However, Jones expands to $O(\varepsilon^2)$ in the analysis, and some progressive wave/progressive wave interaction result in cross-wave resonance at $O(\varepsilon^2)$. Care must be taken to ignore non-essential terms only after all Taylor series expansions are calculated.

3) *Assume a slow streamwise modulation of the cross-wave.* The assumed form of the cross-wave velocity potential in Chapter II had no streamwise x dependence. Figure 10 shows a very distinct streamwise amplitude modulation of the cross-wave, and many other reports also describe this modulation [Underhill, Lichter, and Bernoff, 1991; Barnard and Pritchard, 1972]. Equations (2.25a) for ϕ_c (Chapter II) could be modified to include a streamwise modulation with different time and length scales than those for ϕ_p [Jones, 1984; Miles and Becker, 1988]. This would add a considerable number of terms to the Lagrangian since all $\partial^n \phi_c / \partial x^n$ were zero (Chapter II). The Hamiltonian will likely require an entirely new sequence of canonical transformations.

4) *Determine a mechanical analog.* The large number of terms in the Lagrangian and Hamiltonian equations illustrates the immense labor required to carry out the Melnikov analysis. Finding a mechanical system with similarities in behavior to the cross-wave system would aid considerably in understanding the chaotic behavior of cross-waves. For example, calculating a Melnikov function for a secondary resonance cross-waves is described in 2) above as requiring rescaling, higher order expansions, and additional terms previously neglected. A simple mechanical system, which would not require Taylor series

expansions and so would contain far fewer terms, could be used to explore the Melnikov function analysis for various frequency ratios of the forcing to the natural frequency. It is not known whether this mechanical analog system should contain two masses, one representing the cross-wave and one the progressive wave, each with one type of motion permitted, or if there should be one mass, representing the water surface, with two types of motion permitted.

5) *More secondary resonance experiments.* The two examples of secondary resonance cross-waves described in Chapter III indicate the need for more experiments. Recall that mode 2 in run 11 developed as a secondary resonance (Figure 11) and that mode 4 was visible as a secondary resonance in run 33 until it was overwhelmed by the primary resonance of mode 1. The 1:1 resonance has not been pursued in any other experiments. Determining a neutral stability diagram for the secondary resonance case, whether or not it is chaotic, would aid in a better understanding of parametrically generated cross-waves.

6) *Determine the structure of the neutral stability curve for the primary resonance cross-waves.* The neutral stability curve was described in Chapter III as being ambiguous to define precisely. This ambiguity was hypothesized to be due to very slight differences in the free surface displacement (which are initial conditions), slight differences in wavemaker forcing frequency and amplitude from the conditions specified, or the duration of the forcing. It is the duration of the forcing that might help determine the structure of the neutral stability curve.

The recommendation is to perform a large number of primary resonance cross-wave experiments in a wide region surrounding the neutral stability curve for one given mode. The experimental procedure would again require an initially still surface and a specified constant wavemaker forcing frequency and amplitude. However, the procedure would differ from that described in Chapter III by allowing the wavemaker forcing to continue as

long as necessary (within reason) to generate a cross-wave. The time to the generation of the cross-wave mode would be recorded for that particular wavemaker frequency and amplitude. If the stability diagram in the region of the neutral stability curve were densely filled in with points coded to express the time to cross-wave generation, the structure of the curve may become apparent. The Mandlebrot set, for example, uses a color coding to indicate the number of iterations required for convergence for each initial condition. The color coding in the region of the neutral stability curve would indicate the forcing time required to generate a cross-wave for each wavemaker frequency and amplitude condition. Perhaps this structure would be fractal.

Bibliography

ABRAHAM, R. H. & SHAW, C. D. 1992 *Dynamics: The Geometry of Behavior.* Second Edition. Addison-Wesley.

ALLEN, J. S., SAMELSON, R. M., & NEWBERGER, P. A. 1991 Chaos in a model of forced quasi-qeostrophic flow over topography: an application of Melnikov's method. *J. Fluid Mech.* **226**, 511-547.

BARNARD, B. J. S., MAHONY, J. J. & PRITCHARD, W. G. 1977 The excitation of surface waves near a cut-off frequency. *Phil. Trans. R. Soc. Lond.* A **286**, 87-123.

BARNARD, B. J. S. & PRITCHARD, W. G. 1972 Cross-waves. Part 2. Experiments. *J. Fluid Mech.* **55**, 245-255.

BOGOLIUBOV, N. N. & MITROPOLSKY, Y. A. 1961 *Asymptotic Methods in the Theory of Non-Linear Oscillations.* Gordon and Breach Science Publishers.

FETTER, A. L. & WALECKA, J. D. 1980 *Theoretical Mechanics of Particles and Continua.* McGraw-Hill.

GARRETT, C. J. R. 1976 On cross-waves. *J. Fluid Mech.* **41**, 837-849.

GOLDSTEIN, H. 1980 *Classical Mechanics.* Second Edition. Addison-Wesley.

GRADSHTEYN, I. S. and RYZHIK, I. M. 1980 *Table of Integrals, Series, and Products.* Academic Press.

GRIMSHAW, R. 1990 *Nonlinear Ordinary Differential Equations.* Blackwell Scientific Publications.

GUCKENHEIMER, J. & HOLMES, P. 1983 *Nonlinear Oscillations, Dynamical Systems, and Bifurcations of Vector Fields.* Springer-Verlag.

HOLMES, P. 1986 Chaotic motions in a weakly nonlinear model for surface waves. *J. Fluid Mech.* **162**, 365-388.

HUDSPETH, R. T. & SULISZ, W. 1991 Stokes drift in two-dimensional wave flumes. *J. Fluid Mech.* **230**, 209-221.

JONES, A. F. 1984 The generation of cross-waves in a long deep channel by parametric resonance. *J. Fluid Mech.* **138**, 53-74.

KIT, E. & SHEMER, L. 1989 On the neutral stability of cross-waves. *Phys. Fluids* A **1**(7), 1128-1132.

KIT, E., SHEMER, L. & MILOH, T. 1987 Experimental and theoretical investigation of nonlinear sloshing waves in a rectangular channel. *J. Fluid Mech.* **181**, 265-291.

LICHTER, S. & CHEN, J. 1987 Subharmonic resonance of nonlinear cross-waves. *J. Fluid Mech.* **183**, 451-465.

LICHTER, S. & SHEMER, L. 1986 Experiments on nonlinear cross waves. *Phys. Fluids* **29**(12), 3971-3975.

LIN, J. D. & HOWARD, L. N. 1960 Non-linear standing waves in a rectangular tank due to forced oscillation. *M. I. T. Hydrodynamics Laboratory Technical Report 44.*

LUKE, J. C. 1967 A variational principle for a fluid with a free surface. *J. Fluid Mech.* **27**, 395-397.

MAHONEY, J. J. 1972 Cross-waves. Part 1. Theory. *J. Fluid Mech.* **55**, 229-244.

MEI, C. C. 1989 *The Applied Dynamics of Ocean Surface Waves.* John Wiley & Sons.

MELNIKOV, V. K. 1963 On the stability of the center for time-periodic perturbations. *Trans. Moscow Math. Soc.* **12**, 1-57.

MILDER, D. M. 1977 A note regarding 'On Hamilton's principle for surface waves'. *J. Fluid Mech.* **83**, 159-161.

MILES, J. W. 1976 Nonlinear surface waves in closed basins. *J. Fluid Mech.* **75**, 419-448.

MILES, J. W. 1977 On Hamilton's principle for surface waves. *J. Fluid Mech.* **83**, 153-158.

MILES, J. W. 1988 Parametrically excited, standing cross-waves. *J. Fluid Mech.* **186**, 119-127.

MILES, J. W. & BECKER, J. 1988 Parametrically excited, progressive cross-waves. *J. Fluid Mech.* **186**, 129-146.

MOON, F. C. 1987 *Chaotic Vibrations*. John Wiley & Sons.

MOON, F. C. 1992 *Chaotic and Fractal Dynamics*. John Wiley & Sons.

SHEMER, L. 1990 On the directly generated resonant standing wave in a rectangular tank. *J. Fluid Mech.* **217**, 143-165.

SHEMER, L. & KIT, E. 1989 Long-time evolution and regions of existence of parametrically excited nonlinear cross-waves in a tank. *J. Fluid Mech.* **209**, 249-263.

SHEMER, L., KIT, E. & MILOH. T. 1987 Measurements of two- and three-dimensional waves in a channel, including the vicintiy of cut-off frequencies. *Exps. Fluids* **5**, 66-72.

SHEMER, L. & LICHTER, S. 1987 Identification of cross-wave regimes in the vicinity of a cut-off frequency. *Phys. Fluids* **30**(11), 3427-3433.

TSAI, W. T., YUE, D. K. P. & YIP, K. M. K. 1990 Resonantly excited regular and chaotic motions in a rectangular wave tank. *J. Fluid Mech.* **216**, 343-380.

UNDERHILL, W. B., LICHTER, S. & BERNOFF, A. J. 1991 Modulated, frequency-locked, and chaotic cross-waves. *J. Fluid Mech.* **225**, 371-394.

WIGGINS, S. 1988 *Global Bifurcations and Chaos*. Springer-Verlag.

WIGGINS, S. 1990 *Introduction to Applied Nonlinear Dynamical Systems and Chaos*. Springer-Verlag.

WIGGINS, S. & HOLMES, P. 1987 Homoclinic orbits in slowly varying oscillators. *SIAM J. Math Anal.* **18**(3), 612-629.

APPENDICES

Appendix I

Table 1. Coefficients used in the Lagrangian components.

$A_1 = \cos\xi$	$B_1 = \sin\xi$
$a_1 = \int_0^{\xi} \cos x\, dx = B_1$	$b_1 = \int_0^{\xi} \sin x\, dx = 1 - A_1$
$a_2 = \int_0^{\xi} \cos^2 x\, dx = \frac{1}{2}(\xi + A_1 B_1)$	$b_2 = \int_0^{\xi} \sin^2 x\, dx = \frac{1}{2}(\xi - A_1 B_1)$
$a_3 = \int_0^{\xi} \cos^3 x\, dx = \frac{1}{3} B_1 (A_1^2 + 2)$	$b_3 = \int_0^{\xi} \sin^3 x\, dx = -\frac{1}{3} A_1 (B_1^2 + 2) + \frac{2}{3}$
$c_{11} = \int_0^{\xi} \cos x \sin x\, dx = \frac{1}{2} B_1^2$	$d_{11} = \cos\xi \sin\xi = A_1 B_1$
$c_{12} = \int_0^{\xi} \cos x \sin^2 x\, dx = \frac{1}{3} B_1^3$	$d_2 = \cos 2\xi = A_1^2 - B_1^2$
$c_{21} = \int_0^{\xi} \cos^2 x \sin x\, dx = \frac{1}{3}(1 - A_1^3)$	$\mu_1 = \frac{1}{\beta} + 2\beta$
$\mu_2 = \frac{1}{2\beta^3} + \frac{2}{\beta} + \frac{\beta}{2} - \frac{\beta^2}{2}$	$\mu_5 = \frac{2}{\beta} + \frac{\beta}{2} - \frac{\beta^3}{2}$
$f_1 = \int_{-\alpha}^{0} f(z)\, e^{z/\beta^2}\, dz$	$\Lambda = -\frac{(\mu_2 - 8 - 2/\beta^2)}{2\xi\sqrt{2b\beta\xi}}$

Table 2. Nonautonomous components of the Hamiltonian (3.21) following the Hamilton-Jacobi transformation.

$$H_{\varepsilon}^{*}(t)=-\varepsilon\frac{2\left(p^{*}-P_{2}^{*}\right)}{\beta^{2}\xi\sqrt{2b\beta\xi}}\sqrt{P_{1}^{*}-p^{*}}\cos\left(2Q_{1}^{*}+\frac{t}{\beta}\right)$$
$$-\varepsilon\frac{\left(\mu_{2}+8+2/\beta^{2}\right)}{2\xi\sqrt{2b\beta\xi}}\left(p^{*}-P_{2}^{*}\right)\sqrt{P_{1}^{*}-p^{*}}\cos\left(4Q_{1}^{*}+2q^{*}+\frac{2t}{\beta}\right)$$
$$+\varepsilon\frac{\left(\mu_{2}-2\mu_{5}\right)}{2\xi\sqrt{2b\beta\xi}}\left(p^{*}-P_{2}^{*}\right)\sqrt{P_{2}^{*}}\cos\left(4Q_{1}^{*}+2Q_{2}^{*}+4q^{*}+\frac{2t}{\beta}\right)$$

$$H_{\gamma}^{*}(t)=\frac{\gamma\left(P_{1}^{*}-p^{*}\right)}{8\beta\xi}\left[3\sin\left(4Q_{1}^{*}+\frac{3t}{\beta}\right)-\sin\left(4Q_{1}^{*}+\frac{t}{\beta}\right)\right]$$
$$+\frac{\gamma\sqrt{P_{2}^{*}\left(P_{1}^{*}-p^{*}\right)}}{4\beta\xi}\left[3\sin\left(4Q_{1}^{*}+2Q_{2}^{*}+2q^{*}+\frac{3t}{\beta}\right)-\sin\left(4Q_{1}^{*}+2Q_{2}^{*}+2q^{*}+\frac{t}{\beta}\right)\right]$$
$$+\frac{\gamma P_{2}^{*}}{8\beta\xi}\left[3\sin\left(4Q_{1}^{*}+4Q_{2}^{*}+4q^{*}+\frac{3t}{\beta}\right)-\sin\left(4Q_{1}^{*}+4Q_{2}^{*}+4q^{*}+\frac{t}{\beta}\right)\right]$$
$$+\gamma\left[\frac{f_{1}}{2\varepsilon}\sqrt{\frac{b\left(P_{1}^{*}-p^{*}\right)}{2\beta\xi}}\right]\sin\left(2Q_{1}^{*}+\frac{2t}{\beta}\right)+\frac{\gamma(1+2\beta)}{4\beta\xi}\left(p^{*}-P_{2}^{*}\right)\sin\left(2Q_{1}^{*}+2q^{*}+\frac{2t}{\beta}\right)$$
$$+\gamma\left[\frac{f_{1}}{2\varepsilon}\sqrt{\frac{bP_{2}^{*}}{2\beta\xi}}\right]\sin\left(2Q_{1}^{*}+2Q_{2}^{*}+2q^{*}+\frac{2t}{\beta}\right)$$

Table 3. Nonautonomous components of the Hamiltonian (3.25) following the shift transformation.

$$H_{\varepsilon}''(t) = -\varepsilon\frac{2p''}{\beta^2\xi\sqrt{2b\beta\xi}}\sqrt{P_1''-p''}\cos\left(2Q_1''+\frac{t}{\beta}\right)$$
$$-\varepsilon\frac{\left(\mu_2+8+2/\beta^2\right)}{2\xi\sqrt{2b\beta\xi}}p''\sqrt{P_1''-p''}\cos\left(4Q_1''+2q''+\frac{2t}{\beta}\right)$$
$$+\varepsilon\frac{\left(\mu_2-2\mu_5\right)}{2\xi\sqrt{2b\beta\xi}}p''\sqrt{P_2''}\cos\left(2Q_1''+2Q_2''+2q''+\frac{2t}{\beta}\right)$$

$$H_{\gamma}''(t) = \frac{\gamma(P_1''-p'')}{8\beta\xi}\left[3\sin\left(4Q_1''+\frac{3t}{\beta}\right)-\sin\left(4Q_1''+\frac{t}{\beta}\right)\right]$$
$$+\frac{\gamma\sqrt{P_2''(P_1''-p'')}}{4\beta\xi}\left[3\sin\left(2Q_1''+2Q_2''+\frac{3t}{\beta}\right)-\sin\left(2Q_1''+2Q_2''+\frac{t}{\beta}\right)\right]$$
$$+\frac{\gamma P_2''}{8\beta\xi}\left[3\sin\left(4Q_2''+\frac{3t}{\beta}\right)-\sin\left(4Q_2''+\frac{t}{\beta}\right)\right]$$
$$+\gamma\left[\frac{f_1}{2\varepsilon}\sqrt{\frac{b(P_1''-p'')}{2\beta\xi}}\right]\sin\left(2Q_1''+\frac{2t}{\beta}\right)+\frac{\gamma p''(1+2\beta)}{4\beta\xi}\sin\left(2Q_1''+2q''+\frac{2t}{\beta}\right)$$
$$+\gamma\left[\frac{f_1}{2\varepsilon}\sqrt{\frac{bP_2''}{2\beta\xi}}\right]\sin\left(2Q_2''+\frac{2t}{\beta}\right)$$

Table 4. Nonautonomous components of the Hamiltonian (3.31) following the Nonautonomous Q_2'' transformation.

$$\tilde{H}_\varepsilon(t) = -\varepsilon\frac{2\tilde{p}}{\beta^2\xi\sqrt{2b\beta\xi}}\sqrt{\tilde{P}_1-\tilde{p}}\,\cos\left(2\tilde{Q}_1+\frac{t}{\beta}\right)$$
$$-\varepsilon\frac{\left(\mu_2+8+2/\beta^2\right)}{2\xi\sqrt{2b\beta\xi}}\tilde{p}\sqrt{\tilde{P}_1-\tilde{p}}\,\cos\left(4\tilde{Q}_1+2\tilde{q}+\frac{2t}{\beta}\right)$$
$$+\varepsilon\frac{\left(\mu_2-2\mu_5\right)}{2\xi\sqrt{2b\beta\xi}}\tilde{p}\sqrt{\tilde{P}_2}\,\cos\left(2\tilde{Q}_1+2\tilde{Q}_2+2\tilde{q}+\frac{4t}{\beta}\right)$$

$$\tilde{H}_\gamma(t) = \frac{\gamma\left(\tilde{P}_1-\tilde{p}\right)}{8\beta\xi}\left[3\sin\left(4\tilde{Q}_1+\frac{3t}{\beta}\right)-\sin\left(4\tilde{Q}_1+\frac{t}{\beta}\right)\right]$$
$$+\frac{\gamma\sqrt{\tilde{P}_2\left(\tilde{P}_1-\tilde{p}\right)}}{4\beta\xi}\left[3\sin\left(2\tilde{Q}_1+2\tilde{Q}_2+\frac{5t}{\beta}\right)-\sin\left(2\tilde{Q}_1+2\tilde{Q}_2+\frac{3t}{\beta}\right)\right]$$
$$+\frac{\gamma\tilde{P}_2}{8\beta\xi}\left[3\sin\left(4\tilde{Q}_2+\frac{7t}{\beta}\right)-\sin\left(4\tilde{Q}_2+\frac{5t}{\beta}\right)\right]$$
$$+\gamma\left[\frac{f_1}{2\varepsilon}\sqrt{\frac{b\left(\tilde{P}_1-\tilde{p}\right)}{2\beta\xi}}\right]\sin\left(2\tilde{Q}_1+\frac{2t}{\beta}\right)+\frac{\gamma\tilde{p}(1+2\beta)}{4\beta\xi}\sin\left(2\tilde{Q}_1+2\tilde{q}+\frac{2t}{\beta}\right)$$
$$+\frac{\gamma f_1}{2\varepsilon}\sqrt{\frac{b\tilde{P}_2}{2\beta\xi}}\left[\sin\left(2\tilde{Q}_2+\frac{4t}{\beta}\right)+\sin\left(2\tilde{Q}_2+\frac{2t}{\beta}\right)\right]$$

Table 5. Nonautonomous components of the Hamiltonian (3.35) following the $\tilde{Q}_1$ transformation.

$$\tilde{H}'_{\varepsilon}(t) = -\varepsilon\frac{2\tilde{p}'}{\beta^2\xi\sqrt{2b\beta\xi}}\sqrt{\tilde{P}_1'^2-\tilde{p}'}\cos\left(\frac{\tilde{Q}_1'}{\tilde{P}_1'}+\frac{t}{\beta}\right)$$
$$-\varepsilon\frac{\left(\mu_2+8+2/\beta^2\right)}{2\xi\sqrt{2b\beta\xi}}\tilde{p}'\sqrt{\tilde{P}_1'^2-\tilde{p}'}\cos\left(\frac{2\tilde{Q}_1'}{\tilde{P}_1'}+2\tilde{q}'+\frac{2t}{\beta}\right)$$
$$+\varepsilon\frac{\left(\mu_2-2\mu_5\right)}{2\xi\sqrt{2b\beta\xi}}\tilde{p}'\sqrt{\tilde{P}_2'}\cos\left(\frac{\tilde{Q}_1'}{\tilde{P}_1'}+2\tilde{Q}_2'+2\tilde{q}'+\frac{4t}{\beta}\right)$$

$$\tilde{H}'_{\gamma}(t) = \frac{\gamma\left(\tilde{P}_1'^2-\tilde{p}'\right)}{8\beta\xi}\left[3\sin\left(\frac{2\tilde{Q}_1'}{\tilde{P}_1'}+\frac{3t}{\beta}\right)-\sin\left(\frac{2\tilde{Q}_1'}{P_1}+\frac{t}{\beta}\right)\right]$$
$$+\frac{\gamma\sqrt{\tilde{P}_2'\left(\tilde{P}_1'^2-\tilde{p}'\right)}}{4\beta\xi}\left[3\sin\left(\frac{\tilde{Q}_1'}{\tilde{P}_1'}+2\tilde{Q}_2'+\frac{5t}{\beta}\right)-\sin\left(\frac{\tilde{Q}_1'}{\tilde{P}_1'}+2\tilde{Q}_2'+\frac{3t}{\beta}\right)\right]$$
$$+\frac{\gamma\tilde{P}_2'}{8\beta\xi}\left[3\sin\left(4\tilde{Q}_2'+\frac{7t}{\beta}\right)-\sin\left(4\tilde{Q}_2'+\frac{5t}{\beta}\right)\right]$$
$$+\gamma\left[\frac{f_1}{2\varepsilon}\sqrt{\frac{b\left(\tilde{P}_1'^2-\tilde{p}'\right)}{2\beta\xi}}\right]\sin\left(\frac{\tilde{Q}_1'}{\tilde{P}_1'}+\frac{2t}{\beta}\right)+\frac{\gamma\tilde{p}'(1+2\beta)}{4\beta\xi}\sin\left(\frac{\tilde{Q}_1'}{\tilde{P}_1'}+2\tilde{q}'+\frac{2t}{\beta}\right)$$
$$+\frac{\gamma f_1}{2\varepsilon}\sqrt{\frac{b\tilde{P}_2'}{2\beta\xi}}\left[\sin\left(2\tilde{Q}_2'+\frac{4t}{\beta}\right)+\sin\left(2\tilde{Q}_2'+\frac{2t}{\beta}\right)\right]$$

Table 6. Nonautonomous components of the Hamiltonian (3.40) following the nonautonomous $\tilde{Q}_1'$ transformation.

$$H_\varepsilon(t) = -\varepsilon\frac{2p}{\beta^2\xi\sqrt{2b\beta\xi}}\sqrt{P_1^2-p}\cos\left(\frac{Q_1}{P_1}-\frac{t}{\beta}\right)$$
$$-\varepsilon\frac{(\mu_2+8+2/\beta^2)}{2\xi\sqrt{2b\beta\xi}}p\sqrt{P_1^2-p}\cos\left(\frac{2Q_1}{P_1}+2q-\frac{2t}{\beta}\right)$$
$$+\varepsilon\frac{(\mu_2-2\mu_5)}{2\xi\sqrt{2b\beta\xi}}p\sqrt{P_2}\cos\left(\frac{Q_1}{P_1}+2Q_2+2q+\frac{2t}{\beta}\right)$$

$$H_\gamma(t) = \frac{\gamma(P_1^2-p)}{8\beta\xi}\left[3\sin\left(\frac{2Q_1}{P_1}-\frac{t}{\beta}\right)-\sin\left(\frac{2Q_1}{P_1}-\frac{3t}{\beta}\right)\right]$$
$$+\frac{\gamma\sqrt{P_2(P_1^2-p)}}{4\beta\xi}\left[3\sin\left(\frac{Q_1}{P_1}+2Q_2+\frac{t}{\beta}\right)-\sin\left(\frac{Q_1}{P_1}+2Q_2+\frac{t}{\beta}\right)\right]$$
$$+\frac{\gamma P_2}{8\beta\xi}\left[3\sin\left(4Q_2+\frac{7t}{\beta}\right)-\sin\left(4Q_2+\frac{5t}{\beta}\right)\right]$$
$$+\gamma\left[\frac{f_1}{2\varepsilon}\sqrt{\frac{b(P_1^2-p)}{2\beta\xi}}\right]\sin\left(\frac{Q_1}{P_1}-\frac{2t}{\beta}\right)+\frac{\gamma p(1+2\beta)}{4\beta\xi}\sin\left(\frac{Q_1}{P_1}+2q-\frac{2t}{\beta}\right)$$
$$+\frac{\gamma f_1}{2\varepsilon}\sqrt{\frac{bP_2}{2\beta\xi}}\left[\sin\left(2Q_2+\frac{4t}{\beta}\right)+\sin\left(2Q_2+\frac{2t}{\beta}\right)\right]$$

Calculation of the Melnikov integrals.

The Melnikov function for the cross-wave problem is described in §4 as

$$M(Q_{10}) = 2\cos\frac{Q_{10}}{\overline{P}_1}(I_1 + I_2 + I_3), \tag{A.1}$$

$$I_1 = -\frac{(1-2\beta)}{4\beta\xi\overline{P}_1}\int_0^\infty p_h \cos\frac{2t}{\beta}\,dt, \tag{A.2a}$$

$$I_2 = \frac{f_1\Omega}{2\varepsilon\overline{P}_1\Lambda}\sqrt{\frac{b}{2\beta\xi}}\int_0^\infty \cos\frac{2t}{\beta}\,dt, \tag{A.2b}$$

$$I_3 = -\frac{f_1}{2\varepsilon\overline{P}_1\Lambda}\sqrt{\frac{b}{2\beta\xi}}\int_0^\infty \sqrt{\Lambda^2\left(\overline{P}_1^2 - p_h\right) - \Omega^2}\,\sin\frac{2t}{\beta}\,dt. \tag{A.2c}$$

Each of the component integrals I_j will be described and evaluated below. These integrals use the definition

$$\Theta = \left(\Lambda^2\overline{P}_1^2 - \Omega^2\right). \tag{A.3}$$

Component I_1. Applying (4.10) to (A.2a) makes this component

$$I_1 = -\frac{(1-2\beta)\Theta}{4\beta\xi\overline{P}_1\Lambda^2}\int_0^\infty \operatorname{sech}^2\left(\varepsilon t\sqrt{\Theta}\right)\cos\frac{2t}{\beta}\,dt. \tag{A.4}$$

Using the definite integral from Gradshteyn and Ryzhik [1980, p.505, #3.982(1)],

$$I_1 = -(1-2\beta)\pi\left\{4\beta^2\xi\overline{P}_1\Lambda^2\varepsilon^2\sinh\left(\frac{\pi}{\beta\varepsilon\sqrt{\Theta}}\right)\right\}^{-1}, \tag{A.5}$$

for all $\overline{P}_1^2 > \Omega^2/\Lambda^2$.

Component I_2. The component I_2 does not contain the variable p_h, so the improper integral of (A.2b) must be evaluated. This may be done by applying Proposition 4.1.29 from Wiggins [1988]. This proposition states that the Melnikov integral converges conditionally when the limits of integration $+\infty$ and $-\infty$ are approached along the sequences of times T_j^s and $-T_j^u$, respectively, where $j = 1, 2, \ldots$, and $j \to \infty$. For this problem $T_j^s = T_j^u = j\pi\beta$ is chosen so that

$$\int_{-\infty}^{\infty}[\ ]dt = \lim_{j\to\infty}\int_{-T_j^u}^{T_j^s}[\ ]dt = \lim_{j\to\infty}\int_{-j\pi\beta}^{+j\pi\beta}[\ ]dt = 2\lim_{j\to\infty}\int_{0}^{j\pi\beta}[\ ]dt. \tag{A.6}$$

(See p. 454 in Wiggins, 1988, for an example where time sequences are chosen.) The Melnikov component I_3 is then zero,

$$I_2 = 0. \tag{A.7}$$

Component I_3. Applying (4.10) to the last Melnikov component (A.2c),

$$I_3 = -\frac{f_1\sqrt{\Theta}}{2\varepsilon\overline{P}_1\Lambda}\sqrt{\frac{b}{2\beta\xi}}\int_0^{\infty}\tanh\left(\varepsilon t\sqrt{\Theta}\right)\sin\frac{2t}{\beta}\,dt. \tag{A.8}$$

Integrating by parts and applying the time sequences of (A.6),

$$I_3 = -\frac{f_1\sqrt{\Theta}}{2\varepsilon\overline{P}_1\Lambda}\sqrt{\frac{b}{2\beta\xi}}\left(-\frac{\beta}{2}\lim_{j\to\infty}\tanh\left(\varepsilon t\sqrt{\Theta}\right)\cos\frac{2t}{\beta}\bigg|_0^{j\pi\beta} + \frac{\beta\varepsilon\sqrt{\Theta}}{2}\int_0^{\infty}\frac{\cos 2t/\beta}{\cosh^2\left(\varepsilon t\sqrt{\Theta}\right)}\,dt\right) \tag{A.9a}$$

$$= -\frac{f_1\sqrt{\Theta}}{2\varepsilon\overline{P}_1\Lambda}\sqrt{\frac{b}{2\beta\xi}}\left(-\frac{\beta}{2} + \frac{\beta\varepsilon\sqrt{\Theta}}{2}\int_0^{\infty}\frac{\cos 2t/\beta}{\cosh^2\left(\varepsilon t\sqrt{\Theta}\right)}\,dt\right). \tag{A.9b}$$

Applying the definite integral from Gradshteyn and Ryzhik [1980, p.505, #3.982(1)] to the remaining integral,

$$I_3 = -\frac{f_1\sqrt{\Theta}}{2\varepsilon\overline{P}_1\Lambda}\sqrt{\frac{b}{2\beta\xi}}\left[-\frac{\beta}{2} + \frac{\pi}{2\varepsilon\sqrt{\Theta}}\left(\sinh\frac{\pi}{\varepsilon\beta\sqrt{\Theta}}\right)^{-1}\right] \tag{A.10}$$

for all $\overline{P}_1^2 > \Omega^2/\Lambda^2$.

Since all of the Melnikov components in (A.1) are bounded and only I_2 is zero, the Melnikov function $M(Q_{10}) = 0$ when

$$\cos\frac{Q_{10}}{\overline{P}_1} = 0, \quad Q_{10} = \overline{P}_1\,\pi(2n+1)/2, \quad n = 0,\pm1,\pm2,... \tag{A.11}$$

for all $\overline{P}_1^2 > \Omega^2/\Lambda^2$ and the stable and unstable manifolds of the corresponding hyperbolic periodic orbit intersect transversely yielding Smale horseshoes on the appropriate energy manifold.

Appendix II

Table 7. Wavemaker forcing and amplitude for the experimental runs. The wavemaker frequency is f_{wm} and the waveboard stroke is S, the amplitude of the wavemaker motion, measured at the drive piston. The comments are from notes made during the experiment runs.

Run	f_{wm} (Hz)	S (ft)	kS	Comments
1	1.317	0.025	0.055	No visible mode 2
2	1.317	0.038	0.081	Very steady pattern of mode 2
3	1.317	0.050	0.106	Larger mode 2, not as steady as run 2
4	1.230	0.075	0.139	No visible mode 2
5	1.239	0.075	0.141	No visible mode 2
6	1.245	0.075	0.143	No visible mode 2
7	1.515	0.075	0.211	No visible mode 2
8	1.449	0.075	0.193	No visible mode 2
9	1.285	0.075	0.165	Mode 2 appeared
10	1.423	0.075	0.186	Mode 2 appeared at the very end
11	0.653	0.150	0.078	Could see mode 2 near the wavemaker
12	0.653	0.075	0.039	No visible mode 2
13	1.441	0.050	0.127	No visible mode 2
14	1.411	0.050	0.122	No visible mode 2
15	1.371	0.050	0.115	No visible mode 2
16	1.330	0.050	0.108	Mode 2 appeared
17	1.280	0.050	0.100	No visible mode 2
18	1.292	0.050	0.102	No visible mode 2
19	1.305	0.050	0.104	Mode 2 appeared
20	1.862	0.013	0.055	Mode 4 appeared near the end
21	1.862	0.008	0.034	No visible mode 4
22	1.862	0.025	0.106	Mode 4 appeared
23	1.774	0.038	0.147	No visible mode 4
24	1.814	0.038	0.153	Mode 4 appeared, breaking at board
25	1.965	0.038	0.180	Very steady pattern of mode 4
26	1.995	0.038	0.185	Mode 4 appeared
27	1.975	0.038	0.182	Steady pattern of mode 4
28	1.804	0.025	0.100	No visible mode 4
29	1.834	0.025	0.103	Mode 4 appeared
30	1.945	0.025	0.117	Steady pattern of mode 4
31	1.965	0.025	0.118	No visible mode 4
32	0.922	0.100	0.104	Mode 4 visible at waveboard, then mode 1
33	0.922	0.125	0.130	Mode 4 first, then dominated by mode 1
34	0.922	0.075	0.078	No visible mode 1
35	0.880	0.125	0.119	No visible mode 1
36	0.970	0.125	0.144	No visible mode 1, hint of mode 4
37	0.895	0.125	0.123	No visible mode 1
38	0.950	0.125	0.138	No cross-waves
39	0.910	0.125	0.126	No cross-waves
40	0.935	0.125	0.134	No cross-waves

Appendix III

Table 8. Notation

a_c'	dimensional cross-wave amplitude
a_p'	dimensional progressive wave amplitude
a_w'	dimensional amplitude of the wavemaker motion
b', b	dimensional and nondimensional half width of the wavetank
$f(z)$	wavemaker depth function
f_1	integral over depth of the wavemaker depth function
f_{cn}	cross-wave frequency in Hz for mode n in experiments
f_p	progressive wave frequency in Hz during experiments
f_{wm}	wavemaker forcing frequency in Hz during experiments, also equals to the progressive wave frequency
$\hat{F}, F'', \tilde{F}'$	generating functions used in some canonical transformations
g'	gravitational acceleration
h'	still water depth
H	the original Hamiltonian, before any transforamtions the same notation is also used for the final Hamiltonian
$H_o, H_\varepsilon, H_\gamma$	the $O(1)$, $O(\varepsilon)$, and the perturbed components of H subscripts on subsequent Hamiltonians mean the same thing
H'	transformed Hamiltonian after the rotation of axes transformation
$\hat{H}$	transformed Hamiltonian after the action/angle variables
H^*	transformed Hamiltonian after the application of Hamilton-Jacobi theory
H''	transformed Hamiltonian after the shift transformation
$\tilde{H}$	transformed Hamiltonian after the nonautonomous Q_2'' transformation
$\tilde{H}'$	transformed Hamiltonian after the $\tilde{Q}_1$ transformation
$\overline{H}$	the time-averaged Hamiltonian
H^γ	the perturbed part of the final Hamiltonian

I_1, I_2, I_3	components of the Melnikov integral
$\hat{\mathbf{i}}$	unit vector in the x or x' direction
$\hat{\mathbf{j}}$	unit vector in the y or y' direction
$\hat{\mathbf{k}}$	unit vector in the z or z' direction
k'	dimensional wavenumber for the progressive wave
l'	dimensional length of fluid domain down the wavetank
$\overline{L}'$	total dimensinal Lagrangian from Luke, 1967, an integral over volume
$\overline{L}'_v$	dimensional Lagrangian density from Luke, 1967
$\overline{L}^o$	dimensional terms of the Lagrangian with zero variation
L', L	dimensional and nondimensional total Lagrangian written as surface integrals without the terms with zero variation
$L'_{v'}$, L_v	the component of L', L integrated over volume
$L'_{\chi'}$, L_χ	the component of L', L integrated over the wavemaker surface
$L'_{\xi'}$, L_ξ	the component of L', L integrated over the cross-section down the channel
$L'_{\eta_1'}$, L_{η_1}	the component of L', L integrated over the first set of free surface terms
$L'_{\eta_2'}$, L_{η_2}	the component of L', L integrated over the second set of free surface terms
$M(Q_{10})$	the Melnikov function
M	two dimensional normally hyperbolic invariant manifold of the unperturbed system
M_γ	two dimensional normally hyperbolic locally invariant manifold of the perturbed system
n	mode number of the cross-wave
P'	dimensional fluid pressure
$\mathrm{p}_1, \mathrm{p}_2$	original momenta from Holmes' 1986 paper

P_1, P_2	final transformed momenta from Holmes' 1986 paper
p, P_1, P_2	conjugate momenta in the original untransformed variables and in the final variables
p', P_1', P_2'	conjugate momenta after the rotation of axes transformation
$\hat{p}, \hat{P}_1, \hat{P}_2$	conjugate momenta after the action/angle transformation
p^*, P_1^*, P_2^*	conjugate momenta after the Hamilton-Jacobi transformation
p'', P_1'', P_2''	conjugate momenta after the shift transformation
$\tilde{p}, \tilde{P}_1, \tilde{P}_2$	conjugate momenta after the nonautonomous Q_2'' transformation
$\tilde{p}', \tilde{P}_1', \tilde{P}_2'$	conjugate momenta after the $\tilde{Q}_1$ transformation
$p_{orig}, P_{1orig}, P_{2orig}$	original momenta, denoted this way to avoid confusion with the final transformed momenta in the summary section
q_1, q_2	original coordinates from Holmes' 1986 paper
Q_1, Q_2	final transformed variables from Holmes' 1986 paper
q, Q_1, Q_2	generalized coordinates in the original untransformed variables and in the final variables
q', Q_1', Q_2'	generalized coordinates after the rotation of axes transformation
$\hat{q}, \hat{Q}_1, \hat{Q}_2$	generalized coordinates after the action/angle transformation
q^*, Q_1^*, Q_2^*	generalized coordinates after the Hamilton-Jacobi transformation
q'', Q_1'', Q_2''	generalized coordinates after the shift transformation
$\tilde{q}, \tilde{Q}_1, \tilde{Q}_2$	generalized coordinates after the nonautonomous Q_2'' transformation
$\tilde{q}', \tilde{Q}_1', \tilde{Q}_2'$	generalized coordinates after the $\tilde{Q}_1$ transformation
$q_{orig}, Q_{1orig}, Q_{2orig}$	original coordinates denoted this way to avoid confusion with the final transformed coordinates in the summary section
S	wavemaker stroke in experiments
t, t'	dimensionless and dimensional time
$\boldsymbol{u}'$	dimensional fluid particle velocity

$x,\ x'$	dimensionless and dimensional position down the tank, with $x=0$ and $x'=0$ at the equilibrium position of the wavemaker
$y,\ y'$	dimensionless and dimensional position across the width of the tank, with $y=0$ and $y'=0$ at the centerline of the tank
$z,\ z'$	dimensionless and dimensional position at depth, with $z=0$ and $z'=0$ at the still water level
α	dimensionless depth parameter, $\kappa' h'$
β	dimensionless wavenumber parameter, $\sqrt{\frac{\kappa'}{k'}}$
γ	dimensionless waveboard stroke parameter, $k' a_w'$, which is also called the perturbation pararmeter
Γ	dimensionless ratio of wave amplitudes, $\frac{a_p'}{a_c'}$
δ	indicates the first variation, a derivative of a functional
ε	dimensionless wave amplitude parameter, $\kappa' a_c'$, which is also used as the measure of nonlinearity
λ_{cn}	wavelength for cross-wave of mode n in experiments
Λ	coefficient defined in Table 1, used in Hamiltonian
$\eta,\ \eta'$	dimensionless and dimensional free surface elevation, measured from the still water level
θ	rotation angle for the rotation of axes canoncical transformation
μ_i	coefficients used in Hamiltonians, defined in Table 1
κ'	dimensional wavenumber for the cross-wave
κ_n	cross-wave wavenumber for mode n in experiments
ξ	dimensionless length parameter down the channel, $k' l'$
ρ'	dimensional fluid density
$\rho_o(P_1)$	manifold of the hyperbolic fixed points in the unperturbed system
$\rho_\gamma(P_1)$	manifold of the hyperbolic fixed points in the perturbed system

$\tau(\overline{P}_1)$	tori on M for fixed $P_1 = \overline{P}_1$
ϕ, ϕ'	dimensionless and dimensional fluid velocity potential
ϕ_c, ϕ_c'	dimensionless and dimensional cross-wave velocity potential
ϕ_p, ϕ_p'	dimensionless and dimensional progressive wave velocity potential
χ, χ'	dimensionless and dimensional wavemaker position measured from the equilibrium vertical position
ω_c'	dimensional cross-wave frequency
ω_p'	dimensional progressive wave frequency
ω_{cn}	cross-wave frequency for mode n in experiments
Ω	detuning parameter
$\frac{\partial}{\partial x'}, \frac{\partial}{\partial y'}, \frac{\partial}{\partial z'}$	partial derivatives with respect to the dimensional coordinates x', y', z'
$\frac{\partial}{\partial x}, \frac{\partial}{\partial y}, \frac{\partial}{\partial z}$	partial derivatives with respect to the dimensionless coordinates x, y, z
$\frac{\partial}{\partial t'}$	partial derivative with respect to the dimensional time t'
$\frac{\partial}{\partial t}$	partial derivative with respect to the dimensionless time t, also indicated by a dot over the variable
∇'	dimensional gradient operator, $\frac{\partial}{\partial x'}\hat{\mathbf{i}} + \frac{\partial}{\partial y'}\hat{\mathbf{j}} + \frac{\partial}{\partial z'}\hat{\mathbf{k}}$
∇	dimensionless gradient operator, $\frac{\partial}{\partial x}\hat{\mathbf{i}} + \beta\frac{\partial}{\partial y}\hat{\mathbf{j}} + \beta\frac{\partial}{\partial z}\hat{\mathbf{k}}$
∇_2'	dimensional horizontal gradient operator, $\frac{\partial}{\partial x'}\hat{\mathbf{i}} + \frac{\partial}{\partial y'}\hat{\mathbf{j}}$
∇_2	dimensionless horizontal gradient operator, $\frac{\partial}{\partial x}\hat{\mathbf{i}} + \beta\frac{\partial}{\partial y}\hat{\mathbf{j}}$
∇^2, ∇'^2	dimensionless and dimensional Laplacian, $\nabla\cdot\nabla$ or $\nabla'\cdot\nabla'$